

QUANTUM INFORMATION DYNAMICS: A
PERSPECTIVE FROM FREE FERMION MODELS

Jonathon Riddell

*A Thesis Submitted to the School of Graduate Studies in
Partial Fulfillment of the Requirements for Master of Science*

September 3, 2019

McMaster University
Master of Science (2019)
Hamilton, Ontario (Department of Physics and Astronomy)

TITLE: Quantum Information Dynamics: A Perspective From Free Fermion Models
AUTHOR: Jonathon Riddell
SUPERVISOR: Dr. Erik S. Sørensen
NUMBER OF PAGES: 78

Acknowledgments

Throughout my scientific career I have received guidance, support and encouragement from amazing mentors and collaborators. Most importantly, I have also been given opportunities to do research on subjects for which I am incredibly passionate. I would like to thank Erik for accepting me as his student, and for guiding me through projects we both found interesting and fruitful. I want to specially thank you for helping me with concerns relating to my health, and for making sure that I was comfortable in the department; this has had an immense impact on me, and I am not sure I could have stuck around without your help. I also appreciate the weekly meetings along with a focus on developing my skills as a researcher, and I look forward to another four years of working together! I would like to thank Álvaro for giving me the opportunity to work with him; I have benefited a lot from working with you and I appreciate your patience and willingness to teach. I would also like to thank Luis Pedro for our collaborations and fruitful discussions. Moreover, I am profoundly thankful to my first mentor, Markus, for giving me the first opportunity to become a researcher and for introducing me to the subject I am deeply passionate about. Lastly, I would like to thank Sung-Sik and Duncan for sitting on my committee and Catherine for chairing my defense.

Lastly, I would like to acknowledge my family and friends whose support has been instrumental to my success. While my health has been a constant issue for me, my family and friends are the crutches I lean on to move forward and reach my goals. It is difficult to convey how important they all are for me to succeed in life. I would like to show gratitude to three people who have provided me with vital support through my degree (and more) my mom, my lovely wife, and my little sister; you three are my strength and my inspiration. A special thanks to my friends Steve, Nathan, James and Anton for always being willing to talk about the math or coding related problems in my research. Only you understand how truly confused I can be!

Contents

1	Introduction	1
2	Out of Time Ordered Correlators and Entanglement Growth in the Random Field XX Spin Chain	13
3	Out of Time Order Correlations in the Quasi-Periodic Aubry-André model	29
4	Time evolution of correlation functions in quantum many-body systems	45
5	Conclusions	63

Chapter 1

Introduction

The age old question of how statistical mechanics emerges from the microscopic laws of nature has recently seen a resurgence of interest due to novel experiments with ultra-cold atomic gases and analytic ideas from quantum information theory [1–6]. Traditionally, statistical mechanics was studied in the context of a small sub-system coupled to a thermal bath [2, 7–11]. Coupling to a bath guarantees the subsystem relaxes to the thermal state with identical temperature to the bath [12–15]. Although the composite system must evolve in time according to the Schrodinger equation, the sub-system itself does not demonstrate unitary dynamics and flows towards a mixed state. This strong assumption on the initial state along with the coupling to the bath is not always possible. So-called pure state statistical mechanics in systems isolated from an environment has recently become a topic of interest [2, 7, 8]. Such isolated systems can be simulated with novel experiments involving optical lattices and trapped ions allowing the creation of quantum systems decoupled from the outside environment, making them closed systems with unitary time evolution [1, 16–30]. Such experimental control allows the direct experimental investigation into foundational questions of quantum statistical mechanics, namely, how does unitary dynamics lead to its emergence [21, 23, 31–33]? Suppose we prepare a d -level system with N lattice sites with a time independent local Hamiltonian \hat{H} in a pure state $|\psi\rangle$ where the state is normalized $\langle\psi|\psi\rangle = 1$. We could similarly use the density matrix formalism and write $\rho = |\psi\rangle\langle\psi|$. This state is said to be pure due to a single outer-product defining the density matrix. A mixed state would instead be a weighted sum of pure states $\rho_{\text{mixed}} = \sum_s p_s |\psi_s\rangle\langle\psi_s|$, where $\sum_s p_s = 1$. Let the Hamiltonian have eigenvectors/eigenvalues $\hat{H}|E_m\rangle = E_m|E_m\rangle$. Time evolving our pure state with the Hamiltonian is written as,

$$|\psi(t)\rangle = \sum_{m=1}^{d^N} c_m e^{-iE_m t} |E_m\rangle, \quad (1.1)$$

where $c_m = \langle E_m | \psi \rangle$. We then fix the energy density as the quantity, $\frac{1}{N} \langle \psi | \hat{H} | \psi \rangle = u$. Due to unitary time evolution the purity of a pure state is conserved in time, that is,

$$\text{if } \rho(t) = |\psi(t)\rangle\langle\psi(t)|, \quad \text{tr}(\rho(t)) = \text{tr}(\rho(t)^2) = 1, \quad (1.2)$$

meaning evolution towards a mixed state (ex. microcanonical or Gibbs state) is impossible due to the initial conditions. However the expectation value of some observable \hat{A} could evolve to be similar to that of a mixed state. To begin the quest of recovering statistical mechanics we then need to justify the equilibration of the expectation value of the observable. If equilibration occurs, the equilibrated value of the observable would need to be that of the infinite time average. We may write the time evolution as,

$$\langle \hat{A}(t) \rangle = \sum_{m,n} \bar{c}_m c_n A_{m,n} e^{i(E_m - E_n)t} = \sum_m |c_m|^2 A_{m,m} + \sum_{m \neq n} \bar{c}_m c_n A_{m,n} e^{i(E_m - E_n)t}, \quad (1.3)$$

where $A_{m,n} = \langle E_m | \hat{A} | E_n \rangle$. The last equality features two sums, one of which is a constant of motion, and the other a dephasing term. To proceed, we need to now make assumptions on the energy eigenvalues. If the Hamiltonian \hat{H} is quantum chaotic, the level statistics usually obey Wigner-Dyson statistics implying level repulsion [7]. So we may make the assumption that, for a chaotic Hamiltonian,

$$E_m = E_k \iff m = k. \quad (1.4)$$

Then the infinite time average is,

$$\langle \hat{A}(t \rightarrow \infty) \rangle = \lim_{T \rightarrow \infty} \frac{1}{T} \int_0^T \langle \hat{A}(t) \rangle dt = \sum_m |c_m|^2 A_{m,m}. \quad (1.5)$$

There has been work done to study when and how equilibration like this occurs [2,34–41]. A seemingly strong bound for this form of operator equilibration is given in [37]. First we define the infinite time average state (regularly called the diagonal ensemble),

$$\omega = \lim_{T \rightarrow \infty} \frac{1}{T} \int_0^T \rho(t) dt = \sum_m |c_m|^2 |E_m\rangle\langle E_m|. \quad (1.6)$$

Then we may investigate the average distance between the state and the diagonal ensemble over an infinitely long time window and bound it [37],

$$\sigma_A^2 = \lim_{T \rightarrow \infty} \frac{1}{T} \int_0^T \left| \text{tr}(\rho \hat{A} - \omega \hat{A}) \right|^2 dt \leq \frac{\|\hat{A}\|^2}{d_{\text{eff}}}, \quad (1.7)$$

where $\|\hat{A}\|^2$ is the 2-norm and,

$$d_{\text{eff}} = \frac{1}{\text{tr}(\omega^2)}. \quad (1.8)$$

It is argued from equation 1.7 that the difference between the late time state and ω would be beyond experimental precision to detect due to the tightness of this bound [37, 40]. Note however, that this is an infinite time average. Attempts have been made to extend these arguments to finite time, providing a stronger statement about equilibration [2, 42–55]. Despite these efforts no generic proof of finite time equilibration for local Hamiltonians under reasonable assumptions is known. Most bounds scale poorly with system sizes or are applicable in few scenarios. For an integrable, non-interacting model, namely free fermions, equilibration in finite time for a general class of initial states and operators was recently proven [56]. A free fermionic Hamiltonian in one dimension is written as,

$$\hat{H} = \sum_{i,j} M_{i,j} \hat{f}_i^\dagger \hat{f}_j, \quad (1.9)$$

where $\{\hat{f}_k, \hat{f}_l\} = \{\hat{f}_k^\dagger, \hat{f}_l^\dagger\} = 0$ and $\{\hat{f}_l^\dagger, \hat{f}_k\} = \delta_{l,k}$ are fermionic operators. If the Hamiltonian in equation 1.9 is local, then from [56],

$$|\Gamma_{i,j} - \Gamma_{i,j}^{(\text{eq})}| \leq Ct^{-\gamma}, \quad (1.10)$$

where $\Gamma_{i,j}$ are two point expectation values of the form, $\langle \hat{f}_i^\dagger \hat{f}_j \rangle + \text{h.c.}$, the superscript (eq) implies an infinite time average value, C is some reasonable constant and $\gamma > 0$. This result is true for a generally large class of initial states, requiring only exponentially decaying correlations. This also covers all operators due to the Hamiltonian preserving Gaussian statistics of the initial state, or evolving towards them in time [57]. If we instead investigate an interacting system which is simply quenched away from a thermal ensemble, one may track this equilibration with certain operators using dynamical correlation functions [58, 59],

$$C(t) = \langle \hat{A}(t) \hat{A} \rangle. \quad (1.11)$$

Then for general systems, a rigorous proof of equilibration in finite time has been found [60],

$$\frac{1}{T} \int_0^T \frac{|C(t) - C_\infty|^2}{(C(0))^2} dt \leq 4\pi \left(\frac{a(\epsilon)}{\sigma_G} \frac{1}{T} + \delta(\epsilon) \right), \quad (1.12)$$

where $a(\epsilon)$, σ_G are numbers that are on the order of one, $\delta(\epsilon)$ is very small and the average is over a thermal state.

Once in equilibrium, one needs to justify why the diagonal ensemble (equation 1.5) encodes the same physics as a thermal state. If we again use the ansatz of quantum chaos and formulated our Hamiltonian as simply a random matrix, then one finds that in the eigenbasis of such a Hamiltonian, the observable looks like [7],

$$\hat{A}_{m,n} = \bar{A}\delta_{m,n} + \sqrt{\frac{\bar{A}^2}{D}}R_{m,n}, \quad (1.13)$$

where D is the dimension of the Hilbert space, $\bar{A} = \bar{A}_{m,m} = \frac{1}{D} \sum_m \hat{A}_{m,m}$ and $R_{m,n}$ is a random variable with zero mean and unit variance. Using this result we find that equation 1.5 at equilibrium reads [7],

$$\sum_m |c_m|^2 A_{m,m} \approx \bar{A} \sum_m |c_m|^2 = \bar{A}, \quad (1.14)$$

meaning that this result is independent of temperature, energy density, and other thermodynamic quantities. We know however that such equilibrium values are dependent on these quantities, so this line of reasoning needs to be extended. One success of this ansatz is that the off diagonal elements of our observable shrink with the size of the Hilbert space, meaning the dephasing term in equation 1.3 is a summation over quite small numbers. This then suggests equilibrium can be reached quickly in generic situations. Despite this, the approach needs to be extended in order to predict the emergence of statistical mechanics. It is then insightful to compare the expectation values of statistical ensembles to equation 1.5. Let us define the microcanonical ensemble in the following way (taking the definitions from [41, 61]); the microcanonical subspace is defined as,

$$T_{u,\delta} = \text{span}\{|E_k\rangle : \hat{H}|E_k\rangle = E_k|E_k\rangle \wedge u - \delta \leq \frac{E_k}{N} \leq u\}, \quad (1.15)$$

then the microcanonical ensemble is defined as the uniform mixture of these states,

$$\tau_{u,\delta} = \frac{1}{M} \pi_{u,\delta}, \quad (1.16)$$

where $\pi_{u,\delta}$ is the projector onto the space spanned by $T_{u,\delta}$ and $M = \dim T_{u,\delta}$. Writing this more conventionally,

$$\tau_{u,\delta} = \frac{1}{M} \sum_{k:|E_k\rangle \in T_{u,\delta}} |E_k\rangle \langle E_k|. \quad (1.17)$$

The expectation value of the observable \hat{A} in the microcanonical average is,

$$\text{tr}(\tau_{u,\delta} \hat{A}) = \frac{1}{M} \sum_{k:|E_k\rangle \in T_{u,\delta}} A_{k,k}. \quad (1.18)$$

Alternatively we can define the Gibbs (thermal) ensemble as,

$$\rho_\beta = \frac{1}{Z} e^{-\beta \hat{H}} = \frac{1}{Z} \sum_k e^{-\beta E_k} |E_k\rangle \langle E_k|, \quad Z = \text{tr} \left(e^{-\beta \hat{H}} \right). \quad (1.19)$$

where β is determined by, $\frac{1}{N} \text{tr}(\rho_\beta \hat{H}) = u$. The thermal average of the observable is then given by,

$$\langle \hat{A} \rangle_\beta = \frac{1}{Z} \sum_k e^{-\beta E_k} A_{k,k}. \quad (1.20)$$

Then how could our equilibrated value given in equation 1.5 be equal to the values found in equation 1.18 or 1.20? It is useful to note that, if the observable is local and the model is local then the expectation values of equation 1.18 and 1.20 are identical in the thermodynamic limit, constituting equivalence of ensembles in closed systems [41,61]. A potential answer to the question of reproducing the expectation values is the Eigenstate Thermalization Hypothesis (ETH) where the matrix elements of relevant observables in the energy eigenbasis are conjectured to obey [7, 62–66],

$$A_{m,n} = A(\bar{E}) \delta_{m,n} + e^{-S(\bar{E})/2} f(\bar{E}, \alpha) R_{m,n}. \quad (1.21)$$

Where $\bar{E} = (E_m + E_n)/2$, $\alpha = (E_m - E_n)/2$, $A(\bar{E})$, $f(\bar{E}, \alpha)$ are smooth functions of \bar{E} and α , and $S(\bar{E})$ is the thermodynamic entropy. There exist a large body of numerical evidence supporting this conjecture in non-integrable systems. Evidence has been compiled for its support in hardcore boson, spin and fermionic systems [7, 67–80]. There is however no known analytical proof [2, 7, 81]. Likewise there is no accepted or rigorous definition of what a relevant observable is. It is believed local observables are the most likely candidates to obey the ETH [7,67]. However, it is also argued by Garrison and Grover that observables with support on up to one half of the system size could satisfy the ETH [82]. Progress has been made to analytically show similar statements hold. Equation 1.21 can be commonly referred to as the strong ETH, requiring that all eigenstates obey it. This gives rise to the notion of the so-called eigenstate ensemble, since the physics of the microcanonical ensemble can be captured by the eigenstate with similar energy. This is seen through, for example, the Von Neumann entropy $S = -\text{tr}(\rho \ln \rho)$. Let us partition our closed system into two subsystems A, B such that A encompasses less lattice sites than B . Then let $\rho_A = \text{tr}_B \rho$ and V_A be the volume of the subsystem A . If we take $\rho = |E_k\rangle \langle E_k|$ then the systems obeying equation 1.21 observe a volume law in $S_A = -\text{tr}(\rho_A \ln \rho_A) \sim V_A$ for the energy eigenvectors [7, 81, 83, 84]. ETH models out of equilibrium have entanglement entropy increase linearly with time between subsystems and dephasing and dissipation occurs [81].

Progress has been made with the so called weak ETH where equation 1.21 is relaxed to most eigenstates. The following statement has been rigorously proved by Alhambra et al [60] (see lemma 1, this result is an extension of previous results [85, 86]). There exists a constant $0 < \alpha < 1/(D + 1)$ such that the following holds. Let H be a translation-invariant, non-degenerate Hamiltonian with N sites on a D -dimensional lattice, ρ an equilibrium ensemble $[\rho, H] = 0$ with finite correlation length ξ , and A some observable with support on a connected region of at most N^α sites. Then, for any $\delta > 0$,

$$\Pr_{|E_k\rangle \in \rho}(|\langle E_k|A|E_k\rangle - \text{tr}\rho A| \geq \delta) \leq \exp(-c\delta N^{\frac{1}{D+1}} \xi^{-\frac{D}{D+1}}), \quad (1.22)$$

where $c > 0$ is a constant, and $|E_k\rangle \in \rho$ indicates that the eigenstates are sampled from the equilibrium distribution ρ .

Equation 1.22 tells us that, with large system sizes, the probability that any given eigenstate generated randomly from an ensemble differs from the average of such an ensemble by an amount δ is exponentially suppressed by both δ and system size. This statement still leaves room for the so-called quantum scars, eigenstates which violate equation 1.21, which have been recently investigated [87–89]. These eigenstates, despite making up a vanishing fraction of the total number of eigenstates, do not appear locally thermal, and are important for physically relevant dynamics in several systems [87–89]. Quantum scars are evidence that, even in systems believed to obey ETH, there exist eigenstates that do not obey equation 1.21. In equation 1.21 the off-diagonal elements of these observables in the energy eigenbasis are also predicted to be quite small. Although such a statement is not completely recovered rigorously, it is possible to bound these elements for local observables. The following statement proved by Arad et al. and separately by Oliveira et al. captures the smallness of the off-diagonal elements for a large portion of the spectrum, using [90, 91],

$$|\langle E_i|A|E_j\rangle| \leq \frac{|E_i - E_j|}{R} e^{-\frac{(|E_i - E_j| - R)}{gk}}, \quad (1.23)$$

where R, g, k are constants related to the structure of the Hamiltonian and lattice. Although equation 1.23 does not cover the entire spectrum, if the difference in energy is either small or large, the eigenstate thermalization argument does not seem very far fetched. The intermediate region is however still an open question.

A notable counter examples to the ETH are the so called many body localized (MBL) systems [67, 92]. Localization can be induced in many ways, however a random or quasi-periodic field are the usual mechanisms to induce this phase in spin models. The usual model to study this phenomena is written (here with periodic boundaries) [67],

$$\hat{H} = J \sum_{i=1}^L \hat{S}_i \cdot \hat{S}_{i+1} + \lambda_i \hat{S}_i^Z, \quad (1.24)$$

where $\hat{S}_i = (\hat{S}_i^X, \hat{S}_i^Y, \hat{S}_i^Z)$ is a vector of spin 1/2 matrices, and λ_i is a random field generated from a uniform distribution on the interval $[-\lambda, \lambda]$. When $\lambda \gg J$ the model undergoes a transition from an ETH to an MBL phase [67,81,92,93]. The entanglement entropy observed in the eigenstates of MBL models obey area laws between subsystems, growing like the area of contact [67, 81, 92, 93]. They also do not equilibrate to the usual ensembles of statistical mechanics, due to the lack of dissipation [67,81,92,93]. Arguably one of the most interesting facets of the MBL phase is that out of equilibrium states build up entanglement entropy between their subsystems like $S_A \sim \log t$ [94–98].

Free models, namely quasi-free fermions are integrable and non-interacting, which requires slightly different notions of thermalization and localization. Unsurprisingly, models which fall into the category of equation 1.9 have had much more progress in understanding thermalization and localization properties. If the model is translationally invariant then a generalized form of the weak ETH holds [99, 100]. If selected randomly, eigenstates are locally identical to generalized Gibbs ensembles of the form,

$$\rho = \frac{1}{Z} e^{-\sum_{j=1}^r \beta_j \hat{Q}_j}, \quad (1.25)$$

where r is intensive in the number of lattice sites, β_j are determined by fixing the expectation value of \hat{Q}_j and \hat{Q}_j is a conserved quantity. The \hat{Q}_j need to be of the form,

$$\hat{Q}_j = \sum_k q_j(k) \hat{\eta}_k^\dagger \hat{\eta}_k, \quad (1.26)$$

where $\hat{\eta}_k^\dagger$ are fermionic operators which diagonalize equation 1.9 and $q_j(k)$ is Lipschitz continuous at all but a sub-extensive number of points. Lipschitz continuity requires that there exists some constant c such that,

$$|q_j(k_1) - q_j(k_2)| \leq c|k_1 - k_2|. \quad (1.27)$$

This is remarkably equivalent to the ensemble that free fermions were proved to equilibrate to in [56]. The parameter r is then fixed by the correlation length of the initial state, and the \hat{Q}_j are current operators of the form (in one dimension with L lattice sites),

$$\hat{Q}_z = \frac{1}{L} \sum_{l=1}^L \cos\left(\frac{2\pi lz}{L}\right) \hat{\eta}_l^\dagger \hat{\eta}_l. \quad (1.28)$$

Equation 1.28 gives observables proposed by [56] which connects the generalized ETH (gETH) proved in [100]. Entanglement entropy scaling of the eigenstates has similarly been

studied in these free models, finding that eigenstates experience maximal entanglement entropy only on subsystems of vanishing fractions of the system size and obey volume laws throughout the spectrum [101–103].

If instead we investigate a free fermionic Hamiltonian with onsite disorder by filling the co-efficient matrix M from equation 1.9 with $M_{i,i} = \lambda_i$, where λ_i are drawn from a uniform distribution on the interval of $\lambda_i \in [-\lambda, \lambda]$ one can induce Anderson localization (AL) at any $\lambda > 0$ [81, 83, 104–106]. AL is the free model counterpart to MBL, similar to having gETH to ETH. The AL single particle eigenstates are exponentially localized in real space which is characterized by a localization length [104, 107, 108]. The entanglement entropy also obeys an area law for its subsystems [104, 107–109]. AL systems have exponentially suppressed particle and matter transport. The easiest way to see this is through the AL version of the Lieb Robinson bound. For generic models, one may write a Lieb-Robinson bound of the form,

$$||[\hat{A}_j(t), \hat{B}_k]|| \leq C ||\hat{A}|| ||\hat{B}|| e^{-\frac{(|j-k|-vt)}{\xi}}, \quad (1.29)$$

where \hat{A}_j, \hat{B}_k are operators on lattice sites j, k respectively, C is some positive constant, $\xi > 0$ and v is an upper bound for the maximal group velocity [104, 110]. For AL models, equation 1.29 becomes,

$$||[\hat{A}_j(t), \hat{B}_k]|| \leq C ||\hat{A}|| ||\hat{B}|| e^{-\frac{|j-k|}{\xi}}, \quad (1.30)$$

and we refer to $\xi > 0$ as the localization length [104]. With equation 1.30 we may view AL in the fermionic model as an insulator which lacks particle and energy transport. This lack of transport suppresses generalized thermalization.

Now that we have summarized the two largest classes of models and their properties in the processes of equilibration and thermalization (or lack of thermalization) understanding this process from an information spreading perspective has recently become a popular topic. During the process of equilibration, unitary dynamics must take the local information of our initial state, and scramble or smear it to recover a state resembling a thermal ensemble [67]. This may be concretely seen in the following way. Suppose we prepare two states ρ_1, ρ_2 such that these two states have nearly identical energy, $\text{tr}(\hat{H}\rho_1) \approx \text{tr}(\hat{H}\rho_2)$. However we prepare these states such that they disagree on the initial condition of some local observable \hat{A} , $\text{tr}(\hat{A}\rho_1) \neq \text{tr}(\hat{A}\rho_2)$. Then if \hat{H} satisfies the strong ETH, the two states are expected to equilibrate to the same thermal state, where the inverse temperature β is determined uniquely by the energy. This then implies both states after reaching equilibrium agree on the expectation value of \hat{A} and the information of the initial conditions is lost. This process is referred to as the scrambling of information. Understanding this process of scrambling is crucial in the

pursuit of our understanding of equilibration and thermalization. To study this we first need a function that could track this phenomena. A recently proposed correlation function called the out of time ordered correlator (OTOC) is such a quantity [111, 112],

$$C(x, t) = \langle [\hat{A}(t), \hat{B}]^\dagger [\hat{A}(t), \hat{B}] \rangle, \quad (1.31)$$

where \hat{A}, \hat{B} are local observables which commute at $t = 0$. If the operators are both hermitian and unitary the OTOC can be re-expressed as,

$$C(x, t) = 2 - 2\Re[F(x, t)], \quad (1.32)$$

where,

$$F(x, t) = \langle \hat{A}(t) \hat{B} \hat{A}(t) \hat{B} \rangle. \quad (1.33)$$

From the perspective of condensed matter systems, the OTOC tracks the local operator \hat{A} as it spreads its influence over the lattice through the degree of non-commutativity of the two operators at different times. If $C(x, t)$ remains non-zero for late times, the system is said to have scrambled its information. $F(x, t)$ can be understood from a different perspective, namely as a series of measurements. First acting on a state with operator \hat{B} and allowing the system to evolve for a time t and then measuring \hat{A} . The function $F(x, t)$ is then the overlap of this state and the state where these operations are reversed. The time it takes $C(x, t) \sim 1$ defines the so called scrambling time. The early time approach to scrambling for some models is expected to be of the form, $C(0, t) \sim e^{\lambda_L t}$ with a conjectured bound $\lambda_L \leq 2\pi k_B T / \hbar$ [112]. Systems where this bound is tight are known as fast scramblers [113–118]. There are however a range of models that do not exhibit such growth [83, 96, 119–123]. The OTOC is filled with rich dynamics, it has four dynamical regimes of interest that have various forms. These regimes include two purely quantum mechanical regimes, early time and the wave-front, and then the late time relaxation and infinite time values.

The early time growth is largely an artifact of the local nature of the Hamiltonian. Using the Hadamard formula (see ref. [124] lemma 5.3) one can conclude that the OTOC initially grows with a power law that precedes the classical wave-front,

$$C(x, t) \sim t^{l(x)}, \quad (1.34)$$

where $l(x)$ is some linear function of distance. This power law is independent of the integrability of the model and has been predicted and verified for a variety of models [109, 119, 125–129]. This growth is also known to be independent of disorder and has been found numerically in localized regimes [109, 128].

Following this early growth is the wavefront, the front at which classical information travels. A universal form for the OTOC has been proposed [130, 131],

$$C(x, t) \sim \exp\left(-\lambda \frac{(x - v_B t)^{1+p}}{t^p}\right), \quad (1.35)$$

where λ_L is a Lyapunov exponent, v_B is the butterfly velocity and p is a constant. The wavefront has received considerable interest and has been confirmed analytically and numerically in a variety of cases and has even been used to track an ETH to MBL transition [130–141]. Especially interesting is in a free model (equation 1.9 with nearest neighbour hopping), a standard saddle point approximation reveals the butterfly velocity to be equivalent to the maximal group velocity with $p = 1/2$ [130, 131].

To rigorously define a scrambling time, and to claim whether the system does or does not scramble, one needs to make arguments for late time values of the OTOC. Due to the complicated nature of equation 1.31, rigorous universal results in finite time are rare. Despite this, some model dependent analytic results and many numerical results exist. For example, in the XY spin chain an inverse power law is known to hold [127, 129],

$$C(x, t) \sim \frac{1}{t^\alpha} + \gamma, \quad (1.36)$$

where $\alpha \geq 0$ and the exact value of α depends on the choices of spin operators and the anisotropy co-efficient while γ is the equilibrium value of the OTOC. Inverse power laws are also known to hold for interacting models in both ETH and localized phases, while exponential decay has been observed for Floquet systems [121, 122]. Much less is known on what conditions the OTOC actually goes to equilibrium, and how finite size effects might affect this process. The infinite time average is usually studied using $F(x, t)$ where a decay to zero would imply scrambling and returning to unity would mean an absence of scrambling. It has been shown that γ , the infinite time value of the OTOC, is generally non-zero for interacting models, localized models (neck-tie light-cone or the light-cone which spreads like $\log t$), or in free-models where non-local string operators are used [83, 106, 109, 120–122, 127–129, 142–146]. In the case of local operators in free models, $\gamma = 0$, thus no scrambling occurs [109, 127, 129].

$F(x, t)$ is argued using equation 1.21 to have a specific late time factorization, which is a strong criteria for genuine scrambling [120, 147], particularly at infinite temperature we have,

$$F(x, t \rightarrow \infty) = \lim_{T \rightarrow \infty} \int_0^T \frac{1}{T} \langle \hat{A}(t) \hat{B} \hat{A}(t) \hat{B} \rangle dt = \langle \hat{A}^2 \rangle \langle \hat{B} \rangle^2 + \langle \hat{A} \rangle^2 \langle \hat{B}^2 \rangle - \langle \hat{A} \rangle^2 \langle \hat{B} \rangle^2. \quad (1.37)$$

To arrive at equation 1.37 one needs to assume the strong ETH is true, making it a potential marker of chaotic Hamiltonians. Such a factorization does not appear to be possible using equation 1.22 (weak ETH), meaning late time values of the OTOC should be able to distinguish strong and weak ETH regimes. This is contrary to the time correlation functions of the form,

$$C(t) = \text{tr} \left(\rho \hat{A}(t) \hat{B} \right), \quad (1.38)$$

where the equation has a late time factorization theorem proved using only the weak ETH in [60], restated here for convenience.

Let H be a local, translation-invariant, non-degenerate Hamiltonian on a D -dimensional Euclidean lattice of N sites, and let $[\rho, H] = 0$ be an equilibrium ensemble (such as a thermal state) of finite correlation length $\xi > 0$. Let A, B be local observables with support on at most N^α sites, where α is fixed and such that $0 < \alpha < 1/(D + 1)$. Then,

$$\lim_{T \rightarrow \infty} \int_0^T C(t) \frac{dt}{T} = \text{tr}(\rho \hat{A}) \text{tr}(\rho \hat{B}) + \mathcal{O} \left(\xi^{\frac{2D}{D+1}} \log^2(N) N^{-\frac{2}{D+1}} \right). \quad (1.39)$$

Equation 1.39 shows a dissipation that is present in weak and strong ETH systems. This further suggests using the OTOC, which is equivalent to a four point correlator in time, is necessary to capture physics traditional dynamical correlation functions cannot. The OTOC is known to have an intimate relation with entanglement entropy, namely the second Rényi entropy [83]. Again consider a system split into two sub-systems A, B . The second Rényi entropy of the subsystem A is written as, $S_A^{(2)} = -\log \text{tr}(\rho_A^2)$. This entropy is then related to the OTOC by [83],

$$e^{-S_A^{(2)}} = \sum_{\hat{M}_i \in B} \langle \hat{M}_i(t) \hat{V} \hat{M}_i(t) \hat{V} \rangle_{\beta=0}, \quad (1.40)$$

such that the \hat{M}_i operators are a complete basis in the subspace B and $\hat{V} = \hat{O} \hat{O}^\dagger$ such that the initial state was quenched with \hat{O} . Equation 1.40 can be generalized to finite temperature and presents a deep connection between the function $F(x, t)$ and the entanglement entropy of the system.

Finally, the OTOC has also received attention from the experimental community as well. The primary difficulty for measuring such quantities is the need to reverse time. Recent proposals outline how one might probe the OTOC [148–151]. The OTOC has been recently experimentally realized on small quantum computers, directly probing scrambling [152, 153].

Equilibration, thermalization and scrambling appear to be intimately related, however their exact relation is unknown. As presented above, these fields are at their current stages still quite popular and new directions are appearing regularly. Now that we have put the field

into focus, the following chapters present three manuscripts as my contributions to these fields during my Master of Science project. Further introductions and background are presented in the manuscripts and my contributions are summarized at the beginning of each chapter.

Chapter 2

Out of Time Ordered Correlators and Entanglement Growth in the Random Field XX Spin Chain

In this chapter we present the article [109] which can be found published in Physical Review B with DOI:10.1103/PhysRevB.99.054205. The work can also be found on arXiv as arXiv:1810.00038. I am the primary author and contributor of this work. All numerics, plots and original equations present in the article are created by myself, with helpful guidance from my supervisor, Erik S. Sørensen.

In this article we investigate the OTOC in the random field XX spin chain which exhibits an extended (generalized ETH phase) and an Anderson localized phase. The Hamiltonian of the model is written as,

$$\hat{H} = J \sum_{i=0}^{L-2} (S_i^x S_{i+1}^x + S_i^y S_{i+1}^y) + \sum_{i=0}^{L-1} \lambda_i S_i^z, \quad (2.1)$$

where S_i^x, S_i^y and S_i^z are the spin-1/2 operators at site i , L is the number of sites. J is our coupling co-efficient and the onsite fields λ_i are generated randomly from a uniform distribution $[-\lambda, \lambda]$. With $\lambda > 0$ this model is an Anderson insulator and enters the AL phase [104, 154]. This model can be transformed into a free fermionic model with a Jordan Wigner transformation [155]. Using $S_i^\pm = (S_i^x \pm iS_i^y)/2$,

$$\begin{aligned} S_i^+ &= \prod_{j=1}^{i-1} (1 - 2\hat{f}_j^\dagger \hat{f}_j) \hat{f}_i^\dagger, & S_i^- &= \prod_{j=1}^{i-1} (1 - 2\hat{f}_j^\dagger \hat{f}_j) \hat{f}_i, \\ S_i^z &= \hat{f}_i^\dagger \hat{f}_i - \frac{1}{2}, \end{aligned} \quad (2.2)$$

which recovers,

$$\hat{H} = \frac{J}{2} \sum_{i=0}^{L-2} \left(\hat{f}_i^\dagger \hat{f}_{i+1} + \hat{f}_{i+1}^\dagger \hat{f}_i \right) + \sum_{j=0}^{L-1} \lambda_j \left(\hat{f}_j^\dagger \hat{f}_j - \frac{1}{2} \right), \quad (2.3)$$

which is a free fermionic Hamiltonian of the form given in equation 1.9. We study the OTOC with operators which are strictly local in the Jordan-Wigner transformation ,

$$C(x, t) = \langle [\hat{\sigma}_i^z(t), \hat{\sigma}_j^z]^\dagger [\hat{\sigma}_i^z(t), \hat{\sigma}_j^z] \rangle, \quad (2.4)$$

where $\hat{\sigma}_i^z = 2S_i^z$ are chosen because they are unitary.

The universal power law and wave-front form from equations 1.34 and 1.35 are investigated. We find the power law $l(x) = 2|x|$ for the model. We also find a discrepancy in the description of the wave-front, finding that at the wave-front moving at the maximal group velocity, the OTOC is better described by a Gaussian,

$$C(x, t) \sim e^{a(x, \lambda)t^2 + b(x, \lambda)}, \quad (2.5)$$

where $a(x, \lambda)$ is in general a negative and $b(x, \lambda)$ is positive. We also investigate the entanglement entropy in the AL phase and find slow entanglement growth for weak disorders.

Out-of-time ordered correlators and entanglement growth in the random-field XX spin chain

Jonathon Riddell* and Erik S. Sørensen†

Department of Physics & Astronomy, McMaster University 1280 Main St. W., Hamilton, Ontario, Canada L8S 4M1

 (Received 7 October 2018; revised manuscript received 20 December 2018; published 13 February 2019)

We study out-of-time ordered correlations $C(x, t)$ and entanglement growth in the random-field XX model with open boundary conditions using the exact Jordan-Wigner transformation to a fermionic Hamiltonian. For any nonzero strength of the random field, this model describes an Anderson insulator. Two scenarios are considered: a global quench with the initial state corresponding to a product state of the Néel form, and the behavior in a typical thermal state at $\beta = 1$. As a result of the presence of disorder, the information spreading as described by the out-of-time correlations stops beyond a typical length scale ξ_{OTOC} . For $|x| < \xi_{\text{OTOC}}$, information spreading occurs at the maximal velocity $v_{\text{max}} = J$ and we confirm predictions for the early-time behavior of $C(x, t) \sim t^{2|x|}$. For the case of the quench starting from the Néel product state, we also study the growth of the bipartite entanglement, focusing on the late- and infinite-time behavior. The approach to a bounded entanglement is observed to be slow for the disorder strengths we study.

DOI: [10.1103/PhysRevB.99.054205](https://doi.org/10.1103/PhysRevB.99.054205)

I. INTRODUCTION

A recent conjecture [1] establishing a bound for the rate of growth of chaos in quantum systems has spurred interest in the study correlators of the form [2]

$$C(x, t) = \langle [W(x, t), V(0)]^\dagger [W(x, t), V(0)] \rangle, \quad (1)$$

where W and V are local nonoverlapping operators separated by a displacement x , $[W(x, 0), V(0)] = 0$, and $\langle \cdot \rangle$ is a thermal average. If W, V are both Hermitian and unitary, it follows that

$$C(x, t) = 2(1 - \text{Re}[F(x, t)])$$

with $F(x, t) = \langle W(x, t)V(0)W(x, t)V(0) \rangle$ and F is therefore referred to as an out-of-time ordered correlator (OTOC). While W and V commute at $t = 0$, this may no longer be the case at a later time giving rise to the notion of a growing “operator radius” [3] defined as the distance $R_W(t)$, where $F(x, t)$ significantly deviates from 1 for all $|x| < R_W(t)$. $C(x, t)$ can then be seen as a measure of the degree of noncommutativity of $W(x, t)$ and $V(0)$ for $t > 0$, and if $C(x, t)$ remain large for an extended period of time the system is said to be scrambled. From a state perspective the function $F(x, t)$ describes the process of acting with the local operator V on the state, time evolving to some time t and acting on the state with W some displacement x away, and the overlap it has with the state where these operations are inverted. In a chaotic system, this overlap should decay in time to zero [4].

The time where $C(x, t)$ becomes $O(1)$ defines a “scrambling” time t_* , and for the early-time approach to scrambling it is expected that for some models $C(0, t) \sim e^{\lambda_L t}$ with the conjectured [1] bound $\lambda_L \leq 2\pi k_B T / \hbar$. Systems that approach this bound are known as fast scramblers [5–10]. This is in contrast to a range of models that do not exhibit this early-time exponential growth [3,4,11–15] and are

therefore known as slow scramblers. In particular, OTOCs in many-body localized systems [16,17] (MBL) have been studied [3,4,12–14,18–21] and early-time power-law growth of $C(x, t)$ is expected [3,4,12,14] in such systems. Distinguishing them from Anderson localized (AL) models where $C(x, t)$ is expected to be a constant [14], at least for very strong disorder. The behavior of the correlator $C(x, t)$ is therefore capable of distinguishing different phases.

More generally, if the spatial dependence is taken into account, $C(x, t)$ exhibits the butterfly effect [22–24] with certain models exhibiting the behavior $C \sim e^{\lambda_L(t-x/v_B)}$. Here, v_B is the butterfly velocity that can be viewed as the velocity of information in a strongly correlated systems. Perturbative weak coupling calculations [24,25] recover similar exponential behavior, whereas random circuit models [26–28] show a diffusively spreading $C \sim e^{-\lambda_L(x-v_B t)^2/t}$, and for noninteracting translationally invariant systems it can be shown that [19,20] $C \sim e^{-\lambda_L(x-v_B t)^{3/2}/t^{1/2}}$. A universal form has also been proposed [20]:

$$C(x, t) \sim \exp\left(-\lambda_L \frac{(x - v_B t)^{1+p}}{t^p}\right). \quad (2)$$

It should be noted that these different forms are only expected to be valid close to the “wave front,” where $x - v_B t$ is small. We also note that, in general, v_B can be different from v_E [29], the rate at which entanglement spreads, but for the models we shall consider here $v_B = v_E$ [30].

Recent studies [14,30] have also shown that $C(x, t)$ can be directly related to the second Rényi entropy $S^{(2)}$ of an appropriately defined subsystem, and scrambling in a quantum channel can be defined in terms of the tripartite information of a subsystem [30]. The quasiprobability behind the OTOC [31–33] has also been studied.

The closely related concept of the growth of entanglement after a quench has been intensely studied with the observation of a logarithmic growth with time [15,34–37] as one of the hallmark features of MBL. In contrast, a thermal phase should

*riddeljp@mcmaster.ca

†sorensen@mcmaster.ca

exhibit linear growth of the entanglement and in the AL phase a bounding constant entanglement is expected [14,38–42].

The relationship between scrambling, the OTOC, and thermalization has also been considered [43–45]. Models which can be mapped to a quasi-free-fermionic model with delocalizing dynamics have been studied showing that local two-point correlation functions equilibrate to a generalized Gibbs ensemble [46,47]. An interesting question is then as follows: What signatures of generalized thermalization appear in an OTOC? We address how our results contribute to this discussion in the Conclusion.

There are therefore many aspects that make the OTOC an object of considerable current interest, and exact numerical results are of significant interest in particular in the presence of disorder. Previous studies [14,18] have in particular focused on MBL systems where both disorder and interactions play an important role and severely limit the sizes that can be reached in numerical calculations. If interactions are neglected, the Jordan-Wigner transformation can be used to study OTOCs. In the absence of disorder, such studies have been performed on the quantum Ising chain [48], quadratic fermions [49], and hard-core boson models [50]. In [48] scrambling was observed at the critical point of the quantum Ising model in the OTOC for operators nonlocal in the Jordan-Wigner fermions.

Here, we turn the attention to the one-dimensional XX spin chain with a random field (RFX):

$$\hat{H} = J \sum_{i=0}^{L-2} (S_i^x S_{i+1}^x + S_i^y S_{i+1}^y) + \sum_{i=0}^{L-1} \lambda_i S_i^z, \quad (3)$$

where S_i^x , S_i^y , and S_i^z are the spin- $\frac{1}{2}$ operators at site i , L is the number of sites, J is the interaction coefficient, and the λ_i are the onsite fields applied to the z axis. The λ_i are taken uniformly from the interval $\lambda_i \in [-\lambda, \lambda]$ and we set $\hbar = 1$. We shall refer to λ as the disorder parameter and we shall mainly be concerned with the weak disorder regime $\lambda < J$. This model describes a typical Anderson insulator and is in the AL phase for any nonzero λ . This model is known to be dynamically localized [51] in the sense that it satisfies a zero-velocity Lieb-Robinson bound. Furthermore, entanglement is bounded at all times for this model [38]. However, relatively little is known about the early-time behavior in the model which is the focus of this paper. As we detail below, the Jordan-Wigner transformation is applicable to the random-field XX spin chain also in the presence of disorder and sizable systems can be treated. To simplify the calculation, we exclusively consider open boundary conditions (OBC). We focus on two different scenarios: a quench from a simple Néel-type product state with no entanglement of the following form:

$$|\psi\rangle = \prod_{l \in \mathbb{S}} \hat{S}_l^+ |\downarrow\rangle, \quad (4)$$

where $\mathbb{S} = \{l \in \mathbb{N} : l \bmod 2 = 0\}$. The second scenario corresponds to a typical thermal state

$$\rho = \frac{e^{-\beta \hat{H}}}{Z} \quad (5)$$

with $\beta = 1$ and $Z = \text{tr} \exp(-\beta \hat{H})$. Expectation values for the two scenarios are then determined as

$$\langle O \rangle_{\text{Néel}} = \langle \psi | O | \psi \rangle \quad \text{and} \quad \langle O \rangle_{th} = \text{tr}(\rho O). \quad (6)$$

Our principal findings are the following. The propagation of the OTOCs essentially stops beyond a length ξ_{OTOC} that depends on the strength of the disorder λ . For $|x| > \xi_{\text{OTOC}}$ $C(x, t)$ is essentially a constant, $C(x, t)$ in agreement with previous studies [14] performed at strong disorder and very small ξ_{OTOC} . However, for $|x| < \xi_{\text{OTOC}}$ the OTOC propagates information with the *maximal* group velocity $v_{\text{max}} = J$ in the thermodynamic limit. This is the case for both the product and thermal state. For modest λ , ξ_{OTOC} can be sizable. For $|x| < \xi_{\text{OTOC}}$, the early-time regime of $C(x, t)$ is shown to behave as $t^{2|x|}$ in accordance with a recent proposal [48], even in the presence of disorder, $\lambda \neq 0$. For $\lambda \neq 0$, the light cone therefore has the shape of a necktie with a v-shaped tip. While the bipartite entanglement in the RFX model is bounded at all times [38] we find that the approach to this bound at small λ is rather slow.

The plan of the paper is as follows. In Sec. II we outline some technical aspects of applying the Jordan-Wigner transformation. Section III presents our results for the OTOCs for the two different scenarios detailed above and in Sec. IV discuss our results for the evolution of the entanglement after a quench from the Néel product state. Finally, in Sec. V we attempt to extract a localization length from the bipartite entanglement entropy.

II. JORDAN-WIGNER TRANSFORMATION

In order to study the model (3), we employ the Jordan-Wigner transformation [52]. Using $S_i^\pm = (S_i^x \pm iS_i^y)/2$,

$$S_i^+ = \prod_{j=1}^{i-1} (1 - 2\hat{f}_j^\dagger \hat{f}_j) \hat{f}_i^\dagger, \quad S_i^- = \prod_{j=1}^{i-1} (1 - 2\hat{f}_j^\dagger \hat{f}_j) \hat{f}_i, \\ S_i^z = \hat{f}_i^\dagger \hat{f}_i - \frac{1}{2}, \quad (7)$$

we recover a Hamiltonian

$$\hat{H} = \frac{J}{2} \sum_{i=0}^{L-2} (\hat{f}_i^\dagger \hat{f}_{i+1} + \hat{f}_{i+1}^\dagger \hat{f}_i) + \sum_{j=0}^{L-1} \lambda_j \left(\hat{f}_j^\dagger \hat{f}_j - \frac{1}{2} \right), \quad (8)$$

which is a quasi-free-fermionic Hamiltonian with anticommutation relations $\{\hat{f}_k, \hat{f}_l\} = \{\hat{f}_k^\dagger, \hat{f}_l^\dagger\} = 0$ and $\{\hat{f}_i^\dagger, \hat{f}_k\} = \delta_{l,k}$. We adjust the spectrum to get rid of the constant term and write

$$\hat{H} = \sum_{i,j} M_{i,j} \hat{f}_i^\dagger \hat{f}_j, \quad (9)$$

where M is the effective Hamiltonian with entries $M_{i,i} = \lambda_i$ and $M_{i,j} = \frac{J}{2}$ if $|i - j| = 1$. All other entries are zero. This model can be used to study differences between a thermal phase, with no disorder $\lambda = 0$, and the localized phase with $\lambda \neq 0$. When $\lambda = 0$ and we restrict ourselves to the case of $\langle \hat{N} \rangle = \sum_i^L \langle \hat{f}_i^\dagger \hat{f}_i \rangle = \frac{L}{2}$ a regime where the eigenstates of this model typically look locally identical to the Gibbs state [53,54]. However when $\lambda > 0$ the eigenstates are localized and have exponentially decaying correlations characterized by some localization length [38,55,56].

Since M is real symmetric, for a given field realization we can always diagonalize $M = ADA^T$ where $AA^T = \mathbb{I}$ and D is a diagonal matrix with entries $D_{k,k} = \epsilon_k$. Defining new fermionic operators

$$\hat{d}_k = \sum_j A_{j,k} \hat{f}_j, \quad (10)$$

$$\hat{d}_k^\dagger = \sum_j A_{j,k} \hat{f}_j^\dagger, \quad (11)$$

we can then write the Hamiltonian as

$$\hat{H} = \sum_k \epsilon_k \hat{d}_k^\dagger \hat{d}_k, \quad (12)$$

where the ϵ_k are the eigenmodes. A simple reorganization and applications of Wick's theorem when appropriate allows us to express out-of-time ordered correlators in terms of two-point correlations. More details on evaluating the time evolution of this model are presented in Appendix A.

The problem of locality should be addressed. The Jordan-Wigner transformation does not completely conserve locality, the j th pair of fermionic operators are built from the $1, \dots, j$ site spin operators, making it quasilocal. However, the \hat{S}_i^z spin operators are mapped locally to fermions, so we use these operators in the OTOC. Similarly, for the entanglement entropy we consider subregions $A = \{1, \dots, |A|\}$ which are blocks of spin sites preserved by the transformation. We have not considered OTOCs that are not local in the fermion representation as was considered for the quantum Ising model in Ref. [48].

In the following, we mainly focus on the disorder strength $\lambda = 0, 0.3, 0.8$ and we always fix $J = 1$ and $\hbar = 1$. We exclusively consider open boundary conditions. For the results presented in the following sections, we typically use a system size of $L = 400$ and, unless otherwise noted, 1000 disorder realizations of the Hamiltonian are considered and averaged over. We use a simple average to extract mean values over the disorder, leaving a study of the complete distribution over the disorder for further study. When presenting results for several time slices of $C(x, t)$, each value of $C(x, t)$ is shifted vertically by a value of $0.25t$ for visualization purposes.

III. OUT-OF-TIME ORDERED CORRELATIONS

In this section we investigate the out-of-time ordered correlations of the form

$$C(x, t) = \langle [\hat{\sigma}_i^z(t), \hat{\sigma}_j^z]^\dagger [\hat{\sigma}_i^z(t), \hat{\sigma}_j^z] \rangle, \quad (13)$$

where $x = i - j$ is understood to be the displacement between sites i and j . Since $\hat{\sigma}_i^z$ is unitary, we may write

$$C(x, t) = 2(1 - \text{Re}[F(x, t)]). \quad (14)$$

We note that with this definition of $C(x, t)$ the maximum value it can reach is 2. Here,

$$F(x, t) = \langle \hat{\sigma}_i^z(t) \hat{\sigma}_j^z \hat{\sigma}_i^z(t) \hat{\sigma}_j^z \rangle. \quad (15)$$

We will fix the position of the time-evolved operator as $i = \frac{L}{2}$. Varying j allows us to observe the operator radius spreading over the lattice. As described above, we consider

two scenarios: a product state generated by a set of creation operators where $\mathbb{S} = \{l \in \mathbb{N} : l \bmod 2 = 0\}$,

$$|\psi\rangle = \prod_{l \in \mathbb{S}} \hat{S}_l^+ |\downarrow\rangle = \prod_{l \in \mathbb{S}} \hat{f}_l^\dagger |0\rangle, \quad (16)$$

where $|\downarrow\rangle$ and $|0\rangle$ are the all spin down and the vacuum state, respectively. This state is a classical Néel state which has the advantage of yielding essentially symmetric initial conditions for spins surrounding the middle lattice point $i = \frac{L}{2}$, allowing us to restrict our studies to one directional displacement on the lattice and having initial fermions distributed evenly in real space. For the second scenario of a thermal state, we construct the Gibbs state with an inverse temperature $\beta = 1$. More details on how these initial conditions are handled and how $C(x, t)$ is calculated can be found in Appendix B.

Before a more detailed discussion of our results for the two different scenarios, we discuss general features of the results for the OTOC and compare the two scenarios in Fig. 1 (solid lines represent results for the product state, dashed lines for the thermal state). Here, Fig. 1(a) show results $C(x, t = 64)$ at a fixed time $t = 64$ versus x . For both the thermal and product states the effects of the disorder are immediately noticeable in the smoothening of $C(x, t)$ that is characteristically oscillating with x in the absence of disorder. For $\lambda \neq 0$, $C(x, t)$ is sharply peaked around $x = 0$ and a clear signature of a wave front where $C(x, t)$ first becomes nonzero is starting to disappear for $\lambda = 0.8$ for this time slice. Figure 1(b) show results for $C(x = 7, t)$ at a fixed separation $x = 7$ versus time. Clear differences between the results for the thermal state and the product state are visible. Most notably, additional structures appear in the peaks of $C(x = 7, t)$ for the product state while the thermal state yields a much smoother oscillation. The long-time behavior of $C(x = 7, t)$ is shown in Fig. 1(c). While $C(x = 7, t)$ clearly goes to zero for $\lambda = 0$ for both scenarios, indicating absence of scrambling, it appears plausible that it attains a finite value in the long-time limit for $\lambda = 0.3, 0.8$ for both scenarios. Since $C(x = 7, t)$ does not saturate for $x = 7$ one could consider this weak (partial) scrambling for $\lambda = 0.3, 0.8$. We note that there is a rather large variation in $C(x = x_0, t)$ with x_0 and as we discuss below $C(|x| > \xi_{\text{OTOC}}, t)$ is essentially zero for *all* t when $\lambda \neq 0$ indicating the absence of scrambling beyond this length scale.

We now turn to a more specific discussion of our results for the Néel product state and thermal state.

A. Product states

In Fig. 2 we show different time slices of $C(x, t)$ versus x . This shell-like structure is expected and parallels the results seen in Ref. [48] for the quantum Ising chain when constructing the OTOC with two operators which are local in the fermionic representation. However, key differences emerge when disorder is introduced by increasing λ . When $\lambda = 0$, we are in a thermal phase and we observe operator spreading over the lattice in the sense that $C(x, t)$ eventually becomes nonzero for any x for large enough t . The operator spreads over the lattice at the maximal group velocity $v_{\text{max}} = J$ as expected. For an individual x , the $C(x, t)$ grows initially in time, peaks, and returns to zero with some rebounding with weaker peaks [see Figs. 1(b) and 1(c)]. Thus, $\lambda = 0$ does not

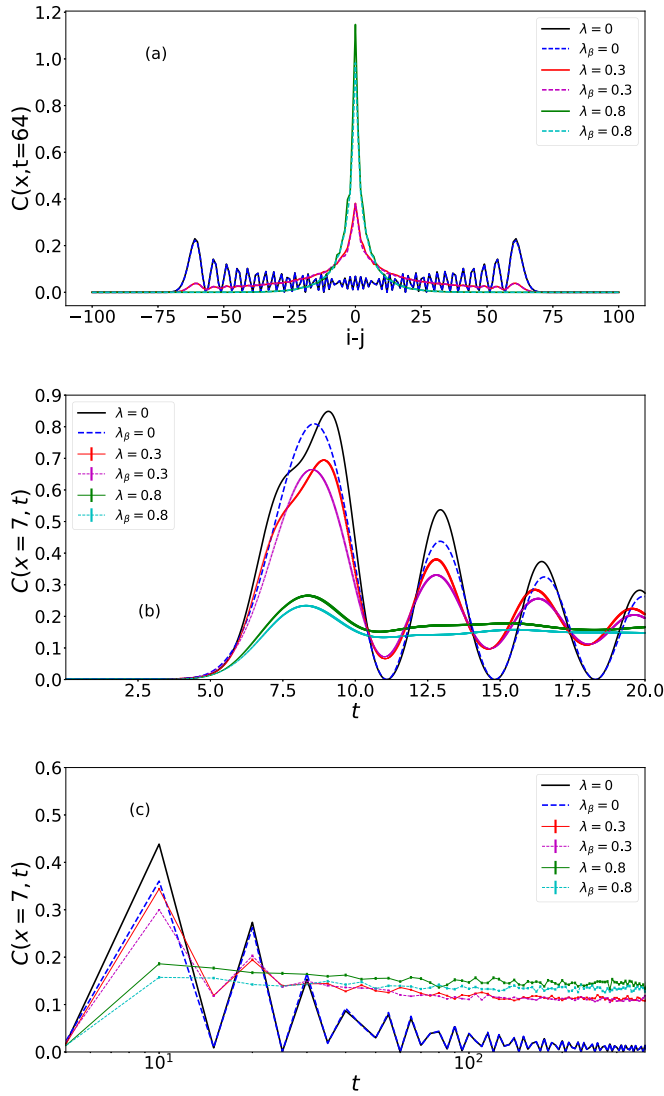


FIG. 1. Results for $C(x, t)$ for three different disorder strengths $\lambda = 0, 0.3, 0.8$. Comparing the product state and thermal state. The labeling λ_β refers to $C(x, t)$ calculated in the thermal state with the specified disorder strength. Solid lines are results for the product state, dashed lines refer to the thermal state at $\beta = 1$. (a) $C(x, t = 64)$ versus x for a fixed $t = 64$, shown as green line in Figs. 2 and 5. (b) Early-time behavior of $C(x = 7, t)$ at $x = 7$, shown as the solid red line in Figs. 2 and 5. (c) Late-time behavior of $C(x = 7, t)$.

scramble. For $\lambda = 0.3$ and 0.8 we observe operator spreading at the *maximal* group velocity for $|x| < \xi_{\text{OTOC}}$ [where ξ_{OTOC} characterizes a length sufficiently large compared to the localization length such that the commutation relation bound is sufficiently small as seen in Eq. (17)]. However, for values of $|x| > \xi_{\text{OTOC}}$, $C(x, t) = 0$ for all times. ξ_{OTOC} is shown in Figs. 2(b) and 2(c) as the dashed vertical red lines and indicated the length scale beyond which $C(x, t) < 10^{-3}$ for all times. Hence, the operator radius is bounded by ξ_{OTOC} and does not spread into regions beyond ξ_{OTOC} . As expected, ξ_{OTOC} shrinks with increasing λ , as seen in Figs. 2(b) and 2(c). For $|x| < \xi_{\text{OTOC}}$, $C(x, t)$ initially grows with t until it peaks and then decreases to weakly oscillate around a nonzero value, and never returns to zero. This is a fundamentally

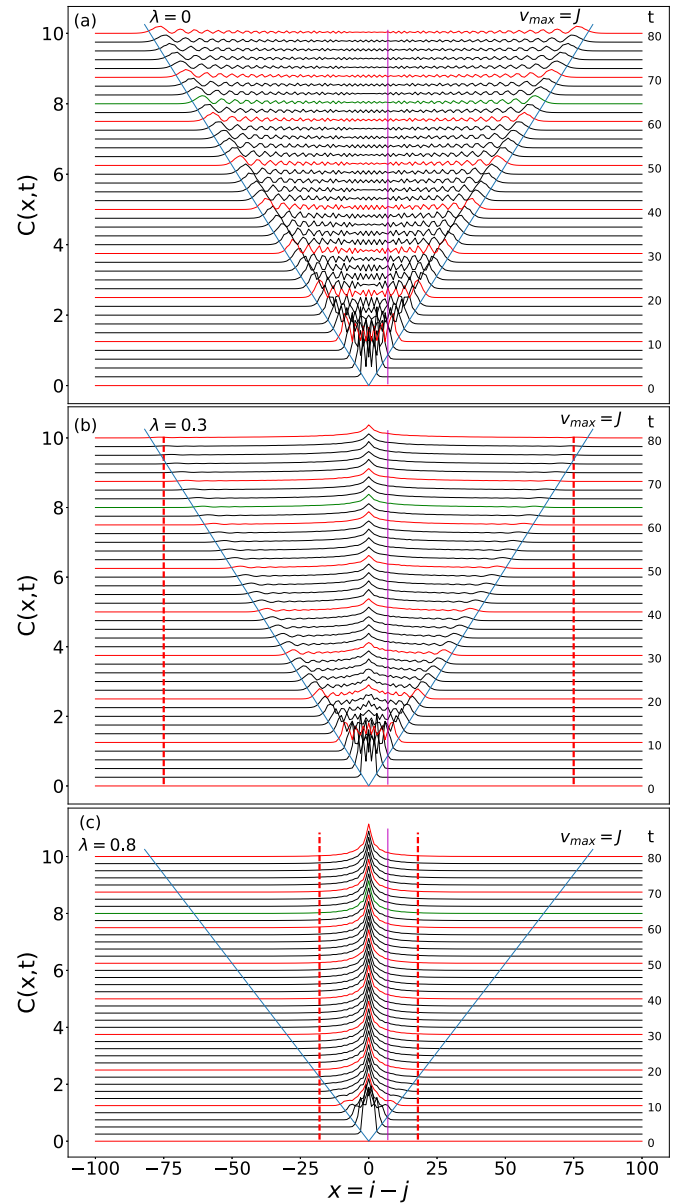


FIG. 2. Wave propagation plot of $C(x, t)$ for the XX spin model at disorder strength (a) $\lambda = 0$, (b) $\lambda = 0.3$, and (c) $\lambda = 0.8$. For visualization, each value of $C(x, t)$ is shifted vertically by a value of $0.25t$, demonstrating the operators radius spreading. The x axis is the displacement from the center of the chain $i = \frac{L}{2}$. The two y axes are the values $C(x, t)$ and the corresponding time. The maximal group velocity $v_{\text{max}} = J$ is also shown (solid blue line). In (b) and (c), the vertical dashed red line indicates ξ_{OTOC} , the x value beyond which $C(x, t) < 10^{-3}$ for any x . $\xi_{\text{OTOC}} = 18$ for $\lambda = 0.8$ and 75 for $\lambda = 0.3$.

different behavior than the no-disorder case. This long-time limit of $C(x, t)$ for $|x| < \xi_{\text{OTOC}}$ increases weakly with λ while it decreases with x . The light cone has therefore the shape of a necktie with a v-shaped tip. This behavior is markedly different from results in MBL systems where a much different logarithmic light cone has been observed [15, 18, 21].

In Refs. [12, 51] it has been noted that the Anderson localized states do exhibit a nonexpanding light cone with the

commutator between two operators being bounded in time by

$$|[A(0, 0), B(x, t)]| \leq C e^{-\frac{|x|}{\xi}}, \quad (17)$$

where $A(0, 0)$ and $B(x, t)$ are operators with local support and x is the displacement in-between them. This result implies that $C(x, t)$ should have the same exponential behavior and we have verified that the results in Fig. 1(a) for $\lambda = 0.8$ and for $|x| < 8$ are well described by

$$C(x, t = 64) \sim e^{-a|x|}, \quad (18)$$

with $a \sim 0.33$. In Ref. [48] it was proposed that a universal power law applies to all lattice systems where the Hamiltonian is constructed from local interactions. For the quantum Ising model this was shown to be [48] $C(x, t) \sim t^{2(2x-1)}$. This is seen by considering the Hadamard formula, and an operator \hat{A} (see Ref. [57], Lemma 5.3):

$$e^{s\hat{H}}\hat{A}e^{-s\hat{H}} = \hat{A} + s[\hat{H}, \hat{A}] + \frac{s^2}{2!}[\hat{H}, [\hat{H}, \hat{A}]] \dots = \sum_{n=0}^{\infty} \frac{s^n}{n!} L_n. \quad (19)$$

For the RFXX spin chain considered here we arrive at a slightly modified power law by repeating the argument of Ref. [48]. This is done by considering $\hat{A} = \hat{\sigma}_{\frac{x}{2}}^z$ and $s = it$ and determining the smallest n of the above sum, such that $[L_n, \sigma_{j=x}^z] \neq 0$. This corresponds to successively evaluating the commutator between the Hamiltonian and the string of operators that grows until it reaches $j = x$. The strings which appear at the smallest order of t for odd n look like (shifting the indexes for simplicity) $\hat{\sigma}_0^x \hat{\sigma}_1^z \hat{\sigma}_2^z \dots \hat{\sigma}_{x-1}^z \hat{\sigma}_x^y$ and $\hat{\sigma}_0^y \hat{\sigma}_1^z \hat{\sigma}_2^z \dots \hat{\sigma}_{x-1}^z \hat{\sigma}_j^x$, while for n even, $\hat{\sigma}_0^x \hat{\sigma}_1^z \hat{\sigma}_2^z \dots \hat{\sigma}_{x-1}^z \hat{\sigma}_x^x$ and $\hat{\sigma}_0^y \hat{\sigma}_1^z \hat{\sigma}_2^z \dots \hat{\sigma}_{x-1}^z \hat{\sigma}_{j=x}^y$, yielding $n = j = x$. At least for regions inside the light cone we expect this behavior to be independent of λ . With $C(x, t)$ the square of the commutator, we then find for the RFXX model at early times

$$C(x, t) \sim t^{2|x|}, \quad (20)$$

with a power law that is independent of λ and is therefore *not* modified by the presence of disorder. This is purely a quantum mechanical phenomenon occurring before the wave front hits and is not a signature of scrambling. This phenomenon is captured in Fig. 3 where results are shown for $\lambda = 0$ [Fig. 3(a)], $\lambda = 0.3$ [Fig. 3(b)], and $\lambda = 0.8$ [Fig. 3(c)] where results are shown for a range of values of x confirming the above power-law dependence. For $|x| = 2, 4$ we include the next leading term in the fits: $t^{2(|x|+1)}$. The power-law growth in this model is thus universal for $\lambda = 0$ as well as in the the localized phase ($\lambda \neq 0$), assuming we are inside the light cone. Interestingly, outside of the light cone, despite the derivation for the power law being independent of λ , the power law breaks down, signifying localization suppressing quantum effects as well. Precisely, how localization effects will start to dominate is not clear, although the clear presence of correction terms for $|x| < \xi_{\text{OTOC}}$ is an indication that such corrections eventually become dominant.

Finally, we study the behavior of $C(x, t)$ at the wave front which moves at a velocity $v_{\text{max}} = J = 1$. Here, we use (following Ref. [48]) the function

$$G(x, t) = \frac{\partial \ln C(x, t)}{\partial t} = \frac{1}{C(x, t)} \frac{\partial C(x, t)}{\partial t}. \quad (21)$$

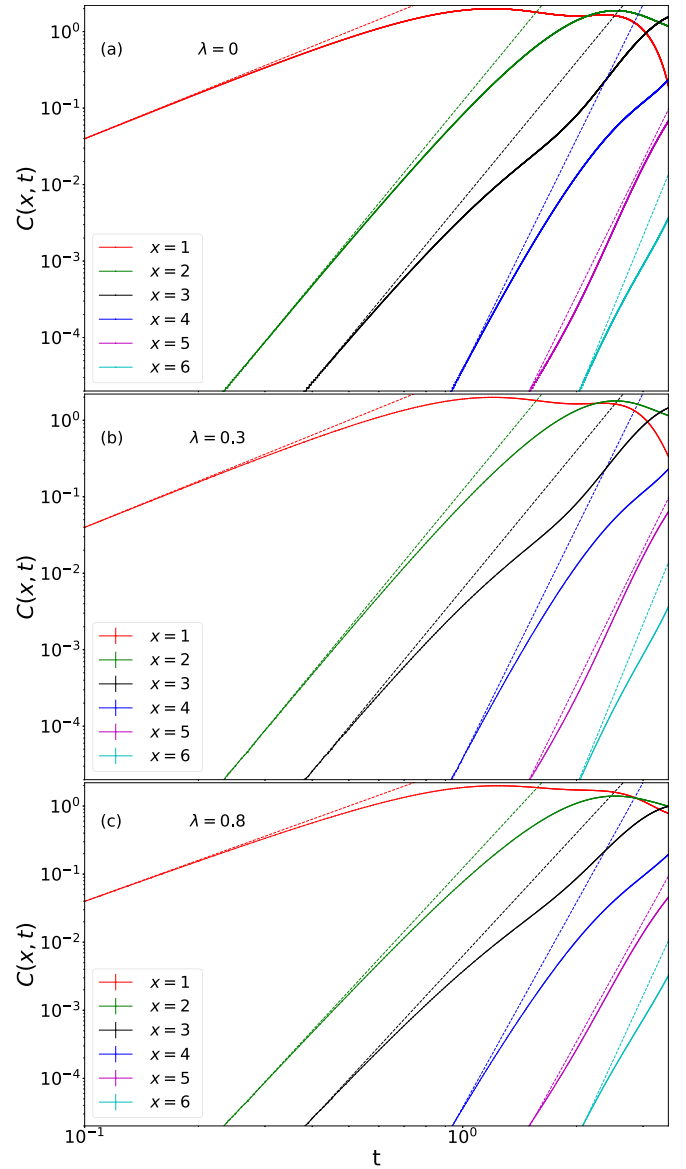


FIG. 3. Early time $C(x, t)$ at different values of x for each studied λ . The dotted lines for $x = 1, 3, 5, 6$ are the power laws $t^{2|x|}$ with appropriate constants in front while the solid lines are the actual data. For $x = 2, 4$ the next leading order power $t^{2(|x|+1)}$ is required to fit the data for every value of λ .

Since we know the expression for $C(x, t)$ exactly $G(x, t)$ can be calculated without resorting to evaluating the derivatives numerically. Our results for this function are plotted in Fig. 4. The wave front hits when $t - \frac{x}{J} = 0$, and we again see the initial purely quantum mechanical growth of $C(x, t)$ before the front hits. After the wave front hits $G(x, t)$ in all cases becomes negative after a short time, and then an oscillatory behavior about 0 is observed. For $\lambda = 0$, the repeating pattern appears to have a discontinuous change when going from negative to positive values of $G(x, t)$, however, this is most likely an artifact of $G(x, t)$ returning to zero and bouncing back upward as seen in Fig. 2. Because this behavior is observed for extremely large values of t and large accessible system sizes, we cannot conclude exactly how $C(x, t)$ goes

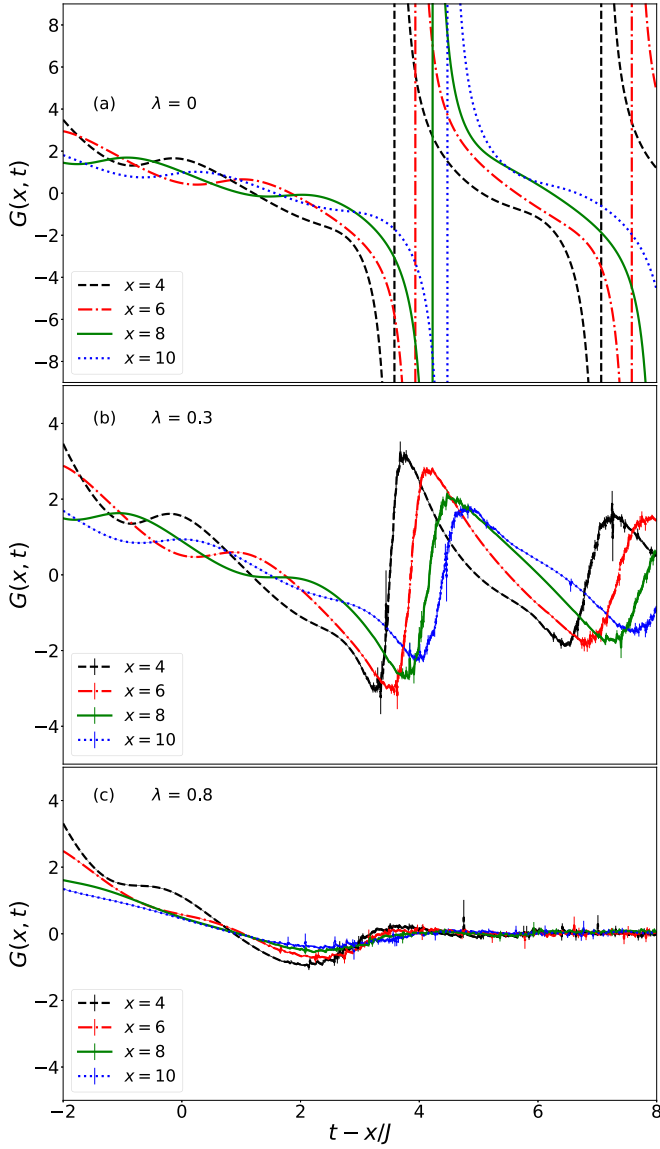


FIG. 4. $G(x, t)$ graphed against $t - \frac{x}{J}$. This simulation required 5000 realizations of the random Hamiltonian to get reasonable error bars. All averages were taken over the function $G(x, t)$ itself.

to zero as $t \rightarrow \infty$ for $\lambda = 0$. For $\lambda \neq 0$ the behavior is different since $C(x, t)$ does not go back to zero, but instead oscillates around a nonzero value. However, we see that as λ is increased, $G(x, t)$ varies much less rapidly. Both $\lambda = 0.3$ and 0.8 show oscillatory behavior in $G(x, t)$ after the wave front reaches but the amplitudes are suppressed with larger λ . Interestingly, we do not observe monotonic behavior on any meaningful interval.

B. Thermal states

Next, we repeat these calculations, but with a thermal state with $\beta = 1$ instead of the product state considered in the previous section. $\beta = 1$ is an arbitrary choice because the dynamics will overall depend primarily on the anticommutator in time (which is β independent), for both disorder and nondisorder. Hence, the variation with β is relatively minor,

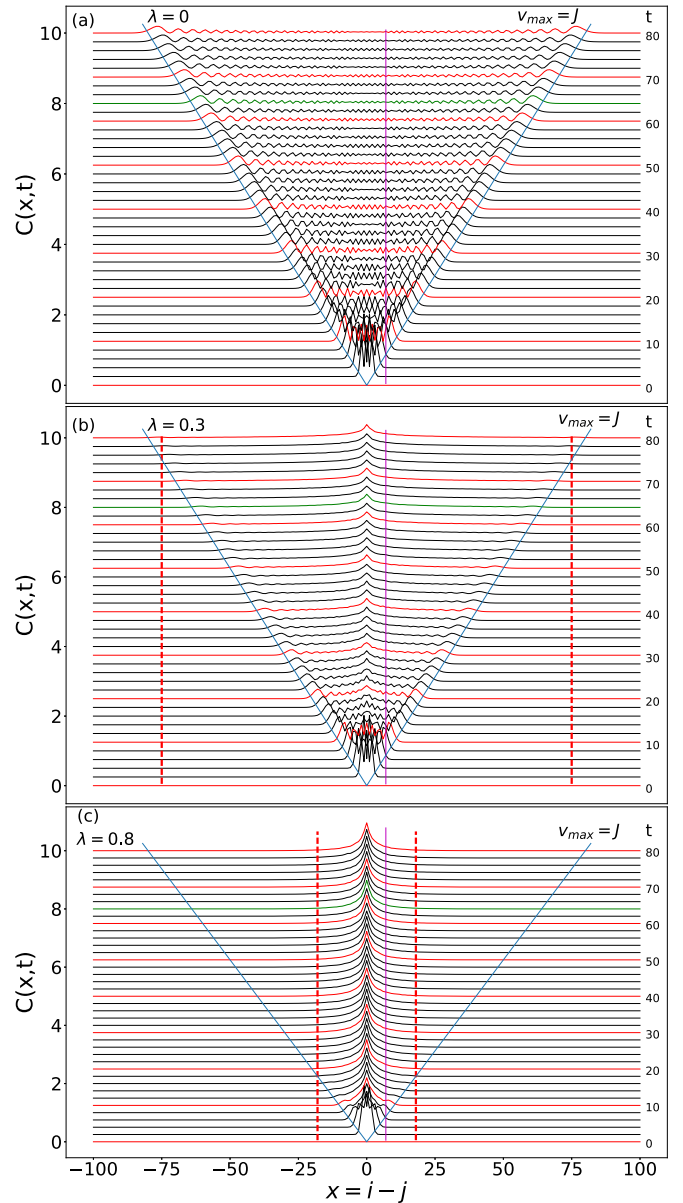


FIG. 5. Wave propagation plot of $C(x, t)$ for the RFX spin chain at disorder strength (a) $\lambda = 0$, (b) $\lambda = 0.3$, and (c) $\lambda = 0.8$ in a thermal state with $\beta = 1$. The x axis is the displacement from the center of the chain $i = \frac{L}{2}$ symmetry about the position i the wave propagates symmetrically. The two y axes are the values $C(x, t)$ and the corresponding time. The maximal group velocity $v_{\max} = J$ is also shown as the solid blue line. In (b) and (c) the vertical dashed red line indicates ξ_{OTOC} , the x value beyond which $C(x, t) < 10^{-3}$ for any x . $\xi_{\text{OTOC}} = 18$ for $\lambda = 0.8$ and 75 for $\lambda = 0.3$.

in particular in the presence of disorder. This state is already in equilibrium and exhibits a significantly different expression for $C(x, t)$ as detailed in Eq. (B8). In Fig. 5 we show $C(x, t)$ at different time slices. Although this plot looks similar to the product state version, Fig. 2, differences emerge. First, the peaks of the $C(x, t)$ are smaller than was the case for the product state, and the $C(x, t)$ is much smoother as seen in Fig. 1, traveling simply as a smooth parabolalike curve in space. However, the oscillatory behavior occurs also in

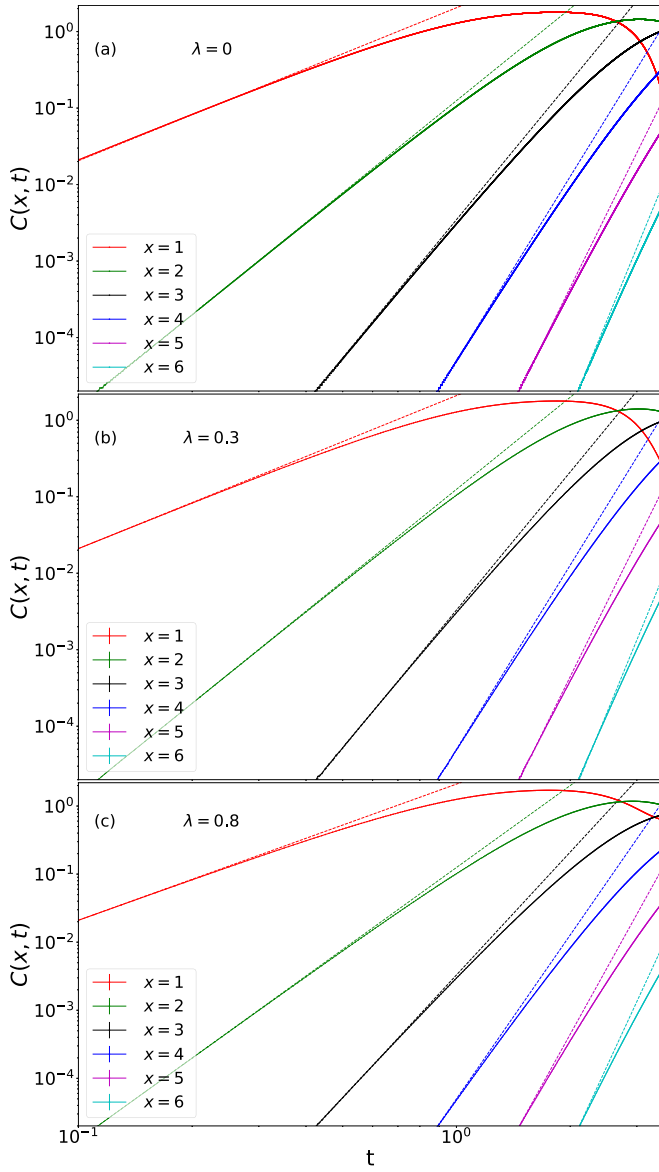


FIG. 6. Early-time $C(x, t)$ thermal correlations at different values of x for $\lambda = 0, 0.3, 0.8$. The dotted lines for $x = 1, 2, 3, 4, 5, 6$ are the power laws $t^{2|x|}$ with appropriate constants in front while the solid lines are the actual data.

this case, and we again do not expect to be able to find a description for how $C(x, t)$ approaches zero in late time. For this value of $\beta = 1$ we find the same values for ξ_{OTOC} as was determined for the Néel product state.

We also see in Fig. 6 that the thermal states obey the power law discussed in Eq. (20). For the thermal state the agreement with the power-law behavior is better than for the product state and no higher-order terms are included in the fits shown in Fig. 6. This is most likely due to the absence of noise, which indicates modeling the wave front will be easier with this initial condition.

Finally, in Fig. 7, we show the wave front as described by $G(x, t)$ evaluated using the thermal state with $\beta = 1$. Unlike the product state we observe monotonic behavior for the approximate region $t - \frac{x}{J} \in [-2, 2]$ and we observe strong

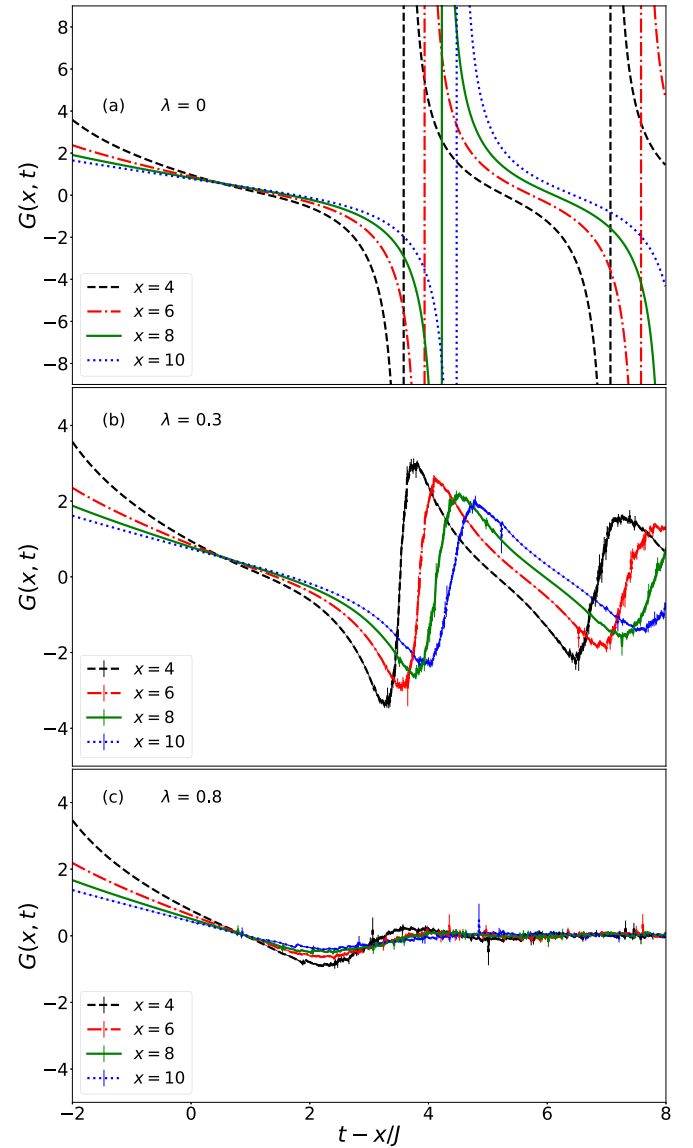


FIG. 7. $G(x, t)$ as a function of $t - \frac{x}{J}$ calculated in the thermal state with $\beta = 1$. This simulation required 5000 realizations of the random Hamiltonian to get reasonable error bars.

x and λ dependence. Once again, the $\lambda = 0$ diverges when $C(x, t)$ goes to zero, and the $\lambda \neq 0$ cases do not exhibit this behavior due to $C(x, t)$ never returning to zero. Similarly, we observe oscillatory behavior after the wave front passes. At the wave front which we define as $t - \frac{x}{J} \in [0, 2]$ we can effectively approximate $G(x, t)$ by a linear equation $G(x, t) \approx m(t - x/J) + c = at + b$, due to the shapes of the functions we expect $a = a(x, \lambda)$ and $b = b(x, \lambda)$. Interestingly, this form suggests that at the wave front

$$C(x, t) \sim e^{\frac{a(x, \lambda)t^2}{2} + b(x, \lambda)t}. \quad (22)$$

To follow the universal form of Eq. (2) one must have

$$G(x, t) \sim \frac{\lambda_L}{t^{p+1}} (x - v_B t)^p (v_B t + px). \quad (23)$$

However, the form of Eq. (23) does not permit a linear equation. Thus, we conclude that our results in Eq. (22) do

TABLE I. Results of fitting the function $G(x, t) \approx m(t - x/J) + c = at + b$ where on the interval $t - \frac{x}{J} \in [0, 2]$ for different values of λ and x . The errors reported are one standard deviation on the parameter.

$\lambda = 0$	m	c
$x = 2$	-0.72948875 ± 0.002	0.94258389 ± 0.002
$x = 4$	-0.59368064 ± 0.001	0.88059725 ± 0.001
$x = 6$	-0.5040499 ± 0.0009	0.82791869 ± 0.001
$x = 10$	-0.44021805 ± 0.0008	0.78445194 ± 0.0009
$\lambda = 0.3$	m	c
$x = 2$	-0.73975833 ± 0.002	0.92284197 ± 0.002
$x = 4$	-0.60431888 ± 0.001	0.85326093 ± 0.001
$x = 6$	-0.51342755 ± 0.001	0.7949133 ± 0.001
$x = 10$	-0.44742463 ± 0.0009	0.74793077 ± 0.001
$\lambda = 0.8$	m	c
$x = 2$	-0.81713901 ± 0.002	0.74741784 ± 0.003
$x = 4$	-0.63429921 ± 0.002	0.60081936 ± 0.003
$x = 6$	-0.52336579 ± 0.003	0.4942889 ± 0.003
$x = 10$	-0.40722873 ± 0.003	0.40339502 ± 0.004

not follow the proposed universal form (2). We currently do not know an exact expression for $a(x, \lambda)$ and $b(x, \lambda)$, however, for completeness we provide a table of the fitted values in Table I. The values for $a = m$ are necessarily negative and c positive. The errors reported are one standard derivation. The small errors indicate that the form given in Eq. (22) is a reasonable description.

IV. BIPARTITE ENTANGLEMENT ENTROPY

We now turn to a discussion of the growth of entanglement in the RFXX starting from the Néel product state which, due to its product form, has zero entanglement. The entanglement entropy between two subsystems A, B is defined with the reduced density matrices $\rho_A = \text{tr}_B \rho$ and $\rho_B = \text{tr}_A \rho$,

$$S_{A,B} = -\text{tr}(\rho_A \ln \rho_A) = -\text{tr}(\rho_B \ln \rho_B), \quad (24)$$

where the equality is taken because regardless of the partition ρ_A and ρ_B have identical nonzero eigenvalues [58]. For the remainder of this section we partition the lattice into halves and denote this quantity as $S_{\frac{L}{2}}$.

Rigorous bounds for the entanglement entropy in the RFXX model in the Anderson localized phase have been derived and it is expected to obey an area law in one dimension [38,55,59]. In particular, it has been shown that the growth of entanglement remains bounded for all times [38]. This means entanglement entropy even for arbitrarily small disorder strengths will be bounded by a constant in the late-time limit. The approach to this limiting value is relatively less explored and that is our focus here. Exact diagonalization results on small systems have been discussed in Ref. [34] where for relatively strong disorder the entanglement entropy reached a constant at very short times.

In order to study the time-dependent entanglement, we time evolve our state, Eq. (16), and calculate the entanglement entropy at late times. We expect that at sufficiently large system sizes we will not observe an increase in entanglement entropy as the system grows since we will be

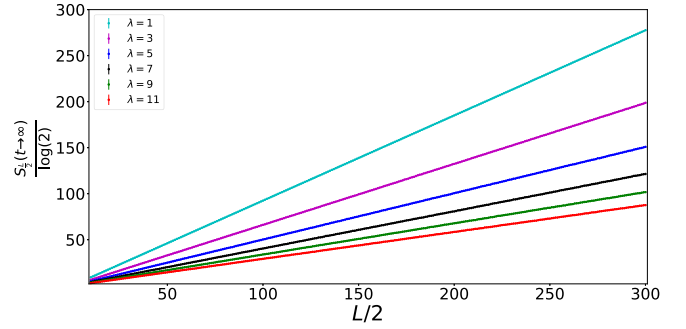


FIG. 8. Infinite-time average $S_{\frac{L}{2}}$ plotted against system size. Each point is an average over 5000 random-field realizations and the error shown is the standard error on the calculated mean. System sizes are taken from $L = 20$ to 600. For these results the approximation yielding the infinite-time average is *not* valid and the resulting volume law is *incorrect*.

close to the theoretical maximum. In Ref. [34] the authors did a similar calculation for both Anderson and many-body localized phases. However, comparing many-body localized systems to Anderson localized systems restricts the system sizes; here we do not have this restriction, focusing entirely on the Anderson localization regime. Using the method in [60] we can efficiently calculate the entanglement entropy from the occupation matrix defined in Eq. (A12). Since we are interested in late-time entanglement entropy, it is tempting to consider the infinite-time average of the occupation matrix. That is, for each element, we define (similar to [61])

$$\begin{aligned} \Lambda^f(\infty)_{i,j} &:= \lim_{T \rightarrow \infty} \int_0^T dt \frac{1}{T} \langle \hat{f}_i^\dagger(t) \hat{f}_j(t) \rangle \\ &= \lim_{T \rightarrow \infty} \int_0^T dt \frac{1}{T} \sum_{k,l} e^{i(\epsilon_k - \epsilon_l)t} A_{i,k} A_{j,l} \langle \hat{a}_k^\dagger \hat{a}_l \rangle \\ &= \sum_k A_{i,k} A_{j,k} \langle \hat{a}_k^\dagger \hat{a}_k \rangle, \end{aligned} \quad (25)$$

which amounts to a “dephasing” of the off-diagonal contributions. Note that we used the fact that the ϵ_k are expected to be nondegenerate [56]. The infinite-time average occupation matrix corresponds to a generalized Gibbs ensemble

$$\rho = \frac{1}{Z} e^{-\sum_k \beta_k \hat{Q}_k}, \quad (26)$$

where $\hat{Q}_k = \hat{a}_k^\dagger \hat{a}_k$.

However in Fig. 8 we see that the infinite-time average occupation matrix predicts volume laws despite large disorder; the disorder only changes the slope, but the entanglement entropy still grows linearly with system size. This is most likely due to the infinite-time average being a valid approximation for the equilibrated occupation matrix *only on small subsystems*, where the difference disappears with the system size. However, here we are focusing on subsystems which are a constant fraction of the system we are growing. Thus, the errors that disappear on a small scale add up on the macroscopic scale and we lose the ability to effectively describe the equilibrated state with the infinite-time average. The above approximation is therefore *not valid* in the present

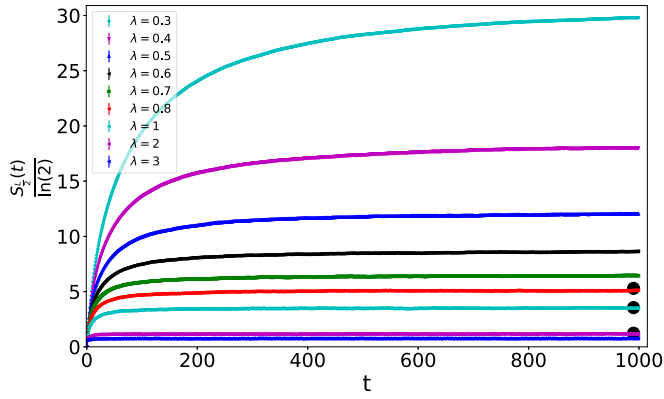


FIG. 9. $S_L(t)$ plotted against time for a system size of $L = 400$. Results are shown for $\lambda = 0.3, 0.4, 0.5, 0.6, 0.7, 0.8, 1, 2, 3$. Each point is an average over 1000 field realizations and the error shown is the standard error on the calculated mean. The black dots pictured are the maximum values observed for times up to $t = 10^8$ for $\lambda = 0.8, 1, 2$.

case. Instead, we must pick an arbitrary late time to calculate the entanglement entropy which we here take to be $t = 10^{11}$.

In Fig. 9 we show results for the growth of the average entanglement entropy with time for the range of disorders we are interested in. It has been proposed that the saturation time for entanglement entropy $\log(t_{\text{sat}}) \sim L$ [34]. Intuitively, for the Anderson insulator, taking a localization value $\xi(\lambda) \ll L$ we would expect the time it takes for the entanglement entropy to get close to this saturated value to be much smaller, as only small subsystems become entangled with each other. This is indeed what we see in Fig. 9, by $t = 500$ all but $\lambda = 0.3$ have little to no growth, and $\lambda = 0.3$ has slowed significantly compared to its initial rise. However, the approach to a constant value could involve logarithmic factors and for subsequent analysis we therefore chose to study the entanglement at $t = 10^{11}$. Three black dots are also included to indicate the maximum value observed at $t = 10^8$. The three dots show the entanglement entropy at the disorder strengths $\lambda = 0.8, 1, 2$. It was recently reported that other localized systems which can be mapped to free fermions show $\log t$ growth at late times [42]. The authors observed this intriguing behavior beginning at around $t = 10^6$ and we confirm here this is *not* observed in the Anderson insulator up to the times considered. The entanglement entropy behavior only marginally changes from $t = 10^3$ to 10^8 .

In Fig. 10 we show results for the entanglement entropy versus $L/2$ at $t = 10^{11}$ as we vary the system size. We observe that as the system size is increased, the slope of $S_{L/2}(t \rightarrow \infty)$ is not constant. Instead, $S_{L/2}(t \rightarrow \infty)$ is indeed approaching a constant value as we increase system size. This means the system is approaching an area law as the system size significantly exceeds the localization length consistent with other studies [38,55]. However, as is particularly evident for $\lambda = 0.3$, there can be an extended range of system sizes for which S is linear in $\log(L)$.

V. LOCALIZATION LENGTH

In this section we use the data from Fig. 10 to define a quantity ξ which is a measure of the localization length

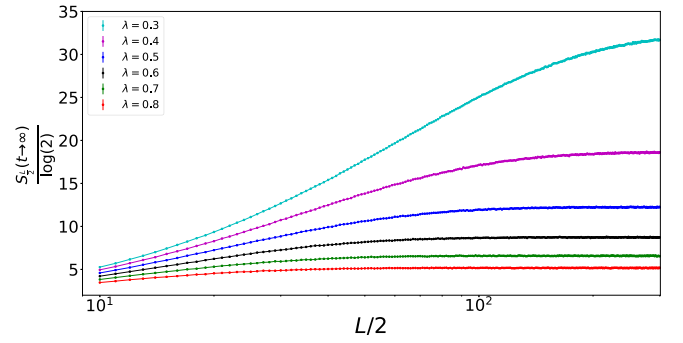


FIG. 10. $S_{L/2}$ plotted against system size at $t = 10^{11}$. Each point is an average over 5000 random-field realizations and the error shown is the standard error on the calculated mean. System sizes are taken from $L = 20$ to 600. Note the logarithmic x axis.

in the RFX. We say the system is completely localized when the entanglement entropy between our two subsystems does not grow as we increase the system. When L is small, unless disorder is extremely large, we expect the entanglement entropy to grow sublinearly in L but it will still grow. So, by adding one site to each subsystem, we grow the lattice and determine the slope of $S_{L/2}$ with $L/2$. We can then define the rate of growth:

$$m(L/2) := S_{L/2} - S_{L/2-1}. \quad (27)$$

In the localized regime we expect that

$$\lim_{L \rightarrow \infty} m(L/2) = 0. \quad (28)$$

The data, however, are not strictly increasing due to noise, so to improve the fitting we use a Savitzky-Golay filter to smooth the data and compute $m(L/2)$ with the smoothed version of the data. Defining a tolerance ϵ , such that $m(L/2) < \epsilon$, we can then define $\xi(\lambda) = \frac{L}{2}$ by the first L for which this occurs. We choose ϵ to be reasonably small since it indicates that the function $m(L/2)$ is approaching the area law. Our results are shown in Fig. 11 clearly indicating a diverging ξ as $\lambda \rightarrow 0$. The fitted function takes the form $a\sqrt{x} + b$ with standard deviations on the variables smaller than 3×10^{-3} . The value of b was found to be $b = -0.00866331$ and we expect this value to approach zero as values closer to $\lambda = 0$ are probed. It

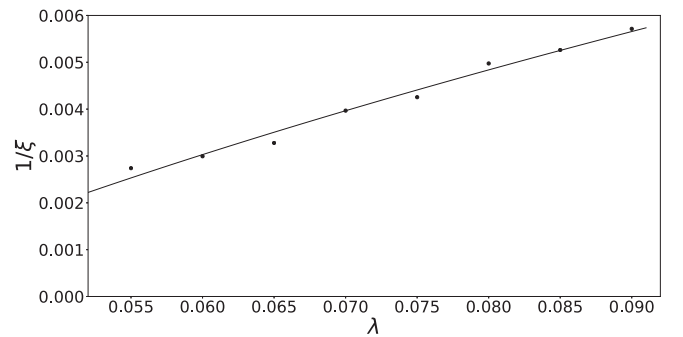


FIG. 11. $\frac{1}{\xi}$ plotted against λ . The data from $S_{L/2}$ were smoothed out using a Savitzky-Golay filter with a polynomial of degree 2 and a window of 11, and a tolerance $\epsilon = 0.37$. Each value of $S_{L/2}$ was computed with over 20 000 realizations of the Hamiltonian.

is at present not clear how reliable the above analysis is for a precise determination of the critical exponents, but the results strongly suggest a diverging length scale as $\lambda \rightarrow 0$.

VI. CONCLUSION

The presence of disorder in the RFXX has been shown to significantly alter the behavior of the OTOCs. At a finite disorder-dependent ξ_{OTOC} information propagation stops and the OTOCs are essentially zero beyond this length scale. However, for $|x| < \xi_{\text{OTOC}}$ we find propagation at the maximal speed $v = J$ and confirm a power-law behavior for the early-time regime of $C(x, t) \sim t^{2x}$ with a position-dependent exponent. An analysis of the behavior of $C(x, t)$ close to the wave front shows a behavior that is not consistent with recent predictions. The growth of the entanglement starting from an unentangled product state shows saturation at sufficiently large times. We have not been able to isolate any specific temperature-dependent effects and, in the light of a temperature-dependent maximal bound on the Lyapunov exponents $\lambda_L \leq 2\pi k_B T / \hbar$, further studies would be of interest.

Finally, our results shed some light on the connection between thermalization and scrambling. We observed *weak* scrambling in the localized phase ($\lambda \neq 0$) of the RFXX. From the results of Ref. [62] it is known that relaxation in a closely related model is described by a generalized Gibbs ensemble with an *extensive* number of conserved quantities. We also observe an absence of scrambling in the nondisordered ($\lambda = 0$) case which requires an *intensive* number of conserved quantities in the corresponding generalized Gibbs ensemble [47]. Hence, the absence of scrambling does not imply the absence of a generalized form of thermalization and a sign of “weak” scrambling does not imply thermalization in the traditional sense.

ACKNOWLEDGMENTS

This research was supported by NSERC and enabled in part by support provided by (SHARCNET) (www.sharcnet.ca) and Compute/Calcul Canada (www.computecanada.ca).

APPENDIX A: TIME-EVOLVING FREE FERMIONS

In this Appendix we review how to time evolve free fermions. A similar treatment can be found in [61]. Starting from the Hamiltonian

$$\hat{H} = \sum_{i,j} M_{i,j} \hat{f}_i^\dagger \hat{f}_j, \quad (\text{A1})$$

where M is a real $L \times L$ symmetric matrix and for generality we do not make any other assumption. This model represents a one-dimensional system of quasi-free fermions hopping on a lattice. The fermionic operators \hat{f}_i^\dagger and \hat{f}_i obey the anticommutation relations

$$\{\hat{f}_j^\dagger, \hat{f}_k\} = \delta_{jk}, \quad \{\hat{f}_j^\dagger, \hat{f}_k^\dagger\} = \{\hat{f}_j, \hat{f}_k\} = 0. \quad (\text{A2})$$

Since M is real symmetric we can always diagonalize it as $M = ADA^T$ where $AA^T = \mathbb{I}$ is real orthogonal transformation and D is a diagonal matrix with entries $D_{k,k} = \epsilon_k$

which are (real) energy eigenmodes. Defining new fermion operators

$$\hat{d}_k = \sum_j A_{j,k} \hat{f}_j, \quad (\text{A3})$$

$$\hat{d}_k^\dagger = \sum_j A_{j,k} \hat{f}_j^\dagger, \quad (\text{A4})$$

we can write the Hamiltonian as

$$\hat{H} = \sum_k \epsilon_k \hat{d}_k^\dagger \hat{d}_k. \quad (\text{A5})$$

The above operators can be referred to as reciprocal space or normal mode operators. These operators inherit fermionic anticommutation relations due to the unitary property of A :

$$\{\hat{d}_l, \hat{d}_k^\dagger\} = \sum_{i,j} A_{i,l} A_{j,k} \{\hat{f}_i, \hat{f}_j^\dagger\} = \delta_{l,k}. \quad (\text{A6})$$

Due to the definition of the annihilation operators, it is easy to see that $|0\rangle_f = |0\rangle_d$. Thus, all eigenstates can be constructed by applying creation operators \hat{d}_k^\dagger . These states are Gaussian, meaning they are completely described by their second moments. Gaussian states can be completely described by the occupation matrix $\Lambda_{i,j}^f = \langle \hat{f}_i^\dagger \hat{f}_j \rangle$ or, in eigenmode space, $\Lambda_{l,k}^d = \langle \hat{d}_l^\dagger \hat{d}_k \rangle$. All time-evolved properties of this model can similarly be deduced by time evolving the occupation matrix. It is simple to time evolve the operators in eigenmode space,

$$\frac{d}{dt}(\hat{d}_k) = i[\hat{H}, \hat{d}_k], \quad (\text{A7})$$

where

$$\hat{H} = \sum_k \epsilon_k \hat{d}_k^\dagger \hat{d}_k. \quad (\text{A8})$$

Using $\{\hat{d}_k, \hat{d}_l^\dagger\} = \delta_{l,k}$ and $\hat{d}_k^2 = 0$, one finds that

$$\hat{d}_k(t) = e^{-i\epsilon_k t} \hat{d}_k, \quad (\text{A9})$$

similarly for the creation operators

$$\hat{d}_k(t)^\dagger = e^{i\epsilon_k t} \hat{d}_k^\dagger, \quad (\text{A10})$$

this then implies

$$\Lambda^d(t) = e^{iDt} \Lambda^d e^{-iDt}, \quad (\text{A11})$$

which means if we know $\Lambda^d(0) = \Lambda^d$ we can compute $\Lambda^d(t)$, giving us all two-point correlators taken at identical times. Because we want to extract local statistics, we need to transform back to the local fermion space. We see this is done by the following transformation:

$$\Lambda^f(t) = A e^{iDt} \Lambda^d e^{-iDt} A^T, \quad (\text{A12})$$

where $\Lambda^d = A^T \Lambda^f A$. Now, since we will also be interested in out-of-time correlations, it becomes important to consider two-point correlations which are taken at different times. For this we introduce the following notation $\Lambda^f(t, t')$, where the left t argument indicates that the creation operators \hat{d}_k^\dagger are at a time t and the right for the annihilation operators. Thus,

Eq. (A12) is $\Lambda^f(t) = \Lambda^f(t, t)$ and the out-of-time two-point correlators are given by

$$\Lambda^f(t, t) = A e^{iDt} \Lambda^d e^{-iDt} A^T, \quad (\text{A13})$$

$$\Lambda^f(t, 0) = A e^{iDt} \Lambda^d A^T, \quad (\text{A14})$$

$$\Lambda^f(0, t) = A \Lambda^d e^{-iDt} A^T. \quad (\text{A15})$$

With Eqs. (A13)–(A15) we can calculate any two-point correlator that might be expressed in the OTOC. Next, it is important to see how the anticommutation rule behaves as we consider creation and annihilation operators at different times. In local space, consider the case where one operator in the Heisenberg picture is taken at $t = 0$ and the other at $t = t$:

$$\{\hat{f}_m^\dagger(t), \hat{f}_n^\dagger\} = \sum_{k,l} A_{n,l} A_{m,k} e^{i\epsilon_k t} (\hat{d}_k^\dagger \hat{d}_l^\dagger + \hat{d}_l^\dagger \hat{d}_k^\dagger) = 0. \quad (\text{A16})$$

Similarly, $\{\hat{f}_m(t), \hat{f}_n\} = 0$, however, the anticommutation between out-of-time creation and annihilation operators is non-trivial:

$$\{\hat{f}_m^\dagger(t), \hat{f}_n\} = \sum_k A_{m,k} A_{n,k} e^{i\epsilon_k t} = a_{m,n}(t). \quad (\text{A17})$$

At $t = 0$ we see $a_{m,n}(0) = \delta_{m,n}$, but time evolution removes this nice behavior. We also see that

$$\bar{a}_{m,n}(t) = \{\hat{f}_m(t), \hat{f}_n^\dagger\} = \sum_k A_{m,k} A_{n,k} e^{-i\epsilon_k t}. \quad (\text{A18})$$

With these tools in place, it is convenient to write the correlations exactly which will be featured in the OTOC. Consider two sites on the lattice labeled by i and j at $t = t$ and 0 , respectively, then the time-dependent correlations are taken from entries of Eqs. (A13)–(A15):

$$\Lambda^f(t, t)_{i,i} = \langle \hat{f}_i^\dagger(t) \hat{f}_i(t) \rangle = \sum_{k,l} e^{i(\epsilon_k - \epsilon_l)t} A_{i,k} A_{i,l} \langle \hat{d}_k^\dagger \hat{d}_l \rangle, \quad (\text{A19})$$

$$\Lambda^f(t, 0)_{i,j} = \langle \hat{f}_i^\dagger(t) \hat{f}_j \rangle = \sum_{k,l} e^{i\epsilon_k t} A_{i,k} A_{j,l} \langle \hat{d}_k^\dagger \hat{d}_l \rangle, \quad (\text{A20})$$

$$\Lambda^f(0, t)_{j,i} = \langle \hat{f}_j^\dagger \hat{f}_i(t) \rangle = \sum_{k,l} e^{-i\epsilon_l t} A_{j,k} A_{i,l} \langle \hat{d}_k^\dagger \hat{d}_l \rangle, \quad (\text{A21})$$

$$\Lambda^f(0, 0)_{j,j} = \langle \hat{f}_j^\dagger \hat{f}_j \rangle = \sum_{k,l} A_{j,k} A_{j,l} \langle \hat{d}_k^\dagger \hat{d}_l \rangle. \quad (\text{A22})$$

With this we have all the ingredients we require to compute an OTOC. In the case of a thermal state or an eigenstate, the expressions in Eqs. (A19)–(A22) are greatly simplified since the occupation matrix in eigenmode space is diagonal. We consider a Gibbs state of the form

$$\rho = \frac{e^{-\beta \hat{H}}}{Z}. \quad (\text{A23})$$

For thermal states we label the correlations with an additional β . The correlations in eigenmode space are well known with different sites decoupled and the occupation numbers

following a Fermi-Dirac statistic with zero chemical potential

$$\Lambda_{k,l}^{d,\beta} = \langle \hat{d}_k^\dagger \hat{d}_l \rangle_\beta = \begin{cases} \frac{1}{1+e^{\beta \epsilon_k}}, & k = l \\ 0, & \text{otherwise.} \end{cases} \quad (\text{A24})$$

In the next Appendix we describe how to use these expressions to compute the OTOC between two S^z operators on different sites.

APPENDIX B: OUT-OF-TIME ORDERED CORRELATIONS

The OTOC we compute in Sec. III relies on the computation of Eq. (15), or rewriting it here,

$$F(t) = \langle \hat{\sigma}_i^z(t) \hat{\sigma}_j^z \hat{\sigma}_i^z(t) \hat{\sigma}_j^z \rangle, \quad (\text{B1})$$

where we have dropped the $x = |i - j|$ term in favor of expressing it as only a function of time. Evaluating this expression is the same as evaluating Eq. (13). For the following, it is easy to represent $\hat{n}_i(t) = \hat{f}_i^\dagger(t) \hat{f}_i(t)$. Substituting the Jordan-Wigner transformation definition,

$$F(t) = 16 \left\langle \left(\hat{n}_i(t) - \frac{1}{2} \right) \left(\hat{n}_j - \frac{1}{2} \right) \left(\hat{n}_i(t) - \frac{1}{2} \right) \left(\hat{n}_j - \frac{1}{2} \right) \right\rangle. \quad (\text{B2})$$

Expanding this and simplifying this using $\hat{n}_i(t)^2 = n_i(t)$ and the anticommutation rules shown in Eq. (A17), we can write

$$F(t) = 16 \left(\hat{n}_i(t) \hat{n}_j \hat{n}_i(t) \hat{n}_j - \frac{1}{2} (\hat{n}_i(t) \hat{n}_j \hat{n}_i(t) + \hat{n}_j \hat{n}_i(t) \hat{n}_j) + \frac{1}{4} [\hat{n}_j \hat{n}_i(t) - \hat{n}_i(t) \hat{n}_j] + \frac{1}{16} \right). \quad (\text{B3})$$

Using Eq. (B3), we can now use the definitions of our initial conditions on Λ^d to derive exact expressions for the OTOCs.

1. Product states

We consider our initial state as one constructed from the vacuum state such that

$$|\Psi\rangle = \prod_{j \in \mathbb{S}} \hat{f}_j^\dagger |0\rangle, \quad (\text{B4})$$

where the cardinality of the set \mathbb{S} represents the conserved number of fermions on the lattice, $\langle \hat{N} \rangle = \sum_j \langle \hat{f}_j^\dagger \hat{f}_j \rangle = |\mathbb{S}|$. This gives us an initial local occupation matrix of the form

$$\Lambda_{i,j}^f(0) = \langle \hat{f}_i^\dagger \hat{f}_j \rangle = \begin{cases} 1, & i = j \wedge i \in \mathbb{S} \\ 0, & \text{otherwise.} \end{cases} \quad (\text{B5})$$

First consider the case that $\hat{\sigma}_j^z$ is selected such that $j \in \mathbb{S}$. Then, using $\hat{f}_j^\dagger |\Psi\rangle = 0$ and Eq. (A17) we get

$$F(t) = 8 |a_{i,j}(t)|^2 \langle \hat{n}_i(t) \rangle - 8 |a_{i,j}(t)|^2 + 1. \quad (\text{B6})$$

Similarly if we assume $j \notin \mathbb{S}$ such that $\hat{f}_j |\Psi\rangle = 0$, then we recover

$$F(t) = 1 - 8 |a_{i,j}(t)|^2 \langle \hat{n}_i(t) \rangle. \quad (\text{B7})$$

Equations (B6) and (B7) reveal that the fundamental behavior of the OTOC relies on $|a_{i,j}(t)|^2$ and $\langle \hat{n}_i(t) \rangle$. The product state OTOC will have two effects coming together:

equilibration of $\langle \hat{n}_i(t) \rangle$ and the out-of-time anticommutation relation $|a_{i,j}(t)|^2$. This extra equilibration is expected to contribute to extra structure not present in the thermal case.

2. Thermal states

The thermal OTOC is computed similarly to the product state, but we exploit its simple structure in eigenmode space as seen in Eqs. (A24). Here, we exploit the fact that $\hat{f}_i^2 = \hat{f}_i^{\dagger 2} = 0$ and use Wicks theorem for thermal states [63]. This gives us

the following form:

$$F(t) = 16|a_{i,j}(t)|^2 (\langle \hat{f}_i^\dagger \hat{f}_i \rangle_\beta \langle \hat{f}_j^\dagger \hat{f}_j \rangle_\beta - \frac{1}{2} (\langle \hat{f}_i^\dagger \hat{f}_i \rangle_\beta + \langle \hat{f}_j^\dagger \hat{f}_j \rangle_\beta) + \bar{a}_{i,j}(t) \langle \hat{f}_i^\dagger(t) \hat{f}_j \rangle_\beta - \langle \hat{f}_i^\dagger(t) \hat{f}_j \rangle_\beta \langle \hat{f}_j^\dagger \hat{f}_i(t) \rangle_\beta) + 1, \quad (\text{B8})$$

where we have used the fact that same time two-point correlators are stationary, $\langle \hat{f}_i^\dagger(t) \hat{f}_i(t) \rangle_\beta = \langle \hat{f}_i^\dagger \hat{f}_i \rangle_\beta$. Equation (B8) is quite a bit more complicated than Eq. (B6), but the defining behavior is still reliant on $|a_{i,j}(t)|^2$ while the quantity $\langle \hat{n}_i(t) \rangle$ is now time independent. Instead, we see out-of-time correlations in the form of $\langle \hat{f}_j^\dagger \hat{f}_i(t) \rangle_\beta$, for example, play a role.

-
- [1] J. Maldacena, S. H. Shenker, and D. Stanford, *JHEP* **08** (2016) 106.
- [2] A. I. Larkin and Y. N. Ovchinnikov, *Zh. Eksp. Teor. Fiz.* **55**, 2262 (1969) [*JETP* **28**, 1200 (1969)].
- [3] B. Swingle and D. Chowdhury, *Phys. Rev. B* **95**, 060201 (2017).
- [4] X. Chen, T. Zhou, D. A. Huse, and E. Fradkin, *Ann. Phys.* **529**, 1600332 (2017).
- [5] Y. Sekino and L. Susskind, *JHEP* **10** (2008) 065.
- [6] S. Sachdev and J. Ye, *Phys. Rev. Lett.* **70**, 3339 (1993).
- [7] S. Sachdev, *Phys. Rev. X* **5**, 041025 (2015).
- [8] D. A. Roberts, D. Stanford, and L. Susskind, *JHEP* **03** (2015) 051.
- [9] W. Fu and S. Sachdev, *Phys. Rev. B* **94**, 035135 (2016).
- [10] J. Maldacena and D. Stanford, *Phys. Rev. D* **94**, 106002 (2016).
- [11] B. Dóra and R. Moessner, *Phys. Rev. Lett.* **119**, 026802 (2017).
- [12] Y. Huang, Y.-L. Zhang, and X. Chen, *Ann. Phys.* **529**, 1600318 (2017).
- [13] K. Slagle, Z. Bi, Y.-Z. You, and C. Xu, *Phys. Rev. B* **95**, 165136 (2017).
- [14] R. Fan, P. Zhang, H. Shen, and H. Zhai, *Sci. Bull.* **62**, 707 (2017).
- [15] D.-L. Deng, X. Li, J. H. Pixley, Y.-L. Wu, and S. Das Sarma, *Phys. Rev. B* **95**, 024202 (2017).
- [16] R. Nandkishore and D. A. Huse, *Annu. Rev. Condens. Matter Phys.* **6**, 15 (2015).
- [17] F. Alet and N. Laflorencie, *C. R. Phys.* (to be published).
- [18] D. J. Luitz and Y. Bar Lev, *Phys. Rev. B* **96**, 020406 (2017).
- [19] S. Xu and B. Swingle, [arXiv:1805.05376](https://arxiv.org/abs/1805.05376).
- [20] S. Xu and B. Swingle, [arXiv:1802.00801](https://arxiv.org/abs/1802.00801).
- [21] S. Sahu, S. Xu, and B. Swingle, [arXiv:1807.06086](https://arxiv.org/abs/1807.06086).
- [22] S. H. Shenker and D. Stanford, *JHEP* **03** (2014) 067.
- [23] Y. Gu, X.-L. Qi, and D. Stanford, *JHEP* **05** (2017) 125.
- [24] A. A. Patel, D. Chowdhury, S. Sachdev, and B. Swingle, *Phys. Rev. X* **7**, 031047 (2017).
- [25] D. Chowdhury and B. Swingle, *Phys. Rev. D* **96**, 065005 (2017).
- [26] A. Nahum, S. Vijay, and J. Haah, *Phys. Rev. X* **8**, 021014 (2018).
- [27] V. Khemani, A. Vishwanath, and D. A. Huse, *Phys. Rev. X* **8**, 031057 (2018).
- [28] T. Rakovszky, F. Pollmann, and C. W. von Keyserlingk, *Phys. Rev. X* **8**, 031058 (2018).
- [29] H. Liu and S. J. Suh, *Phys. Rev. Lett.* **112**, 011601 (2014).
- [30] P. Hosur, X.-L. Qi, D. A. Roberts, and B. Yoshida, *JHEP* **02** (2016) 004.
- [31] N. Yunger Halpern, *Phys. Rev. A* **95**, 012120 (2017).
- [32] N. Yunger Halpern, B. Swingle, and J. Dressel, *Phys. Rev. A* **97**, 042105 (2018).
- [33] J. R. G. Alonso, N. Yunger Halpern, and J. Dressel, *Phys. Rev. Lett.* **122**, 040404 (2019).
- [34] J. H. Bardarson, F. Pollmann, and J. E. Moore, *Phys. Rev. Lett.* **109**, 017202 (2012).
- [35] M. Serbyn, Z. Papić, and D. A. Abanin, *Phys. Rev. Lett.* **110**, 260601 (2013).
- [36] M. Žnidarič, T. Prosen, and P. Prelovšek, *Phys. Rev. B* **77**, 064426 (2008).
- [37] G. D. Chiara, S. Montangero, P. Calabrese, and R. Fazio, *J. Stat. Mech.* (2006) P03001.
- [38] H. Abdul-Rahman, B. Nachtergaele, R. Sims, and G. Stolz, *Lett. Math. Phys.* **106**, 649 (2016).
- [39] F. Iglói, Z. Szatmári, and Y.-C. Lin, *Phys. Rev. B* **85**, 094417 (2012).
- [40] W. Son, L. Amico, F. Plastina, and V. Vedral, *Phys. Rev. A* **79**, 022302 (2009).
- [41] A. Nahum, J. Ruhman, and D. A. Huse, *Phys. Rev. B* **98**, 035118 (2018).
- [42] M. McGinley, A. Nunnenkamp, and J. Knolle, *Phys. Rev. Lett.* **122**, 020603 (2019).
- [43] C. W. von Keyserlingk, T. Rakovszky, F. Pollmann, and S. L. Sondhi, *Phys. Rev. X* **8**, 021013 (2018).
- [44] A. Bohrdt, C. B. Mendl, M. Endres, and M. Knap, *New J. Phys.* **19**, 063001 (2017).
- [45] R. J. Lewis-Swan *et al.*, [arXiv:1808.07134](https://arxiv.org/abs/1808.07134).
- [46] C. Murthy and M. Srednicki, [arXiv:1809.03681](https://arxiv.org/abs/1809.03681).
- [47] M. Gluza, J. Eisert, and T. Farrelly, [arXiv:1809.08268](https://arxiv.org/abs/1809.08268).
- [48] C.-J. Lin and O. I. Motrunich, *Phys. Rev. B* **97**, 144304 (2018).
- [49] S. Byju, K. Lochan, and S. Shankaranarayanan, [arXiv:1808.07742](https://arxiv.org/abs/1808.07742).
- [50] C.-J. Lin and O. I. Motrunich, *Phys. Rev. B* **98**, 134305 (2018).
- [51] E. Hamza, R. Sims, and G. Stolz, *Commun. Math. Phys.* **315**, 215 (2012).
- [52] P. Coleman, *Introduction to Many-Body Physics* (Cambridge University Press, Cambridge, UK, 2015).
- [53] J. Riddell and M. P. Müller, *Phys. Rev. B* **97**, 035129 (2018).
- [54] H.-H. Lai and K. Yang, *Phys. Rev. B* **91**, 081110 (2015).

- [55] H. Abdul-Rahman, B. Nachtergaele, R. Sims, and G. Stolz, *Ann. Phys.* **529**, 1600280 (2017).
- [56] G. Stolz, *Contemp. Math.* **552**, 71 (2011).
- [57] W. Miller, *Symmetry Groups and Their Applications*, Computer Science and Applied Mathematics (Academic, New York, 1972).
- [58] I. Peschel and V. Eisler, *J. Phys. A: Math. Theor.* **42**, 504003 (2009).
- [59] M. Pouranvari, Y. Zhang, and K. Yang, *Adv. Condens. Matter Phys.* **2015**, 4 (2015).
- [60] J. I. Latorre and A. Riera, *J. Phys. A: Math. Theor.* **42**, 504002 (2009).
- [61] M. Perarnau-Llobet, A. Riera, R. Gallego, H. Wilming, and J. Eisert, *New J. Phys.* **18**, 123035 (2016).
- [62] C. Gramsch and M. Rigol, *Phys. Rev. A* **86**, 053615 (2012).
- [63] M. Gaudin, *Nucl. Phys.* **15**, 89 (1960).

Chapter 3

Out of Time Order Correlations in the Quasi-Periodic Aubry-André model

In this chapter we present the article [156] which will be submitted to Physical Review B. The article can be found at arXiv:1908.03292. I am the primary author and contributor of this work. All numerics, plots and original equations present in the article are created by myself with helpful guidance from my supervisor, Erik S. Sørensen.

In this chapter we investigate OTOCs again, this time in a different model. In this case we study the Aubry-André (AA) model [157, 158]:

$$H = -\frac{J}{2} \sum_j (|j\rangle\langle j+1| + \text{h.c.}) + \lambda \sum_j \cos(2\pi\sigma j) |j\rangle\langle j|. \quad (3.1)$$

Where $\sigma = (\sqrt{5} - 1)/2$ is taken as the golden ratio, an irrational number making the model quasi-periodic. This model features a transition from an extended phase to a localized phase at $\lambda = J$. Interestingly it is possible to simulate this model effectively in experiment [159–164]. For convenience we formulate this model in terms of free fermions,

$$\hat{H} = \sum_{i,j} M_{i,j} \hat{f}_i^\dagger \hat{f}_j, \quad (3.2)$$

where if $|i - j| = 1$, $M_{i,j} = -J/2$, the diagonal reads $M_{i,i} = \lambda \cos(2\pi\sigma j)$ and all other terms are zero. We fix the system size to L . We study the OTOC with operators which are local in both the spin and fermionic operators,

$$C(x, t) = \langle [\hat{A}(t), \hat{B}]^\dagger [\hat{A}(t), \hat{B}] \rangle, \quad (3.3)$$

$$\hat{A}(t) = 2\hat{f}_{\frac{L}{2}}^\dagger(t) \hat{f}_{\frac{L}{2}}(t) - 1, \quad \hat{B} = 2\hat{f}_j^\dagger \hat{f}_j - 1. \quad (3.4)$$

We investigate all four usual time regimes and propose a fifth time regime of interest. First we investigate the early time growth and confirm the findings of [109], that the early time regime is independent of disorder and follows the power law,

$$C(x, t) \sim t^{2|x|}. \quad (3.5)$$

Next we investigate the wave-front and resolve the discrepancy between the universal form of equation 1.35 and the Gaussian form found in the previous chapter, equation 2.5. We find that both forms are equally true but correspond to different dynamical regimes. The universal form corresponds, to times such that $t \ll \frac{x}{v_B}$, where v_B is the velocity at which the wave-front propagates. We also find that the prediction of $p = 1/2$ and $v_B = J$ to be true for the non-disordered case of this model. We re-express the Gaussian form as,

$$C(x = x_0, t) \sim e^{-m(x, \lambda) \left(t - \frac{x}{v_B}\right)^2 + b(x, \lambda)t}, \quad (3.6)$$

where $m(x, \lambda) = a(x, \lambda)/2$. The position dependence of $m(x, \lambda)$ and $b(x, \lambda)$ is then investigated and we find that the functions approach a fixed value in the large x limit. This form appears to be universal and is valid for the interval surrounding $x = v_B t$. Our main result is the proof of equilibration of the OTOC. To simplify the proof we switch to the OTOC,

$$C(x, t) = \text{tr} \left(\{ \hat{f}_m^\dagger(t), \hat{f}_n \} \{ \hat{f}_m(t), \hat{f}_n^\dagger \} \right) \equiv |a_{m,n}(t)|^2. \quad (3.7)$$

We then prove for the extended regime that the OTOC equilibrates to its infinite time average as,

$$\frac{1}{T} \int_0^T \left| |a_{m,n}(t)|^2 - |\omega_{m,n}|^2 \right|^2 dt \leq 4\pi Q^2 \left(\frac{a(\epsilon)}{\sigma_G T} + \delta(\epsilon) \right). \quad (3.8)$$

where $|\omega_{m,n}|^2$ is the infinite time average of $|a_{m,n}|^2$, $a(\epsilon)$, Q^2 and σ_G are order unity constants and $\delta(\epsilon)$ is very small. We also show that the infinite time average disappears in the thermodynamic limit signifying no scrambling,

$$|\omega_{m,n}|^2 \sim \frac{1}{L}. \quad (3.9)$$

We also bound the infinite time average of the distance between the OTOC and its infinite time average,

$$\lim_{T \rightarrow \infty} \frac{1}{T} \int_0^T \left| |a_{m,n}(t)|^2 - |\omega_{m,n}|^2 \right|^2 dt \leq \frac{c^4}{L^2}, \quad (3.10)$$

where c is a constant independent of the system size.

Out of Time Order Correlations in the Quasi-Periodic Aubry-André model

Jonathon Riddell¹ and Erik S. Sørensen¹

¹*Department of Physics & Astronomy, McMaster University 1280 Main St. W., Hamilton ON L8S 4M1, Canada.*

(Dated: September 2, 2019)

We study out of time ordered correlators (OTOC) in a free fermionic model with a quasi-periodic potential. This model is equivalent to the Aubry-André model and features a phase transition from an extended phase to a localized phase at a non-zero value of the strength of the quasi-periodic potential. We investigate five different time-regimes of interest for out of time ordered correlators; early, wavefront, $x = v_B t$, late time equilibration and infinite time. For the early time regime we observe a power law for all potential strengths. For the time regime preceding the wavefront we confirm a recently proposed universal form and use it to extract the characteristic velocity of the wavefront for the present model. A Gaussian waveform is observed to work well in the time regime surrounding $x = v_B t$. Our main result is for the late time equilibration regime where we derive a finite time equilibration bound for the OTOC, bounding the correlator's distance from its late time value. The bound impose strict limits on equilibration of the OTOC in the extended regime and is valid not only for the Aubry-André model but for any quadratic model. Finally, momentum out of time ordered correlators for the Aubry-André model are studied where large values of the OTOC are observed at late times at the critical point.

I. INTRODUCTION

Recently out of time ordered correlators (OTOCs) have experienced a resurgence of interest from different fields of physics ranging from the black hole information problem [1] to information propagation in condensed matter systems [2–9]. The OTOC is of particular interest due to its role in witnessing the spreading or “scrambling” of locally stored quantum information across all degrees of freedom of the system, something traditional dynamical correlation functions of the form $\langle A(t)B \rangle$ cannot. Thus, thermalization must have information scrambling as a precursor since the thermal state necessarily will have lost information about any initial state, although thermalization typically occurs at a significantly longer time-scale [10]. An upper bound for the initial exponential growth, $e^{\lambda_L t}$, of the OTOC, with $\lambda_L \leq 2\pi k_B T / \hbar$ has been conjectured [1]. Models approaching or saturating this bound are known as fast scramblers, in contrast to many condensed matter systems which exhibit a much slower growth and are therefore known as slow scramblers. The introduction of disorder significantly alters the information spreading, restricting it within a localization length in Anderson insulators [11] and partially halting the growth of the OTOC in many-body localized states [3]. The OTOC is directly related to the Loschmidt Echo [5] and it has been established that the second Renyi entropy can be expressed in terms of a sum over appropriately defined OTOCs [12]. Any bound that can be established on the growth of the OTOC therefore implies a related bound on the entanglement. A further understanding of the dynamics of quantum information in models with both extended and localized states is therefore of considerable interest and our focus here is on understanding how this arises in the quasi-periodic Aubry-André (AA) model where a critical potential strength separates an extended and localized phase.

An OTOC is generally written in the form,

$$C(x, t) = \langle [\hat{A}(t), \hat{B}]^\dagger [\hat{A}(t), \hat{B}] \rangle, \quad (1)$$

where \hat{A}, \hat{B} are local observables which commute at $t = 0$. If

the observables are both hermitian and unitary the OTOC can be re-expressed as,

$$C(x, t) = 2 - 2\Re[F(x, t)], \quad (2)$$

where,

$$F(x, t) = \langle \hat{A}(t) \hat{B} \hat{A}(t) \hat{B} \rangle. \quad (3)$$

Often one refers to both F and C as the OTOC. From a condensed matter perspective the OTOC is a measure of an operator spreading its influence over a lattice, and quantifies the degree of non-commutativity between two operators at different times. If the initially zero $C(x, t)$ remains non-zero for an extended period of time we say the system has scrambled. A closely analogous diagnostic tool, capable of detecting information scrambling, can be defined in terms of the mutual information between two distant intervals [13].

From a measurement perspective $F(x, t)$ can be understood as a series of measurements. First acting on the state with operator \hat{B} at $t = 0$ and evolving in time to $t > 0$, then acting on the state with operator \hat{A} , then evolving for time $-t < 0$. The OTOC is then obtained by calculating the overlap between the resulting state and the state that is first evolved by t , then acted upon by A , then evolved by $-t$ and finally acted upon by B . Typically in the context of the OTOC one uses $\langle \dots \rangle$ as the thermal average, often at infinite temperature, but studies in a non-equilibrium setting starting from product states have also been done [11, 14, 15]. Out of time correlators have also sparked experimental interest and significant progress has been made to reliably measure these quantities [16–20]. The correlators have even been reliably simulated on a small quantum computer [21] and recently on an ion trap quantum computer [22].

The dynamics of the OTOC has five important regimes; early time, the wavefront, $x = v_B t$, late time dynamics and the infinite time limit. The early time growth of OTOCs has been of interest as an initial growth of the OTOC that precedes classical information. If the Hamiltonian is local in interactions then use of the Hadamard formula (see ref. [23] lemma

5.3) allows one to conclude that in the early time regime the OTOC grows with a power law in time,

$$C(x, t) \sim t^{l(x)}, \quad (4)$$

where t is small and $l(x)$ is a linearly increasing function of the distance. The early power law growth in time occurs before the wavefront hits and is known to be independent of the integrability of the model [11, 14, 24–28]. This polynomial form is also known to be independent of disorder strength and has been observed to hold in localized regimes [11, 14].

More interestingly, the wavefront tracks the passage of classical information in the system. A universal wavefront form has been proposed [29, 30], valid for $t \ll x/v_B$,

$$C(x, t) \sim \exp\left(-\lambda_L \frac{(x - v_B t)^{1+p}}{t^p}\right), \quad (5)$$

where λ_L is the Lyapunov exponent and v_B is the butterfly velocity. Several other forms have been proposed, for a review see Ref. [29]. The above wavefront form, Eq. (5), has been confirmed in several cases, and even used to show a chaotic to many body localization transition [29–40]. For free models one can show with a saddle point approximation that the form from Eq. (5) takes $p = \frac{1}{2}$ and v_B is the maximal group velocity of the model [29, 30, 35]. A particular appealing feature of Eq. (5) is the appearance of a well-defined Butterfly velocity, v_B for a large range of models. A recent numerical study focusing on the random field XX-model suggested that for this disordered model a different form could be made to fit better over an extended region [11] surrounding $x = v_B t$. This result suggests further studies are important for understanding how quantum information is spreading through the system.

The late time dynamics of OTOCs are a similarly rich regime of interest. Understanding how the function $g(t) = |C(x, t) - C(x, t \rightarrow \infty)|^2$ decays in time has received attention in many models. In the case of the anisotropic XY model the decay of the OTOC to its equilibrium value is an inverse power law [27, 28],

$$C(x, t) \sim \frac{1}{t^\alpha} + \gamma, \quad (6)$$

where $\alpha \geq 0$ depending on the choices of spin operators and the anisotropy, and γ is the equilibrium value. Other work has been done on interacting systems where both inverse power laws were observed for chaotic and many body localized phases, and even an exponential decay in time for Floquet systems [3, 15]. However, these results are mostly numerical, and do not give rigorous bounds or arguments as to whether or not the OTOC reaches equilibrium and if it does, to what resolution. Another aspect of the late time regime, the quantity $C(x, t \rightarrow \infty)$ in it self, is naturally of considerable interest. In this setting $F(x, t \rightarrow \infty)$ is often chosen as the quantity to study. In the presence of chaos we expect F to equilibrate to zero, and in other cases settle at a finite value between zero and one [3, 11, 12, 14, 15, 27, 28, 41–47]. A particularly important case for our purposes are the non-interacting models where the observables defining the OTOC

are both local in fermionic and spin representations on the lattice. Here $F(x, t)$ is expected to initially decay towards zero, but eventually return to $F(x, t) = 1$ and in the presence of disorder need not decay back to its initial value or even equilibrate [11, 27, 28, 42, 47]. Of course, C is then predicted to follow the opposite behaviour, starting at zero then reaching a maximum. It is also noteworthy that, in the proximity of a quantum critical point the OTOC has been shown to follow dynamical scaling laws [48].

The introduction of disorder, with the potential of leading to localization, significantly changes the behaviour of the OTOC and propagation of quantum information as a whole. Naturally, quantum information dynamics is expected to be dramatically different between localized and extended phases. We therefore focus on the one-dimensional quasiperiodic Aubry-André (AA) model [49, 50]:

$$H = -\frac{J}{2} \sum_j (|j\rangle\langle j+1| + \text{h.c.}) + \lambda \sum_j \cos(2\pi\sigma j) |j\rangle\langle j|. \quad (7)$$

Here, J is the hopping strength and λ the strength of the quasiperiodic potential. This model has been extensively studied [51–60] and since it is quadratic large-scale exact numerical results can be obtained from the exact solution. In particular quench dynamics has recently been studied [61]. Crucially, it is well established that a critical potential strength $\lambda_c = J$ separates an extended and localized regime if σ is chosen to be the golden mean $\sigma = (\sqrt{5} - 1)/2$. For finite lattices this strictly only holds if the system size is chosen as $L = F_i$, with F_i a Fibonacci number, and $\sigma = F_{i-1}/F_i$ approaching the golden mean as $i \rightarrow \infty$. A dual model can then be formulated [49, 51] by introducing the dual basis $|\bar{k}\rangle = L^{-1/2} \sum_j \exp(i2\pi\bar{k}\sigma j) |j\rangle$. $\lambda_c = J$ is then the self-dual point. The extended phase is characterized by ballistic transport as opposed to diffusive [49]. The nature of the quasi-periodic potential is also special since no rare regions exists and it has recently been argued that localization in the AA model is fundamentally more classical than disorder-induced Anderson localization [54]. It is possible to realize this model quite closely in optical lattices and studies of both bosonic and fermionic experimental realizations have been pursued using ^{39}K bosons [62–64], ^{87}Rb bosons [65], and ^{40}K fermions [66–68].

The AA model has also recently been studied in the presence of an interaction term [69, 70]. While no longer exactly solvable, a many-body localized phase can be identified in studies of small chains [69, 70] and by analyzing the OTOC it has been suggested that an intermediate ‘S’ phase occurs between the extended and many-body localized phases with a power-law like causal lightcone [70].

The structure of this paper is as follows, in section II we discuss our formulation of the Aubry-André model and describe the quench protocol we use. In section III we investigate the dynamics of an out of time ordered correlator in real space and break the section into three subsections dedicated to three dynamical regions of interest. In subsection III A we show that when quenching into either the extended, localized, or critical phase a power-law growth is observed in the early time regime. In III B we investigate the discrepancies between

[29, 30] and [11] for times closer to the wave-front. Section III C contains a proof that, in the extended phase of a free model, we expect the out of time ordered correlator to equilibrate even in the presence of the quasi-periodic potential. The infinite time value is also shown to be *zero* regardless of the strength of the quasi-periodic potential indicating a lack of scrambling regardless of disorder in the extended phase. Finally in section IV we investigate OTOCs constructed from momentum occupation operators and find that they obey a simple waveform.

II. THE MODEL AND OTOCS

As outlined, we focus on the quasi-periodic AA model. We chose a fermionic representation and write the Hamiltonian as follows:

$$\hat{H} = \sum_{i,j} M_{i,j} \hat{f}_i^\dagger \hat{f}_j, \quad (8)$$

where the effective elements of the Hamiltonian matrix M is filled by, $M_{i,j} = -\frac{J}{2}$ if $|i - j| = 1$ and $M_{j,j} = \lambda \cos(2\pi\sigma j)$. The operators are fermionic so we have $\{\hat{f}_k, \hat{f}_l\} = \{\hat{f}_k^\dagger, \hat{f}_l^\dagger\} = 0$ and $\{\hat{f}_l^\dagger, \hat{f}_k\} = \delta_{l,k}$. All other entries of the effective Hamiltonian are zero. Note that this corresponds to open boundary conditions with nearest neighbour hopping which is the most convenient for the calculations. The constant σ is the inverse golden ratio, $\sigma = (\sqrt{5} - 1)/2$. For the very large system sizes we use we have not been able to observe any numerical difference between using $L = F_i$, $\sigma = F_{i-1}/L$ and using a large L with $\sigma = (\sqrt{5} - 1)/2$ even though the model is strictly no longer self-dual. For convenience we therefore use the latter approach. Since the inverse golden ratio is irrational, this creates a quasi-periodic potential controlled by the value of λ . For the rest of our discussion we set $J = 1$ and $\hbar = 1$. This model is identical to the Aubry-André model as can be seen through a series of transformations [49, 71]. One can easily diagonalize and time evolve states in this model, the details of which are presented in the Appendix A. As described above, this model is known to have a localization transition at a critical point $\lambda_c = J$. For $\lambda < \lambda_c$ all states are extended, and $\lambda > \lambda_c$ all states are localized with localization length $\xi = \frac{1}{\ln \lambda}$ [49]. Relaxation and thermalization following a quench into both extended and localized phases has recently been investigated in this model [61]. While most one-body observables thermalize to a generalized Gibbs ensemble in the extended state, and some in the localized, special dynamics was observed for a quench to the critical points where the observables investigated did not reach a clear stationary value in the time intervals investigated. Similar quadratic fermionic models have been used to investigate OTOCs at large system sizes, showing non-trivial behaviour of both non-disordered and disordered OTOC investigations in integrable models [11, 27, 72].

The OTOCs we will be interested in are written in the form Eq. (1) where we choose \hat{A} and \hat{B} such that they commute at $t = 0$ and are unitary. The operators being hermitian and

unitary then obey Eq. (2), (3). In general we choose our operators such that at $t = 0$ $[\hat{A}, \hat{B}] = 0$, making $C(x, 0) = 0$ in all cases. This gives us a convenient reference point in time. Because we are talking about fermionic operators, it makes sense to only consider operators which are quadratic, and further, we choose to restrict ourselves to operators that can be expressed as number operators in real or momentum space. In momentum space the operators we consider are :

$$\eta_k := \frac{1}{\sqrt{L}} \sum_j e^{ikj} \hat{f}_j \quad (9)$$

$$\eta_k^\dagger := \frac{1}{\sqrt{L}} \sum_j e^{-ikj} \hat{f}_j^\dagger. \quad (10)$$

Where, $k \in 2\pi m/L$ with $m = 1, 2, \dots, L$. These operators are extremely non-local in the real space operators, and for the case of $\lambda = 0$ and periodic boundary conditions, are the operators which diagonalize M (strictly speaking only when periodic boundary conditions are used). It has been observed previously that operators not local in the fermionic representation show fundamentally different behaviour than the local ones [27]. These however were spin operators, which were non-local in the Jordan-Wigner transform, so investigating OTOCs with momentum number operators is not entirely an exact analogue.

III. REAL SPACE OTOCS

We start by considering OTOCs based on operators defined in real space. To be specific we study the following operators,

$$\hat{A}(t) = 2\hat{f}_{\frac{L}{2}}^\dagger(t)\hat{f}_{\frac{L}{2}}(t) - 1, \quad \hat{B} = 2\hat{f}_j^\dagger\hat{f}_j - 1 \quad (11)$$

Where we have fixed the location of \hat{A} in space at the middle point of the lattice, and we will vary the location of \hat{B} , so we see can observe the effect of \hat{A} spreading over the lattice. The operators are written with a factor of 2 and a subtraction of 1 to make them unitary. The dynamics and calculations of the OTOC in this setting is presented in Appendix A, B and C.

A. Early time

In this section we explore the early time behavior of the real space OTOCs. As seen in Eq. C33 the dynamics of the OTOC are dominated by the squared anti-commutator relation of the fermionic operators in time, $a_{m,n}(t)$ (defined in Eq. A8). If one sets $\lambda = 0$ and assumes periodic boundary conditions, one finds that in the thermodynamic limit that the squared anti-commutator behaves as the square of a Bessel function in time (see for example Appendix C of [29]),

$$C(x, t) \sim |a_{m,n}(t)|^2 \sim J_x^2(t), \quad (12)$$

then in the limit of small t one finds that,

$$C(x, t) \sim t^{2|x|}. \quad (13)$$

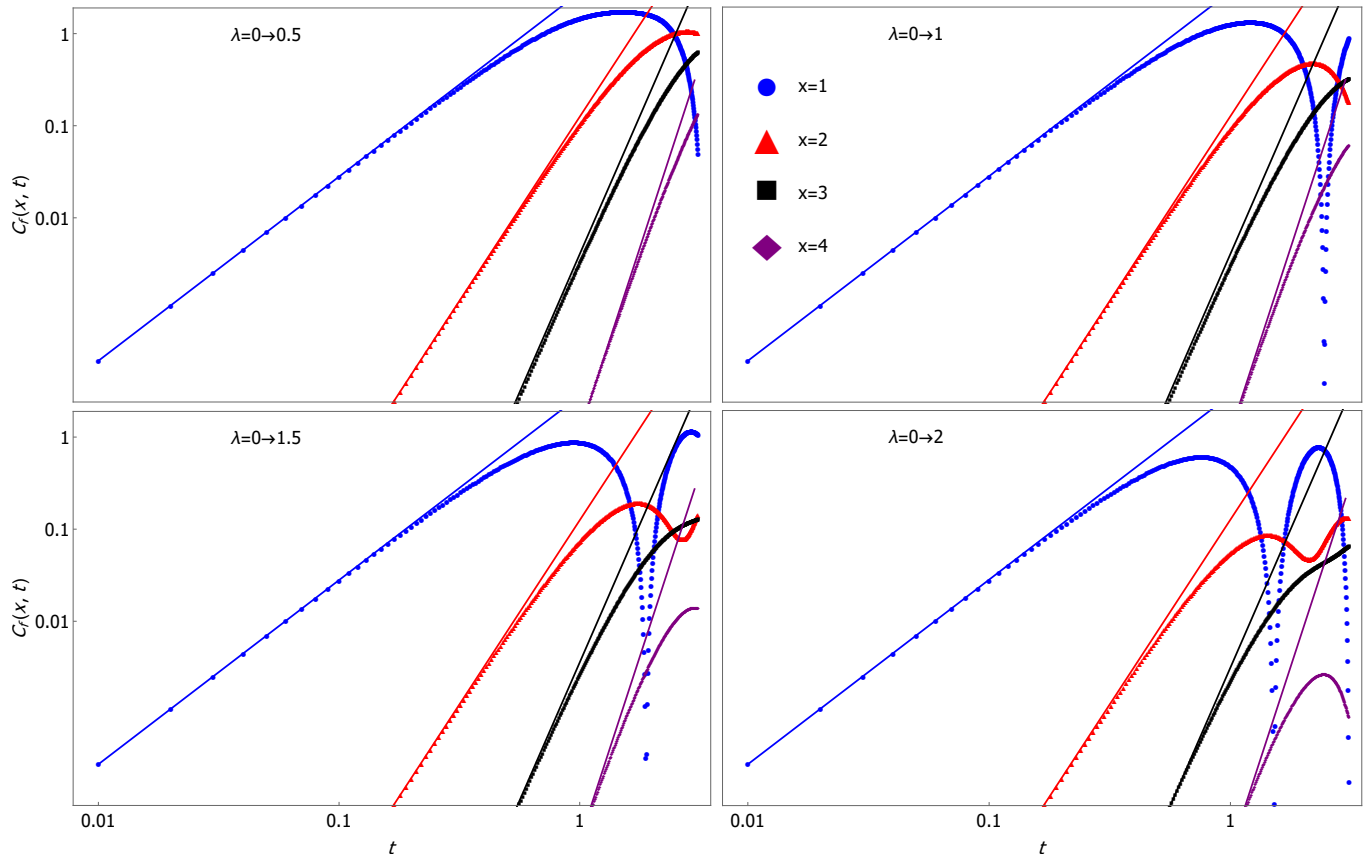


Figure 1. Early time behavior of $C(x, t)$ at different distances. The solid curve is the power law and the dotted curve is the data collected for the OTOC. The system size is $L = 1200$. Results are shown for quenches to four different values of λ starting from the ground state of the model at $\lambda = 0$.

For our purposes the derivation sketched above is too restrictive as we are also interested in non-translationally invariant models and our OTOC features more dynamical terms than just the squared anti-commuter. However, the result, Eq. (13) still remains correct even in the presence of non-zero quasi-periodic potential. This can be seen through the use of the Hadamard formula as shown in [11].

We study this prediction in the most dynamically rich way possible, by quenching from the half-filled ground-state at $\lambda = 0$ to $\lambda = 0.5, 1, 1.5, 2$. Our results are shown in Fig. 1. For a detailed discussion of the starting state see Appendix B. The results here do not significantly change if the quench is to the localized phase ($\lambda = 1.5, 2$), critical ($\lambda = 1$) or extended phase ($\lambda = 0.5$). For all strengths of the quasi-periodic potential is a power-law behaviour observed following Eq. (13). This results agree with [11] which found that in an Anderson localized model regardless of the strength of the localization, if the OTOC significantly grows, then the polynomial early time growth Eq. (13) is observed to hold. This follows naturally from the fact that Eq. (13) is independent of the potential strength, the first contributing dynamics to the OTOC are unaffected by the potential term and come solely from the hopping terms. The early time behaviour can therefore be ob-

tained by studying the $\lambda = 0$ case.

B. Wavefront

In this section we study the wavefront at different potential strengths and address discrepancies from the results shown in [29, 30] and [11]. Recently, the universal form was claimed to be confirmed in the XX spin chain, contradictory to earlier claims [28]. Here we discuss these seemingly contradictory claims. The universal wave form predicted for the out of time ordered correlator in free theories by means of a standard saddle point approximation scheme is given by Eq. (5) in terms of the Lyapunov exponent, λ_L and the Butterfly velocity, v_B . Often this form is applied at surprisingly early times [70] where $-50 < \log(C) < -10$. For the AA model with $\lambda = 0$, corresponding to free fermions, we expect the $v_B = J$ as the maximal group velocity, and $p = \frac{1}{2}$. The universal form, Eq. (5), cannot be re-expressed in a form equivalent to the 'Gaussian' form characterized by two spatial and disorder dependent functions $a(x, \lambda)$, $b(x, \lambda)$ proposed in Ref. 11, for

times surrounding $x = v_B t$, for a fixed $x = x_0$:

$$C(x = x_0, t) \sim e^{-a(x, \lambda) \left(t^2 - \frac{x^2}{v_B^2} \right) + b(x, \lambda) t}. \quad (14)$$

We can rewrite Eq. 14 as,

$$C(x = x_0, t) \sim e^{-m(x, \lambda) \left(t - \frac{x}{v_B} \right)^2 + b(x, \lambda) t}, \quad (15)$$

where $m(x, \lambda) = a(x, \lambda)/2$.

We expect that the discrepancy is most likely due the existence two unique time regimes that are close together. To eliminate noise in our OTOC we drop all of the dynamical terms except the squared anti-commutator. which is equivalent to instead studying the OTOC,

$$C(x, t) = \text{tr} \left(\{ \hat{f}_m^\dagger(t), \hat{f}_n \} \{ \hat{f}_m(t), \hat{f}_n^\dagger \} \right) \equiv |a_{m,n}(t)|^2. \quad (16)$$

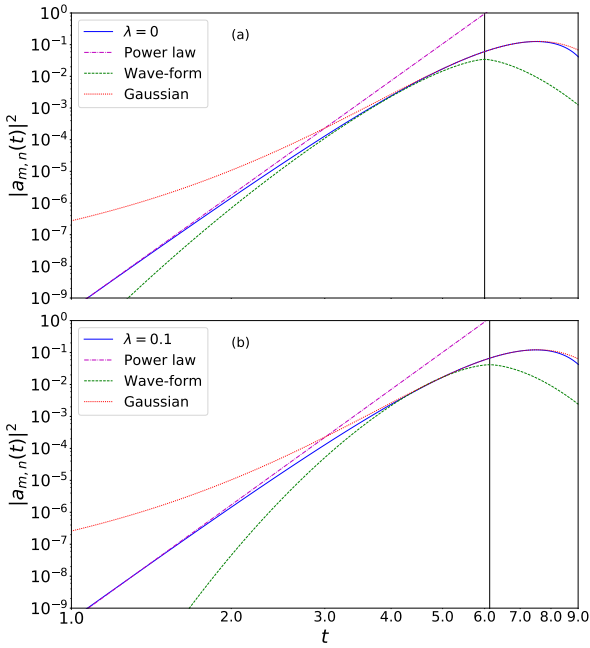


Figure 2. $|a_{m,n}(t)|^2$ for $\lambda = 0$ (a) and $\lambda = 0.1$ (b) plotted with the fitting functions of the early time form, Eq. (13), the proposed universal wave form, Eq. (5) and the Gaussian form, Eq. (15). Results are for a fixed $x = 6$ with $L = 1600$ and $\lambda = 0$. The vertical solid line in both panels corresponds the arrival of the classical wave front at $t = x/v_B$ using the fitted v_B .

To further facilitate the analysis we include a phase, ϕ , in the potential $\lambda \cos(2\pi\sigma j + \phi)$ and smooth our data by averaging over ϕ . Our results are shown in Fig. 2 where we follow an analysis similar to [36]. By varying both time and space we fit the OTOC for $\lambda = 0$ in the region such that $\log(|a_{m,n}|^2) \in [-10, -6]$. With this fit we find $v_B = 0.9950 \pm 0.0002$, $p = 0.50 \pm 0.08$ and $\lambda_L = 1.78 \pm 0.03$ for the universal form, Eq. (5). Where the errors reported are one standard deviation of the parameter estimate. These values are in close agreement

with the expected values of $v_B = 1$ and $p = \frac{1}{2}$. Similarly we investigated the $\lambda = 0.1$ case for $\log(|a_{m,n}|^2) \in [-12, -8]$ and found $v_B = 0.9783 \pm 0.0003$, $p = 0.647 \pm 0.03$ and $\lambda_L = 2.153 \pm 0.09$ for the universal form, Eq. (5). However, these fits correspond to times that significantly precede the classical wavefront. For larger values of the potential strength, λ , we have found it more difficult to obtain good fits to the universal form, Eq. (5).

At later times the OTOC enters a dynamical regime where the Gaussian form of Eq. 15 is valid. Fixing $x = 6$ and using the v_B found for the universal form we find that for $\lambda = 0$ $m(x, \lambda) = 0.3027 \pm 0.0001$ and $b(x, \lambda) = 0.9470 \pm 0.0001$. For $\lambda = 0.1$ we find $m(x, \lambda) = 0.3052 \pm 0.0001$ and $b(x, \lambda) = 0.8597 \pm 0.0002$.

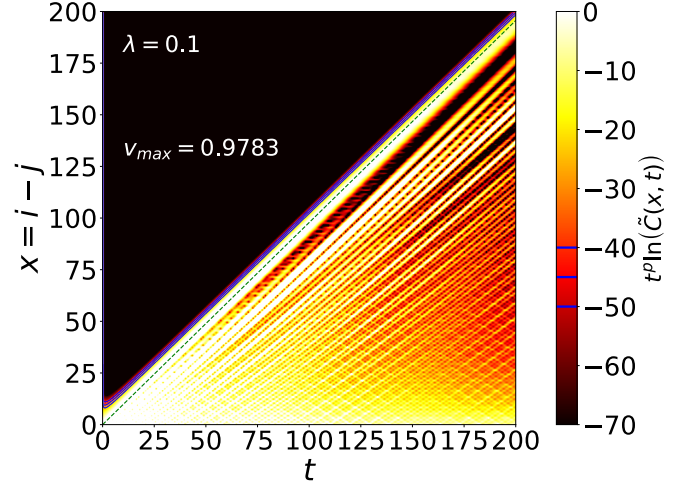


Figure 3. Density plot of $t^p \log(\tilde{C})$, with \tilde{C} an appropriately normalized OTOC from Eq. 16 and $p = 0.6470$. Results are shown for $\lambda = 0.1$ and $L = 1600$. Contour lines are plotted as solid blue lines. The dashed green line indicates $x = v_b t$ with $v_b = 0.9783$ which appear closely parallel to the contour lines.

To further illustrate the universal form, Eq. (5), we show in Fig. 3 results for the entire $C(x, t)$ over a large range of x and t for $\lambda = 0.1$. As above we have smoothed the data over the phase ϕ . We first appropriately normalize C to obtain \tilde{C} and then plot $t^p \log(\tilde{C})$ using the fitted $p = 0.6470$. We then expect that contour lines should be straight lines defined by $x = v_b t$. This is clearly observed in Fig. 3 although we note that it is only contour lines for extremely small values of $t^p \log(\tilde{C})$ (of the order of -40 to -50) that are completely parallel to the determined $v_B t$. Although the universal form of Eq. 5 seems to work well, it is only applicable at times $t \ll \frac{x}{v_B}$.

Let us return to the Gaussian form of Eq. 15, expected to be valid close to $x = v_B t$. We consider the behaviour of the functions $m(x, \lambda)$ and $b(x, \lambda)$ by varying x and fixing v_B as the velocities found fitting the universal waveform. These functions appear to asymptotically approach a fixed value in the large x limit. For large x and $\lambda = 0$ $m(x, \lambda) \approx 0.01$ and $b(x, \lambda) \approx 0.2$. For $\lambda = 0.1$ we see the values $m(x, \lambda) \approx 0.008$ and $b(x, \lambda) \approx 0.1$. This result is shown in Fig. 4. Errors

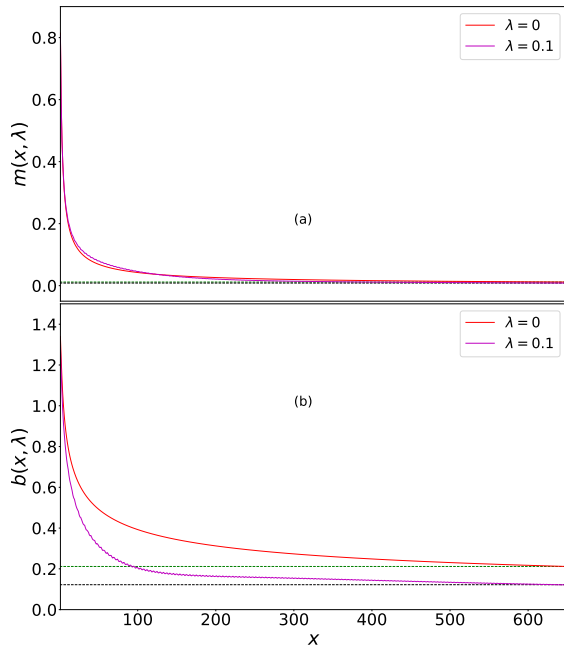


Figure 4. Functions $m(x, \lambda)$ (a) and $b(x, \lambda)$ (b) behaviour for fixed λ at different x . Results are shown for no ϕ averaging and $L = 1600$. The dashed green horizontal line corresponds to the observed value of the function at $x = 650$ for $\lambda = 0$ and the dashed black line to the value for $\lambda = 0.1$.

on this parameters are on the order of 10^{-4} or smaller. This means that taking large values of distance between the two observables \hat{A} and \hat{B} , we may write,

$$C(x, t) \sim e^{-m(t - \frac{x}{v_B})^2} e^{bt}, \quad (17)$$

where m and b are positive constants. Intuitively this corresponds to a Gaussian wave travelling at velocity v_B , augmented by e^{bt} . This form is expected to be valid on the interval surrounding the passage of classical information around $x = v_B t$. Hence, this form works rather close to $x = v_B t$. It seems likely that in interacting systems this might be apparent for much smaller values of x .

If we instead of using the OTOC defined from the anti-commutator, Eq. (16), use the full $C(x, t)$ with a thermal average where we fixed the inverse temperature $\beta = 1$ we find typical results as shown in Fig. 5 for $\lambda = 0.5$. In this case, as is this case for the remainder of our results we do not smoothen the data using the phase ϕ . From Fig. 5 we see that the velocity predicted from the universal fit, Eq. (5), of $v_B = 0.838$ seems to be a good fit for predicting the spread of classical information. For larger values of λ we have not found it possible to use the universal form Eq. (16) in contrast to recent results by Xu et al [70]. A possible explanation for this is that Xu et al [70] study the behaviour of the OTOC in a thermal state at infinite temperature in an interacting model, a somewhat different setting.

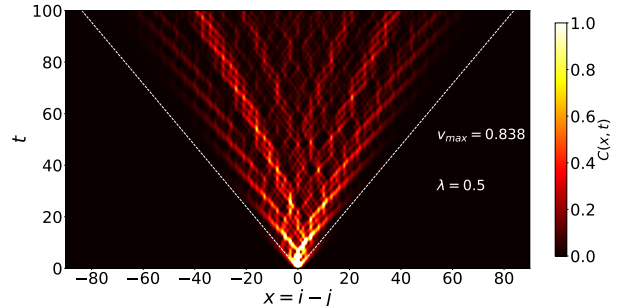


Figure 5. Wavefront spreading in both x and t for $\lambda = 0.5$, the center being taken as $\frac{L}{2}$. System size $L = 1200$.

C. Late time

It is also interesting to investigate the late time dynamics of the OTOC. In prior studies it was pointed out that a $C(x, t) \sim \frac{1}{t}$ behaviour was expected in late time [27, 28]. These results however are for disorder-free models and do not in general hold for our discussion. So instead we look to analytically show that these OTOCs indeed go to an equilibrium value in the late time regime in the extended phase, regardless of strength of the quasi-periodic potential. To bound this behaviour and prove equilibration we again focus on studying the OTOC defined in terms of the squared anti-commutator, Eq. (16). From Eq. (A8) this can be written as:

$$\begin{aligned} C(x, t) &= \text{tr} \left(\{ \hat{f}_m^\dagger(t), \hat{f}_n \} \{ \hat{f}_m(t), \hat{f}_n^\dagger \} \right) \equiv |a_{m,n}(t)|^2 \\ &= \sum_{k,l} A_{m,k} A_{n,k} A_{m,l} A_{n,l} e^{i(\epsilon_k - \epsilon_l)t}. \end{aligned} \quad (18)$$

The infinite time average is defined as,

$$|\omega_{m,n}|^2 = \lim_{T \rightarrow \infty} \frac{1}{T} \int_0^T |a_{m,n}|^2 dt, \quad (19)$$

using the fact that $\epsilon_k = \epsilon_l \Leftrightarrow k = l$,

$$|\omega_{m,n}|^2 = \sum_k A_{m,k}^2 A_{n,k}^2. \quad (20)$$

From Eq. (20) we can come to the intuitive conclusion that when the system is extended, in the thermodynamic limit $L \rightarrow \infty$, we expect the infinite time average to go to zero. The argument for this is as follows. In the extended phase, the values of $A_{m,k}$ will go like $A_{m,k} \sim \frac{1}{\sqrt{L}}$. Which leads to,

$$|\omega_{m,n}|^2 \sim \frac{1}{L}, \quad (21)$$

approaching zero in the thermodynamic limit. This is opposed to the localized phase where we expect, $A_{m,k} \sim e^{-|k-m|/\xi}$, with ξ the localization length and $k = 1, \dots, L$ [73] (see lemma 8.1). This makes the infinite time average go like,

$$|\omega_{m,n}|^2 \sim \max_k e^{-(|k-m| + |k-n|)/\xi}, \quad (22)$$

Hence, the infinite time average of the OTOC is in this case non-zero within a distance of the order of the localization length.

Next we focus on bounding the relaxation process in time, following [74–76]. To study the relaxation we define the positive function,

$$g_{m,n}(t) = \left| |a_{m,n}(t)|^2 - |\omega_{m,n}|^2 \right|^2. \quad (23)$$

Eq. (23) can be interpreted as the distance the OTOC is from its late time value, assuming such a value exists. To be precise we will work with the time average of the function,

$$\langle g_{m,n}(t) \rangle_T = \frac{1}{T} \int_0^T \left| \sum_{k \neq l} A_{m,k} A_{n,k} A_{m,l} A_{n,l} e^{i(\epsilon_k - \epsilon_l)t} \right|^2 dt, \quad (24)$$

to make notation easier let $\alpha = (k, l)$ and,

$$v_\alpha = A_{m,k} A_{n,k} A_{m,l} A_{n,l}, \quad G_\alpha = \epsilon_k - \epsilon_l. \quad (25)$$

This allows us to instead write the expression as,

$$\langle g_{m,n}(t) \rangle_T = \frac{1}{T} \int_0^T \sum_{\alpha \neq \beta} v_\alpha v_\beta e^{i(G_\alpha - G_\beta)t} dt, \quad (26)$$

Since Eq. (23) is a positive function we can use the so-called Lorentzian profile trick [74],

$$\langle g_{m,n}(t) \rangle_T \leq \frac{5\pi}{4} \int_{-\infty}^{\infty} \frac{g_{m,n}(t)T}{T^2 + (t-T/2)^2} \frac{dt}{\pi} = \frac{5\pi}{4} \langle g_{m,n}(t) \rangle_{L_T} \quad (27)$$

Next using the identity, $|\langle e^{i(G_\alpha - G_\beta)t} \rangle_{L_T}| = e^{-|G_\alpha - G_\beta|T}$, we arrive at,

$$\langle g_{m,n}(t) \rangle_T \leq \frac{5\pi}{4} \sum_{\alpha \neq \beta} v_\alpha v_\beta e^{-|G_\alpha - G_\beta|T}. \quad (28)$$

We make use of the triangle inequality to make all elements of the sum positive, and then normalize, defining, $Q = \sum_\alpha |v_\alpha|$,

$$\langle g_{m,n}(t) \rangle_T \leq \frac{5\pi Q^2}{4} \sum_{\alpha \neq \beta} p_\alpha p_\beta e^{-|G_\alpha - G_\beta|T}. \quad (29)$$

It is important to consider how big Q might be. Trivially, $Q \leq \sum_\alpha \max_\alpha |v_\alpha|$. Since this sum over α is quadratic in L and since from Eq. (25) may write $\max_\alpha |v_\alpha| \sim \frac{1}{L^2}$, it then follows that $Q = O(1)$.

We now introduce the function,

$$\xi_p(x) = \max_\beta \sum_{\alpha: G_\beta \in [G_\alpha, G_\alpha + x]} p_\alpha \quad (30)$$

$$a(\epsilon) = \frac{\xi_p(\epsilon)}{\epsilon} \sigma_G, \quad \delta(\epsilon) = \xi_p(\epsilon), \quad (31)$$

where $\sigma_G = \sqrt{\sum_\alpha p_\alpha G_\alpha^2 - (\sum_\alpha p_\alpha G_\alpha)^2}$ is the standard deviation of our distribution of frequencies. From here on we assume $a(\epsilon)$ and $\delta(\epsilon)$ are implicitly dependent on m, n . It can be shown that [74, 75]:

$$\xi_p(x) \leq \frac{a(\epsilon)}{\sigma_G} x + \delta(\epsilon). \quad (32)$$

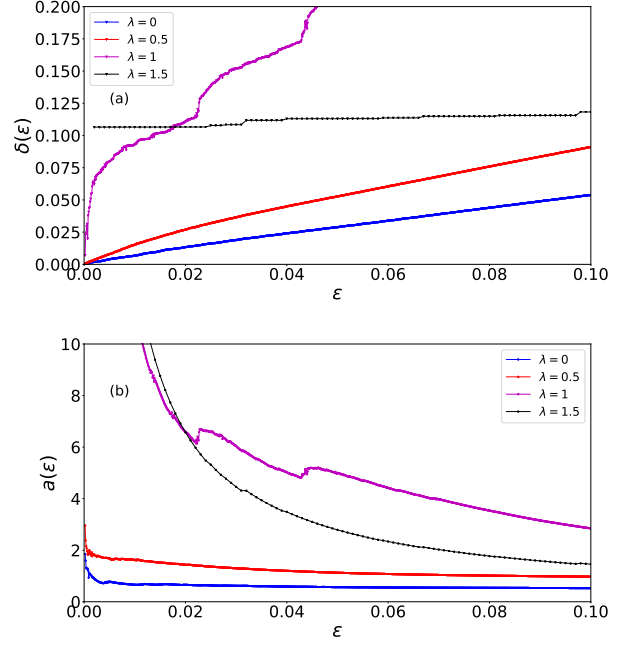


Figure 6. Numerical example of $\delta(\epsilon)$ (panel (a)) and $a(\epsilon)$ (panel (b)) at different system sizes and potential strength for $m = \frac{L}{2}$, $n = \frac{L}{2} + 6$, for $L = 800$.

Using this result along with proposition 5 of [75] (for a similar statement see theorem 6) we finally arrive at:

$$\langle g_{m,n}(t) \rangle_T \leq 4\pi Q^2 \xi_p \left(\frac{1}{T} \right). \quad (33)$$

Using Eq. (32) we can rewrite this as:

$$\langle g_{m,n}(t) \rangle_T \leq 4\pi Q^2 \left(\frac{a(\epsilon)}{\sigma_G T} + \delta(\epsilon) \right). \quad (34)$$

Eq. 34 allows us to upper bound the time scale at which the OTOC equilibrates as $T_{eq} = \frac{\pi a(\epsilon) Q^2}{\sigma_G}$. Now all that is left to numerically show that δ is quite small. In Fig. 6 we show our results for $a(\epsilon)$ and $\delta(\epsilon)$ at different system sizes and potential strength. From these results we can conclude that the bound perform poorly in the localized regime, and at the critical point of the model, while in the extended regime the bound appears to perform quite well. For the extended regime it appears we may pick an $a(\epsilon) O(1)$ while picking $\delta \approx 0$, meaning in these cases we expect the OTOC to equilibrate to its infinite time average.

Next we illustrate the bound, Eq. (33), by numerically evaluating $\langle g_{m,n}(t) \rangle_T$ and $\xi(\frac{1}{T})$. Our results are shown in Fig. 7 where we see that, as predicted, the time average defined in Eq. (24) is not only upper bounded by Eq. (33), but as the time interval T is increase this upper bound decays to zero in the extended region. Thus, this constitutes equilibration of an OTOC in both a translationally invariant case ($\lambda = 0$), and a case with a non-zero quasi-periodic potential ($\lambda = 0.5$). This result is expected to hold for $\lambda \in [0, \lambda_{critical})$ where for the

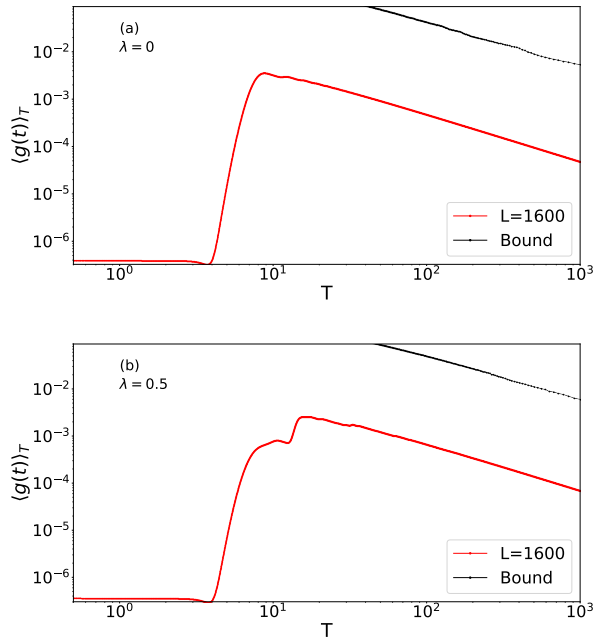


Figure 7. Bound from Eq. (33) for potential strengths $\lambda = 0$ (panel (a)) and $\lambda = 0.5$ (panel (b)). Both results were computed with $L = 1600$ and used $m = \frac{L}{2}$, $n = \frac{L}{2} + 6$, $L = 1600$.

present numerics we have, $\lambda_{\text{critical}} = 1$. Furthermore, we stress that this result should be applicable to *all quadratic models* in their *extended* phases.

Next we consider relaxation in the infinite time limit $T \rightarrow \infty$. Here, the quantity to bound (assuming non-degenerate mode gaps, i.e excluding the localized phase) is,

$$\lim_{T \rightarrow \infty} \langle g_{m,n}(t) \rangle_T = \sum_{k \neq l} A_{m,k}^2 A_{n,k}^2 A_{m,l}^2 A_{n,l}^2. \quad (35)$$

From Eq. (35), using $A_{m,k}^2 \sim \frac{1}{L}$, we see that with four such terms and only a quadratic summation over these terms $\lim_{T \rightarrow \infty} \langle g_{m,n}(t) \rangle_T$ must go to zero in the extended region. To put this into more rigorous terms we may define the constant $c = L \max_k \{A_{m,k}^2, A_{n,k}^2\}$ such that,

$$\lim_{T \rightarrow \infty} \langle g_{m,n}(t) \rangle_T \leq c^4 \sum_{k \neq l} \frac{1}{L^4} \leq \frac{c^4}{L^2}, \quad (36)$$

where c is independent of system size due to the terms $\sqrt{L} A_{m,k} = O(1)$.

IV. MOMENTUM OTOCS

In this section we study the out of time order correlators with momentum number operators, and set,

$$\hat{A}(t) = 2\hat{\eta}_\pi^\dagger(t)\hat{\eta}_\pi(t) - 1, \quad \hat{B} = 2\hat{\eta}_\pi^\dagger\hat{\eta}_\pi - 1. \quad (37)$$

The OTOC then corresponds to the $k = \pi$ momentum operator commuting with itself in time. We make this choice since,

although two momenta k and l could be neighbours in momentum space, this distance isn't physical and no wave front can be defined. The choice of $k = \pi$ is arbitrary but sits in the "middle" of momentum space. To distinguish our results from the previous sections, where real space OTOCs were discussed, we denote the OTOC $C_p(t)$ in this section, suppressing the x dependence of C . The system size throughout this section is set to $L = 400$, no significant differences were observed for systems sizes up to $L = 1200$.

A. Quenching

The momentum OTOCs are studied by quenching from the ground state of the initial Hamiltonian. This is done in a manner identically to section III. First we consider quenching from an initial potential strength $\lambda_i = 0$.

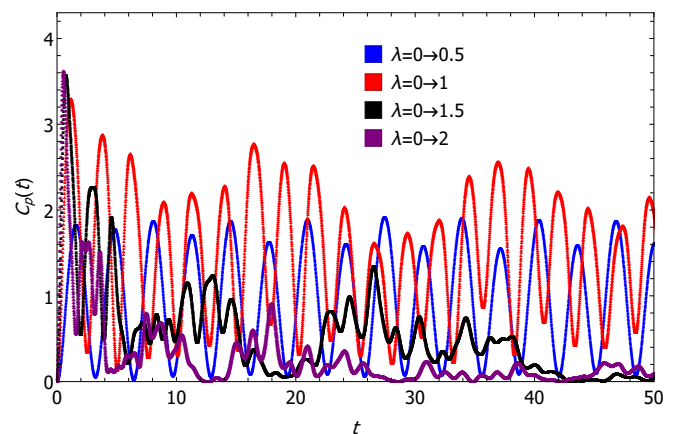


Figure 8. $C_p(t)$ plotted from the dynamics of a ground state of a Hamiltonian characterized by $\lambda_i = 0$ to various final Hamiltonians. This corresponds to quenching from the extended region into the critical point at $\lambda = 1$, extended phase $\lambda = 0.5$ and two examples of the localized phase $\lambda = 1.5, 2$. Results are for $L = 400$.

Fig. 8 shows $C_p(t)$ quenched from the ground state of the Hamiltonian with $\lambda_i = 0$ then quenched and time evolved with new values of $\lambda_f = 0.5, 1, 1.5, 2$. Interestingly, the OTOCs all attain a maximum, at quite early times $t < 4$, and then display a slow decay from the largest value. The localized phase dynamics for potential strengths of $\lambda_f = 1.5, 2$ clearly show that the momentum OTOC eventually decay to zero, and oscillate near it. The extended phase oscillates away from zero, but does not appear to reach it. At the critical point, $\lambda_c = 1$ pronounced oscillations is observed exceeding all other λ_f . The extended state is characterized by oscillations around a fixed non-zero with this value rising with λ_f as it approaches $\lambda_f = \lambda_c$.

As can be clearly seen from Fig. 8, the dynamics are quite complex and it is desirable to understand the asymptotic behaviour at the wavefront, which we can tentatively define as the first occurrence where $C(t)$ decreases. Since the momentum OTOCs are highly non-local in real space the proposed universal form, Eq. (5), is not directly applicable and we there-

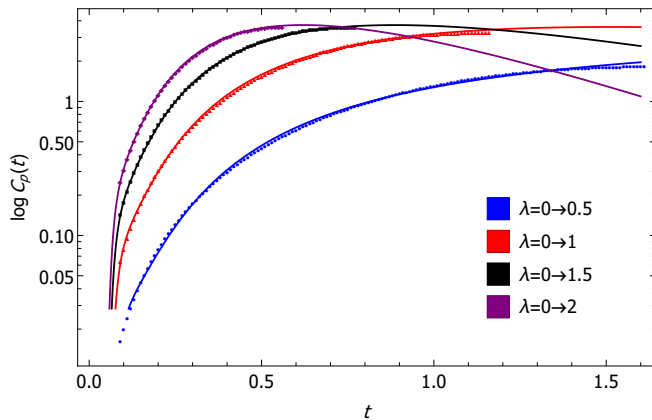


Figure 9. $\log C_p(t)$ plotted from the dynamics of a ground state of a Hamiltonian characterized by $\lambda_i = 0$ to various final Hamiltonians characterized by different λ_f . This data is then fitted to the function, $f(t) = C \exp(at + b/t + c/t^2 + d/t^3)$, which is then graphed. Results are for $L = 400$

fore consider an ad-hoc form

$$f(x) = C \exp(at + b/t + c/t^2 + d/t^3). \quad (38)$$

Results by fitting to the form, Eq. (38) are shown in Fig. 9 for several different values of λ_f . Extremely good fits are obtained and we have verified that adding more terms does not significantly improve the fits.

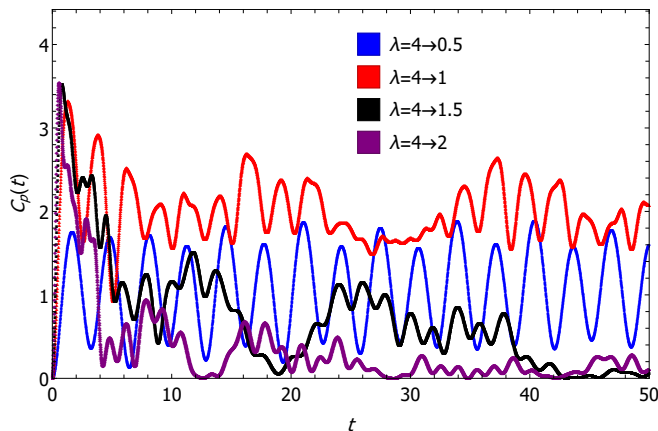


Figure 10. $C_p(t)$ plotted from the dynamics of a ground state of a Hamiltonian characterized by $\lambda = 4$ to various final Hamiltonians. This corresponds to quenching from the extended region into the critical point at $\lambda = 1$, extended phase $\lambda = 0.5$ and two examples of the localized phase $\lambda = 1.5, 2$. Results are for $L = 400$.

Next we consider a different quench where we instead start from the localized phase with $\lambda_i = 4$ and evolve with the four different $\lambda_f = 0.5, 1, 1.5, 2$. Our results for this case are shown in Fig. 10. The oscillations in this case comparably to

quenching from $\lambda_i = 0$ shown in Fig. 8. However, their quasi-periodicity is much smaller and less chaotic. Both examples, $\lambda_i = 0, 4$, are characterized by the same oscillations that appear to never dissipate. However, the wavefront for $\lambda_i = 4$ is near identical to the one shown in Fig. 9 for $\lambda_i = 0$. The same function, Eq. (38), used to fit the results for $\lambda_i = 0$ can be used to characterize the wavefront for $\lambda_i = 4$ producing extremely high quality fits almost indistinguishable from the fits shown in Fig. 9. Thus we conclude that the initial rise of the OTOC goes like Eq. (38) in both quench scenarios. The form given in Eq. (A9) was also observed to hold for momentum OTOCs defined in a thermal states, as well as for initial states in the form of a product state:

$$|\psi\rangle = \prod_{l \in \mathbb{S}} \hat{f}_l^\dagger |0\rangle. \quad (39)$$

where $\mathbb{S} = \{l \in \mathbb{N} : l \bmod 2 = 0\}$. This then allows us to conclude that this form of the wavefront for momentum OTOCs is rather generic, and doesn't depend on initial conditions.

V. CONCLUSION

The AA model with a quasi-periodic potential represents a unique opportunity to investigate quantum information dynamics in the presence of a phase transition between an extended localized phase using exact numerics. Here we have explicitly demonstrated equilibration of the real-space OTOCs to zero in the extended phase of the model, a result that generalizes to any model with quadratic interactions in an extended regime. The early time behavior of the real-space OTOCs are largely independent of the strength of the quasi-periodic potential and follow a simple power-law with position dependent exponent even in the localized phase. The regime close to the classical wavefront, $x = v_B t$, has been shown to propagate as a Gaussian (Eq. 15) with distance dependent parameters which converge to constants in the large distance limit, signifying a fifth time regime of interest for the OTOC. At earlier times $t \ll \frac{x}{v_B}$ it is possible to apply the universal waveform Eq. 5 which is often applied to thermal OTOCs at infinite temperature. The spreading of information in momentum space as obtained from analyzing momentum space OTOCs is significantly more complex and a complete understanding is currently lacking. Here we propose an ad-hoc form for the early time behaviour of the momentum OTOCs that seem to work exceedingly well.

VI. ACKNOWLEDGEMENTS

J.R would like to thank Álvaro M. Alhambra, Luis Pedro García-Pintos and Shenglong Xu for helpful discussions. This research was supported by NSERC and enabled in part by support provided by (SHARCNET) (www.sharcnet.ca) and Compute/Calcul Canada (www.computeCanada.ca).

Appendix A: Time evolution

In this appendix entry we review time evolution of free fermions and present out the numerical method required to carry out of quench protocol. For more detailed treatments of the time evolution of free fermions see [11],[77]. We are given in general a Hamiltonian written in the form,

$$\hat{H} = \sum_{i,j} M_{i,j} \hat{f}_i^\dagger \hat{f}_j. \quad (\text{A1})$$

Where we assume M is real symmetric and thus can be diagonalized with a real orthogonal matrix A such that $M = ADA^\dagger$. This solves the model, and we recover new fermionic operators and a diagonal Hamiltonian,

$$\hat{H} = \sum_k \epsilon_k \hat{d}_k^\dagger \hat{d}_k, \quad (\text{A2})$$

where we refer to ϵ_k as energy eigenmodes which are the entries of the diagonal matrix and the corresponding space, eigenmode space (normal modes is also regularly used). Since the states we are interested in are Gaussian (product states, thermal states, ground states), we can completely deduce all statistics of the model with the occupation matrix. Defining arbitrary fermionic operators as $\hat{b}_k^\dagger, \hat{b}_l$ we define the matrix in b space as,

$$\Lambda_{k,l}^{(b)} = \langle \hat{b}_k^\dagger \hat{b}_l \rangle. \quad (\text{A3})$$

Where the superscript denotes the space we are describing. In this document we refer to real space with f , eigenmode space with d and momentum space with p superscripts. Time evolving individual eigenmodes is easily deduced from Eq. (A2),

$$\hat{d}_k(t) = e^{-i\epsilon_k t} \hat{d}_k. \quad (\text{A4})$$

For the creation operators simply take the Hermitian adjoint. As seen in Eq. (C33), we are interested in time evolving one or two operators in the expectation value. Thus we see that evolving the whole matrix in real space we get,

$$\Lambda^{(f)}(t,t) = A e^{iDt} \Lambda^{(d)} e^{-iDt} A^T. \quad (\text{A5})$$

Where the double time arguments signify we are time evolving both the creation and annihilation part. Similarly the out of time correlations in real space can be calculated from,

$$\Lambda^{(f)}(t,0) = A e^{iDt} \Lambda^{(d)} A^T, \quad \Lambda^{(f)}(0,t) = A \Lambda^{(d)} e^{-iDt} A^T. \quad (\text{A6})$$

From here we can calculate the correlation functions of the momentum operators given by,

$$\eta_k := \frac{1}{\sqrt{L}} \sum_j e^{ikj} \hat{f}_j,$$

$$\eta_k^\dagger := \frac{1}{\sqrt{L}} \sum_j e^{-ikj} \hat{f}_j^\dagger.$$

Then the correlations in momentum space are given by,

$$\Lambda_{k,l}^{(p)} = \sum_{m,n} e^{-i(mk-nl)} \Lambda_{m,n}^{(f)}. \quad (\text{A7})$$

The time evolution is then found by time evolving $\Lambda_{m,n}^{(f)}$ in the desired way. Now all we need to describe is the out of time anti-commutation relations. For the real space operators,

$$\{\hat{f}_m^\dagger(t), \hat{f}_n\} = \sum_k A_{m,k} A_{n,k} e^{i\epsilon_k t} = a_{m,n}(t), \quad (\text{A8})$$

simply taking the conjugate recovers the relationship where \hat{f}_n is time evolved. We also have, $\{\hat{f}_m(t), \hat{f}_n\} = \{\hat{f}_m^\dagger(t), \hat{f}_n^\dagger\} = 0$. For the momentum operators ,

$$\{\eta_k^\dagger(t), \eta_p\} = \frac{1}{L} \sum_{m,n} e^{-i(km-pn)} \left(\hat{f}_m^\dagger(t) \hat{f}_n + \hat{f}_n \hat{f}_m^\dagger(t) \right) = \frac{1}{L} \sum_{m,n} e^{-i(km-pn)} a_{m,n}(t) = u_{k,p}(t). \quad (\text{A9})$$

Eq. (A9) is simply a discrete Fourier transform of Eq. (A8). With these pieces we can now calculate the necessary correlators and out of time anti-commutators for the OTOC.

Appendix B: Quench protocol

We now turn to a discussion of the quench protocol. We define two Hamiltonians written identically to the one written in Eq. (A1), with $\hat{H}^{(1)}$ and $\hat{H}^{(2)}$. We first prepare the ground state of $\hat{H}^{(1)}$ by diagonalizing $M^{(1)}$, let $\epsilon_k^{(1)}$ be its eigenvalues, and preparing the eigenmode state with,

$$\Lambda_{k,l}^{(d,1)} = \langle \hat{d}_k^\dagger \hat{d}_l \rangle = \begin{cases} 1 & k = l \wedge \epsilon_k^{(1)} < 0 \\ 0 & \text{otherwise.} \end{cases} \quad (\text{B1})$$

Note that in some cases we might have $\epsilon_k^{(1)} = 0$ for some value of k , making the ground state degenerate. We then choose to construct the ground state which only has negative eigenmodes occupied and neglect the zero. We then transform the occupation matrix to real space,

$$\Lambda^{(f)}(0,0) = A^{(1)T} \Lambda^{(d,1)} A^{(1)}. \quad (\text{B2})$$

This gives us the initial correlation functions. Next we imagine suddenly changing the Hamiltonian to $\hat{H}^{(2)}$. We can now find this states representation in the eigenmode of the new Hamiltonian by using its orthogonal transform, $\Lambda^{(d,2)} = A^{(2)T} \Lambda^{(f)} A^{(2)}$. Thus the time evolution we are interested in is written as,

$$\Lambda^{(f)}(t,t) = A^{(2)} e^{iD^{(2)}t} \Lambda^{(d,2)} e^{-iD^{(2)}t} A^{(2)T}, \quad (\text{B3})$$

$$\Lambda^{(f)}(t,0) = A^{(2)} e^{iD^{(2)}t} \Lambda^{(d,2)} A^{(2)T}, \quad (\text{B4})$$

$$\Lambda^{(f)}(0,t) = A^{(2)} \Lambda^{(d,2)} e^{-iD^{(2)}t} A^{(2)T}. \quad (\text{B5})$$

This representation allows us to compute statistic we could be interested in for a Gaussian state.

Appendix C: Calculating the OTOCs

Here we present the calculation of the OTOCs in terms of second moments. In all three cases we are interested in; product states, thermal states and ground states, are Gaussian. Thus we can use Wick's theorem to calculate the OTOC. This is done similarly to [11]. Here we present the derivation for $F_b(x,t)$ for arbitrary lattice points and fermionic operators. Consider arbitrary fermionic operators \hat{b}_i such that $\{\hat{b}_k, \hat{b}_l\} = \{\hat{b}_k^\dagger, \hat{b}_l^\dagger\} = 0$, $\{\hat{b}_l^\dagger, \hat{b}_k\} = \delta_{l,k}$ and $a_{m,n}(t) = \{\hat{b}_m^\dagger(t), \hat{b}_n\}$, where we assume $\{\hat{b}_m(t), \hat{b}_n\} = \{\hat{b}_m^\dagger(t), \hat{b}_n^\dagger\} = 0$. Then we are interested in the real part of the function,

$$F_b(x,t) = \left\langle \left(\hat{b}_i^\dagger(t) \hat{b}_i(t) - \frac{1}{2} \right) \left(\hat{b}_j^\dagger \hat{b}_j - \frac{1}{2} \right) \left(\hat{b}_i^\dagger(t) \hat{b}_i(t) - \frac{1}{2} \right) \left(\hat{b}_j^\dagger \hat{b}_j - \frac{1}{2} \right) \right\rangle. \quad (\text{C1})$$

Adopting the notation $\hat{n}_i = \hat{b}_i^\dagger \hat{b}_i$ and using $\hat{n}_i(t)^2 = n_i(t)$ we can write,

$$F(t) = 16 \langle \hat{n}_i(t) \hat{n}_j \hat{n}_i(t) \hat{n}_j - \frac{1}{2} (\hat{n}_i(t) \hat{n}_j \hat{n}_i(t) + \hat{n}_j \hat{n}_i(t) \hat{n}_j) + \frac{1}{4} (\hat{n}_j \hat{n}_i(t) - \hat{n}_i(t) \hat{n}_j) + \frac{1}{16} \rangle. \quad (\text{C2})$$

Here we present the derivation for the thermal state, but since all states considered are Gaussian the end result will be equivalent. Throughout the derivation we abuse the fact that $\hat{b}_i^2 = (\hat{b}_i^\dagger)^2 = 0$, the out of time anti-commutation rules, and assuming

that each \hat{b}_k is a linear combination of \hat{d}_l terms only. Now we can focus on treating each term based on our initial conditions as before. Let us deal with each term of $F(t)$ individually. First consider the fourth order correlations,

$$\langle \hat{n}_j \hat{n}_i(t) - \hat{n}_i(t) \hat{n}_j \rangle_\beta. \quad (\text{C3})$$

Let us derive a rule to contract these fourth moments. Consider,

$$\langle \hat{n}_i(t) \hat{n}_j \rangle_\beta = \langle \hat{b}_i^\dagger(t) \hat{b}_i(t) \hat{b}_j^\dagger \hat{b}_j \rangle_\beta = \sum_{m,n,k,l} A_{i,k} A_{i,l} A_{j,m} A_{j,n} e^{i(\epsilon_k - \epsilon_l t)} \langle \hat{d}_k^\dagger \hat{d}_l \hat{d}_m^\dagger \hat{d}_n \rangle_\beta. \quad (\text{C4})$$

Using the fact that,

$$\Lambda_{k,l}^{d,\beta} = \langle \hat{d}_k^\dagger \hat{d}_l \rangle_\beta = \begin{cases} \frac{1}{1+e^{\beta\epsilon_k}} & k=l, \\ 0 & \text{otherwise.} \end{cases} \quad (\text{C5})$$

$$\text{tr} \left(\hat{d}_k^\dagger \hat{d}_l \hat{d}_m^\dagger \hat{d}_n \rho_\beta \right) = \delta_{k,l} \text{tr}(\hat{d}_m^\dagger \hat{d}_n \rho_\beta) + \delta_{k,n} \text{tr}(\hat{d}_l \hat{d}_m^\dagger \rho_\beta) - \text{tr}(\hat{d}_l \hat{d}_m^\dagger \hat{d}_n \hat{d}_k^\dagger \rho_\beta). \quad (\text{C6})$$

Using $e^{-\beta\epsilon_k \hat{n}_k} \hat{d}_k^\dagger = e^{-\beta\epsilon_k} \hat{d}_k^\dagger e^{-\beta\epsilon_k \hat{n}_k}$ we get,

$$(1 + e^{\beta\epsilon_k}) \text{tr} \left(\hat{d}_k^\dagger \hat{d}_l \hat{d}_m^\dagger \hat{d}_n \rho_\beta \right) = \delta_{k,l} \text{tr}(\hat{d}_m^\dagger \hat{d}_n \rho_\beta) + \delta_{k,n} \text{tr}(\hat{d}_l \hat{d}_m^\dagger \rho_\beta), \quad (\text{C7})$$

$$\implies \text{tr} \left(\hat{d}_k^\dagger \hat{d}_l \hat{d}_m^\dagger \hat{d}_n \rho_\beta \right) = \langle \hat{d}_k^\dagger \hat{d}_l \rangle \text{tr}(\hat{d}_m^\dagger \hat{d}_n \rho_\beta) + \langle \hat{d}_k^\dagger \hat{d}_n \rangle \text{tr}(\hat{d}_l \hat{d}_m^\dagger \rho_\beta). \quad (\text{C8})$$

This then gives,

$$\langle \hat{n}_i(t) \hat{n}_j \rangle_\beta = \langle \hat{b}_i^\dagger(t) \hat{b}_i(t) \rangle_\beta \langle \hat{b}_j^\dagger \hat{b}_j \rangle_\beta + \langle \hat{b}_i^\dagger(t) \hat{b}_j \rangle_\beta \langle \hat{b}_i(t) \hat{b}_j^\dagger \rangle_\beta. \quad (\text{C9})$$

Similarly,

$$\langle \hat{n}_j \hat{n}_i(t) \rangle_\beta = \langle \hat{b}_j^\dagger \hat{b}_j \rangle_\beta \langle \hat{b}_i^\dagger(t) \hat{b}_i(t) \rangle_\beta + \langle \hat{b}_j^\dagger \hat{b}_i(t) \rangle_\beta \langle \hat{b}_j \hat{b}_i^\dagger(t) \rangle_\beta \quad (\text{C10})$$

From here we see that,

$$\langle \hat{n}_j \hat{n}_i(t) \rangle_\beta - \langle \hat{n}_i(t) \hat{n}_j \rangle_\beta = \langle \hat{b}_j^\dagger \hat{b}_i(t) \rangle_\beta \langle \hat{b}_j \hat{b}_i^\dagger(t) \rangle_\beta - \langle \hat{b}_i^\dagger(t) \hat{b}_j \rangle_\beta \langle \hat{b}_i(t) \hat{b}_j^\dagger \rangle_\beta, \quad (\text{C11})$$

$$= \langle \hat{b}_j^\dagger \hat{b}_i(t) \rangle_\beta \left(a_{i,j}(t) - \langle \hat{b}_i^\dagger(t) \hat{b}_j \rangle_\beta \right) - \langle \hat{b}_i^\dagger(t) \hat{b}_j \rangle_\beta \left(\bar{a}_{i,j}(t) - \langle \hat{b}_j^\dagger \hat{b}_i(t) \rangle_\beta \right) = a_{i,j}(t) \langle \hat{b}_j^\dagger \hat{b}_i(t) \rangle_\beta - \bar{a}_{i,j}(t) \langle \hat{b}_i^\dagger(t) \hat{b}_j \rangle_\beta, \quad (\text{C12})$$

this is however a purely imaginary number and therefore does not contribute to the OTOC. Now the sixth order term,

$$\hat{n}_j \hat{n}_i(t) \hat{n}_j = \hat{b}_j^\dagger \hat{b}_j \hat{b}_i^\dagger(t) \hat{b}_i(t) \hat{b}_j^\dagger \hat{b}_j, \quad (\text{C13})$$

$$= \hat{b}_j^\dagger \left(a_{i,j}(t) - \hat{b}_i^\dagger(t) \hat{b}_j \right) \hat{b}_i(t) \hat{b}_j^\dagger \hat{b}_j, \quad (\text{C14})$$

$$= a_{i,j}(t) \hat{b}_j^\dagger \hat{b}_i(t) \hat{b}_j^\dagger \hat{b}_j - \hat{b}_j^\dagger \hat{b}_i^\dagger(t) \hat{b}_j \hat{b}_i(t) \hat{b}_j^\dagger \hat{b}_j, \quad (\text{C15})$$

$$= a_{i,j} \hat{b}_j^\dagger \left(\bar{a}_{i,j}(t) - \hat{b}_j^\dagger \hat{b}_i(t) \right) \hat{b}_j + \hat{b}_j^\dagger \hat{b}_i^\dagger(t) \hat{b}_i(t) \hat{b}_j \hat{b}_j^\dagger \hat{b}_j, \quad (\text{C16})$$

$$|a_{i,j}|^2 \hat{b}_j^\dagger \hat{b}_j + \hat{b}_j^\dagger \hat{b}_i^\dagger(t) \hat{b}_i(t) \left(1 - \hat{b}_j^\dagger \hat{b}_j \right) \hat{b}_j, \quad (\text{C17})$$

$$= |a_{i,j}|^2 \hat{b}_j^\dagger \hat{b}_j + \hat{b}_j^\dagger \hat{b}_i^\dagger(t) \hat{b}_i(t) \hat{b}_j. \quad (\text{C18})$$

Then applying the expectation value,

$$|a_{i,j}|^2 \langle \hat{b}_i^\dagger(t) \hat{b}_i(t) \rangle_\beta + \langle \hat{b}_i^\dagger(t) \hat{b}_j^\dagger \hat{b}_j \hat{b}_i(t) \rangle_\beta, \quad (\text{C19})$$

$$= |a_{i,j}|^2 \langle \hat{b}_i^\dagger(t) \hat{b}_i(t) \rangle_\beta + \sum_{m,n,k,l} A_{i,k} A_{j,l} A_{j,m} A_{i,n} e^{i(\epsilon_k - \epsilon_n t)} \langle \hat{d}_k^\dagger \hat{d}_l \hat{d}_m^\dagger \hat{d}_n \rangle_\beta, \quad (\text{C20})$$

$$= |a_{i,j}|^2 \langle \hat{b}_i^\dagger(t) \hat{b}_i(t) \rangle_\beta + \sum_{m,n,k,l} A_{i,k} A_{j,l} A_{j,m} A_{i,n} e^{i(\epsilon_k - \epsilon_n t)} \left(-\langle \hat{d}_k^\dagger \hat{d}_m \rangle_\beta \langle \hat{d}_l \hat{d}_n \rangle_\beta + \langle \hat{d}_k^\dagger \hat{d}_n \rangle_\beta \langle \hat{d}_l \hat{d}_m \rangle_\beta \right), \quad (\text{C21})$$

$$= |a_{i,j}|^2 \langle \hat{b}_i^\dagger(t) \hat{b}_i(t) \rangle_\beta + \langle \hat{b}_j^\dagger \hat{b}_j \rangle_\beta \langle \hat{b}_i(t) \hat{b}_i(t) \rangle_\beta - \langle \hat{b}_j^\dagger \hat{b}_i(t) \rangle_\beta \langle \hat{b}_i^\dagger(t) \hat{b}_j \rangle_\beta \quad (\text{C22})$$

Next we look at the other 6th moment,

$$\hat{n}_i(t)\hat{n}_j\hat{n}_i(t) = \hat{b}_i^\dagger(t)\hat{b}_i(t)\hat{b}_j^\dagger\hat{b}_j\hat{b}_i^\dagger(t)\hat{b}_i(t). \quad (\text{C23})$$

The strategy here is identical, and we arrive at,

$$\hat{n}_i(t)\hat{n}_j\hat{n}_i(t) = |a_{i,j}|^2\hat{b}_i^\dagger(t)\hat{b}_i(t) + \hat{b}_i^\dagger(t)\hat{b}_j^\dagger\hat{b}_j\hat{b}_i^\dagger(t). \quad (\text{C24})$$

Applying the thermal expectation value,

$$\langle\hat{n}_i(t)\hat{n}_j\hat{n}_i(t)\rangle_\beta = |a_{i,j}|^2\langle\hat{b}_i^\dagger(t)\hat{b}_i(t)\rangle_\beta + \langle\hat{b}_i^\dagger(t)\hat{b}_j^\dagger\hat{b}_j\hat{b}_i^\dagger(t)\rangle_\beta, \quad (\text{C25})$$

$$= |a_{i,j}|^2\langle\hat{b}_i^\dagger(t)\hat{b}_i(t)\rangle_\beta + \langle\hat{b}_j^\dagger\hat{b}_j\rangle_\beta\langle\hat{b}_i(t)\hat{b}_i(t)\rangle_\beta - \langle\hat{b}_j^\dagger\hat{b}_i(t)\rangle_\beta\langle\hat{b}_i^\dagger(t)\hat{b}_j\rangle_\beta. \quad (\text{C26})$$

So we finally need the eighth order term which is made easier by knowing the results from the 6th order terms,

$$\hat{n}_i(t)\hat{n}_j\hat{n}_i(t)\hat{n}_j = \hat{b}_i^\dagger(t)\hat{b}_i(t)\left(\hat{b}_j^\dagger\hat{b}_j\hat{b}_i^\dagger(t)\hat{b}_i(t)\hat{b}_j^\dagger\hat{b}_j\right), \quad (\text{C27})$$

$$= \hat{b}_i^\dagger(t)\hat{b}_i(t)\left(|a_{i,j}(t)|^2\hat{b}_j^\dagger\hat{b}_j + \hat{b}_j^\dagger\hat{b}_i^\dagger(t)\hat{b}_i(t)\hat{b}_j\right), \quad (\text{C28})$$

$$= |a_{i,j}(t)|^2\hat{b}_i^\dagger(t)\hat{b}_i(t)\hat{b}_j^\dagger\hat{b}_j + \hat{b}_i^\dagger(t)\hat{b}_i(t)\hat{b}_j^\dagger\hat{b}_i^\dagger(t)\hat{b}_i(t)\hat{b}_j, \quad (\text{C29})$$

$$= |a_{i,j}(t)|^2\hat{b}_i^\dagger(t)\hat{b}_i(t)\hat{b}_j^\dagger\hat{b}_j + \hat{b}_j^\dagger\hat{b}_i^\dagger(t)\hat{b}_i(t)\hat{b}_j. \quad (\text{C30})$$

Now, taking the thermal expectation value we can use previous results, (the first term is from the fourth moments, and second from the sixth),

$$= |a_{i,j}(t)|^2\langle\hat{b}_i^\dagger(t)\hat{b}_i(t)\rangle_\beta\langle\hat{b}_j^\dagger\hat{b}_j\rangle_\beta + \langle\hat{b}_i^\dagger(t)\hat{b}_j\rangle_\beta\langle\hat{b}_i(t)\hat{b}_j^\dagger\rangle_\beta + \langle\hat{b}_i^\dagger(t)\hat{b}_i(t)\rangle_\beta\langle\hat{b}_j^\dagger\hat{b}_j\rangle_\beta - \langle\hat{b}_i^\dagger(t)\hat{b}_j\rangle_\beta\langle\hat{b}_j^\dagger\hat{b}_i(t)\rangle_\beta, \quad (\text{C31})$$

$$= |a_{i,j}(t)|^2\langle\hat{b}_i^\dagger(t)\hat{b}_i(t)\rangle_\beta\langle\hat{b}_j^\dagger\hat{b}_j\rangle_\beta + \langle\hat{b}_i^\dagger(t)\hat{b}_j\rangle_\beta\langle\bar{a}_{i,j}(t) - \hat{b}_j^\dagger\hat{b}_i(t)\rangle_\beta + \langle\hat{b}_i^\dagger(t)\hat{b}_i(t)\rangle_\beta\langle\hat{b}_j^\dagger\hat{b}_j\rangle_\beta - \langle\hat{b}_i^\dagger(t)\hat{b}_j\rangle_\beta\langle\hat{b}_j^\dagger\hat{b}_i(t)\rangle_\beta \quad (\text{C32})$$

Grouping everything together finally gives us,

$$F_b(x, t) = 16|a_{i,j}(t)|^2\left(\langle\hat{b}_i^\dagger(t)\hat{b}_i(t)\rangle_\beta\langle\hat{b}_j^\dagger\hat{b}_j\rangle_\beta - \frac{1}{2}\left(\langle\hat{b}_i^\dagger(t)\hat{b}_i(t)\rangle_\beta + \langle\hat{b}_j^\dagger\hat{b}_j\rangle_\beta\right) + \bar{a}_{i,j}(t)\langle\hat{b}_i^\dagger(t)\hat{b}_j\rangle_\beta - \langle\hat{b}_i^\dagger(t)\hat{b}_j\rangle_\beta\langle\hat{b}_j^\dagger\hat{b}_i(t)\rangle_\beta\right) \quad (\text{C33})$$

Note in the case of product states this form is significantly reduced and in the case of the ground state, one can simply drop the thermal expectation values. This form is general and recovers both cases used in [11].

-
- [1] J. Maldacena, S. H. Shenker, and D. Stanford, *Journal of High Energy Physics* **2016**, 106 (2016).
[2] B. Yoshida, (2019), arXiv:1902.09763.
[3] B. Swingle and D. Chowdhury, *Phys. Rev. B* **95**, 060201 (2017).
[4] J. R. González Alonso, N. Yunger Halpern, and J. Dressel, *Phys. Rev. Lett.* **122**, 040404 (2019).
[5] B. Yan, L. Cincio, and W. H. Zurek, (2019), arXiv:1903.02651.
[6] J. Tuziemski, (2019), arXiv:1903.05025.
[7] D. Mao, D. Chowdhury, and T. Senthil, (2019), arXiv:1903.10499.
[8] R. J. Lewis-Swan, A. Safavi-Naini, J. J. Bollinger, and A. M. Rey, *Nature Communications* **10**, 1581 (2019).
[9] S. Nakamura, E. Iyoda, T. Deguchi, and T. Sagawa, “Universal scrambling in gapless quantum spin chains,” (2019), arXiv:1904.09778.
[10] A. Bohrdt, C. B. Mendl, M. Endres, and M. Knap, *New Journal of Physics* **19**, 063001 (2017).
[11] J. Riddell and E. S. Sørensen, *Phys. Rev. B* **99**, 054205 (2019).
[12] R. Fan, P. Zhang, H. Shen, and H. Zhai, *Science Bulletin* **62**, 707 (2017).
[13] V. Alba and P. Calabrese, arXiv.org (2019), 1903.09176.
[14] J. Lee, D. Kim, and D. H. Kim, (2018), arXiv:1812.00357.
[15] X. Chen, T. Zhou, D. A. Huse, and E. Fradkin, *Annalen der Physik* **529**, 1600332 (2017).
[16] B. Swingle, G. Bentsen, M. Schleier-Smith, and P. Hayden, *Phys. Rev. A* **94**, 040302 (2016).
[17] G. Zhu, M. Hafezi, and T. Grover, *Phys. Rev. A* **94**, 062329 (2016).
[18] N. Y. Yao, F. Grusdt, B. Swingle, M. D. Lukin, D. M. Stamper-Kurn, J. E. Moore, and E. A. Demler, (2016), arXiv:1607.01801.
[19] I. Danshita, M. Hanada, and M. Tezuka, *Progress of Theoretical and Experimental Physics* **2017** (2017), 10.1093/ptep/ptx108, <http://oup.prod.sis.lan/ptep/article-pdf/2017/8/083I01/19650704/ptx108.pdf>.
[20] M. Gärttner, J. G. Bohnet, A. Safavi-Naini, M. L. Wall, J. J. Bollinger, and A. M. Rey, *Nature Physics* **13**, 781 (2017).
[21] J. Li, R. Fan, H. Wang, B. Ye, B. Zeng, H. Zhai, X. Peng, and J. Du, *Phys. Rev. X* **7**, 031011 (2017).
[22] K. A. Landsman, C. Figgatt, T. Schuster, N. M. Linke, B. Yoshida, N. Y. Yao, and C. Monroe, *Nature Publishing Group* **567**, 1 (2019).
[23] W. Miller, *Symmetry Groups and Their Applications*, Computer

- Science and Applied Mathematics (Academic Press, 1972).
- [24] B. Dóra and R. Moessner, *Phys. Rev. Lett.* **119**, 026802 (2017).
- [25] D. A. Roberts and B. Swingle, *Phys. Rev. Lett.* **117**, 091602 (2016).
- [26] X. Chen, T. Zhou, and C. Xu, *Journal of Statistical Mechanics: Theory and Experiment* **2018**, 073101 (2018).
- [27] C.-J. Lin and O. I. Motrunich, *Phys. Rev. B* **97**, 144304 (2018).
- [28] J. Bao and C. Zhang, *arXiv.org* (2019), 1901.09327.
- [29] S. Xu and B. Swingle, *arXiv.org* (2018), 1802.00801.
- [30] V. Khemani, D. A. Huse, and A. Nahum, *Phys. Rev. B* **98**, 144304 (2018).
- [31] A. Nahum, S. Vijay, and J. Haah, *Phys. Rev. X* **8**, 021014 (2018).
- [32] C. W. von Keyserlingk, T. Rakovszky, F. Pollmann, and S. L. Sondhi, *Phys. Rev. X* **8**, 021013 (2018).
- [33] S.-K. Jian and H. Yao, (2018), *arXiv:1805.12299*.
- [34] Y. Gu, X.-L. Qi, and D. Stanford, *Journal of High Energy Physics* **2017**, 125 (2017).
- [35] S. Xu and B. Swingle, *arXiv.org* (2018), 1805.05376v1.
- [36] S. Sahu, S. Xu, and B. Swingle, *arXiv cond-mat.str-el* (2018), 1807.06086.
- [37] T. Rakovszky, F. Pollmann, and C. W. von Keyserlingk, *Phys. Rev. X* **8**, 031058 (2018).
- [38] S. H. Shenker and D. Stanford, *Journal of High Energy Physics* **2014**, 67 (2014).
- [39] A. A. Patel, D. Chowdhury, S. Sachdev, and B. Swingle, *Phys. Rev. X* **7**, 031047 (2017).
- [40] D. Chowdhury and B. Swingle, *Phys. Rev. D* **96**, 065005 (2017).
- [41] Y. Huang, Y.-L. Zhang, and X. Chen, *Annalen der Physik* **529**, 1600318 (2017).
- [42] Y. Chen, *arXiv.org* (2016), *arXiv:1608.02765*.
- [43] R.-Q. He and Z.-Y. Lu, *Phys. Rev. B* **95**, 054201 (2017).
- [44] D. A. Roberts and B. Yoshida, *Journal of High Energy Physics* **2017**, 121 (2017).
- [45] Y. Huang, F. G. S. L. Brandao, and Y.-L. Zhang, (2017), *arXiv:1705.07597*.
- [46] Y. Chen, *arXiv.org* (2016), *arXiv:1608.02765*.
- [47] J. K. Max McGinley, Andreas Nunnenkamp, *arXiv.org* (2018), 1807.06039.
- [48] B.-B. Wei, G. Sun, and M.-J. Hwang, (2019), 1906.00533.
- [49] S. Aubry and G. Andr, *Proceedings, VIII International Colloquium on Group-Theoretical Methods in Physics* **3** (1980).
- [50] H. Hiramoto and M. Kohmoto, *Physical Review B* **40**, 8225 (1989).
- [51] C. Aulbach, A. Wobst, G.-L. Ingold, P. Hänggi, and I. Varga, *New Journal Of Physics* **6**, 70 (2004).
- [52] D. J. Boers, B. Goedeke, D. Hinrichs, and M. Holthaus, *Phys. Rev. A* **75**, 063404 (2007).
- [53] M. Modugno, *New Journal Of Physics* **11**, 033023 (2009).
- [54] M. Albert and P. Leboeuf, *Phys. Rev. A* **81**, 013614 (2010).
- [55] P. Ribeiro, M. Haque, and A. Lazarides, *Phys. Rev. A* **87**, 043635 (2013).
- [56] C. Danieli, K. Rayanov, B. Pavlov, G. Martin, and S. Flach, *International Journal of Modern Physics B* **29**, 1550036 (2015).
- [57] X. Wang and P. Tong, *Journal of Statistical Mechanics: Theory and Experiment* **2017**, 113107 (2017).
- [58] X. Li, X. Li, and S. Das Sarma, *Phys. Rev. B* **96**, 085119 (2017).
- [59] A. J. Martínez, M. A. Porter, and P. G. Kevrekidis, *Philosophical Transactions of the Royal Society A: Mathematical, Physical and Engineering Sciences* **376**, 20170139 (2018).
- [60] G. A. D. Castro and R. Paredes, *European Journal of Physics* (2019).
- [61] C. Gramsch and M. Rigol, *Phys. Rev. A* **86**, 053615 (2012).
- [62] G. Roati, C. D’Errico, L. Fallani, M. Fattori, C. Fort, M. Zaccanti, G. Modugno, M. Modugno, and M. Inguscio, *Nature* **453**, 895 (2008).
- [63] B. Deissler, M. Zaccanti, G. Roati, C. D’Errico, M. Fattori, M. Modugno, G. Modugno, and M. Inguscio, *Nature Physics* **6**, 354 (2010).
- [64] E. Lucioni, B. Deissler, L. Tanzi, G. Roati, M. Zaccanti, M. Modugno, M. Larcher, F. Dalfovo, M. Inguscio, and G. Modugno, *Physical Review Letters* **106**, 133 (2011).
- [65] L. Fallani, J. E. Lye, V. Guarrera, C. Fort, and M. Inguscio, *Physical Review Letters* **98**, 39 (2007).
- [66] M. Schreiber, S. S. Hodgman, P. Bordia, H. P. Lüschen, M. H. Fischer, R. Vosk, E. Altman, U. Schneider, and I. Bloch, *Science* **349**, 842 (2015).
- [67] H. P. Lüschen, P. Bordia, S. S. Hodgman, M. Schreiber, S. Sarkar, A. J. Daley, M. H. Fischer, E. Altman, I. Bloch, and U. Schneider, *Physical Review X* **7**, 37 (2017).
- [68] H. P. Lüschen, P. Bordia, S. Scherg, F. Alet, E. Altman, U. Schneider, and I. Bloch, *Physical Review Letters* **119**, 18 (2017).
- [69] S. Iyer, V. Oganessian, G. Refael, and D. A. Huse, *Phys. Rev. B* **87**, 134202 (2013).
- [70] S. Xu, X. Li, B. Swingle, and S. Das Sarma, *arXiv.org* (2019), 1902.07199.
- [71] P. Coleman, *Introduction to Many-Body Physics* (Cambridge University Press, 2015).
- [72] S. Muralidharan, K. Lochan, and S. Shankaranarayanan, *Phys. Rev. E* **97**, 012142 (2018).
- [73] H. Abdul-Rahman, B. Nachtergaele, R. Sims, and G. Stolz, *Annalen der Physik* **529**, 1600280 (2017).
- [74] A. S. L. Malabarba, L. P. García-Pintos, N. Linden, T. C. Farrelly, and A. J. Short, *Phys. Rev. E* **90**, 012121 (2014).
- [75] L. P. García-Pintos, N. Linden, A. S. L. Malabarba, A. J. Short, and A. Winter, *Phys. Rev. X* **7**, 031027 (2017).
- [76] Álvaro M. Alhambra, J. Riddell, and L. P. García-Pintos, *arXiv:1906.11280* (2019).
- [77] M. Perarnau-Llobet, A. Riera, R. Gallego, H. Wilming, and J. Eisert, *New Journal of Physics* **18**, 123035 (2016).

Chapter 4

Time evolution of correlation functions in quantum many-body systems

In this chapter we present the article [60] which is currently under review by the journal Physical Review letters. The article can be found at arXiv:1906.11280. I am a primary author of this paper, contributing all numerical results, plots and the preliminary proof of theorem 1.

We investigate universal properties of dynamical correlation functions of the form,

$$C(t) = \text{tr} \left(\rho \hat{A}(t) \hat{B} \right), \quad (4.1)$$

where $\rho = \sum_k p_{k,k} |E_k\rangle\langle E_k|$ is a matrix diagonal in the energy eigenbasis and \hat{A}, \hat{B} are observables with finite support on the lattice. The Hamiltonian is assumed to be translationally invariant and local,

$$\hat{H} = \sum_j h_j, \quad (4.2)$$

where h_j acts non-trivially on a finite region. We also assume that the spectrum of the Hamiltonian has non-degenerate energy gaps. The state ρ is assumed to have exponentially decaying correlations of the form,

$$\max_{X \in M, Y \in N} \frac{|\text{tr} \rho X \otimes Y - \text{tr} \rho X \text{tr} \rho Y|}{\|X\| \|Y\|} \leq e^{-\frac{\text{dist}(M, N)}{\xi}}, \quad (4.3)$$

where M, N are regions on the lattice separated by a distance of at least $\text{dist}(M, N)$ and X, Y are operators. These mild assumptions leave us with a generic model away from a phase transition. We rigorously prove the D dimensional statement of the weak ETH found in equation 1.22 and use it to prove the dissipation found in equation 1.39. Following this

we show that the average distance between the correlator and its infinite time average over an infinite interval is extremely small. This statement can be summarized as,

$$\lim_{T \rightarrow \infty} \int_0^T \frac{dt}{T} (C(t) - C_\infty)^2 \leq \|A\| \|B\| \max_{j \neq k} \{|A_{kj} B_{jk}|\} \text{tr} \rho^2. \quad (4.4)$$

We further prove the equilibration of correlation functions $C(t) = \text{tr}(\rho \hat{A}(t) \hat{A})$ in finite time. The rigorous statement can be found in equation 1.12.

Time evolution of correlation functions in quantum many-body systems

Álvaro M. Alhambra,^{1,*} Jonathon Riddell,^{2,†} and Luis Pedro García-Pintos^{3,‡}

¹*Perimeter Institute for Theoretical Physics, Waterloo, ON N2L 2Y5, Canada*

²*Department of Physics & Astronomy, McMaster University 1280 Main St. W., Hamilton ON L8S 4M1, Canada.*

³*Department of Physics, University of Massachusetts, Boston, MA 02125, USA*

(Dated: September 2, 2019)

We give rigorous analytical results on the temporal behavior of two-point correlation functions –also known as dynamical response functions or Green’s functions– in closed many-body quantum systems. We show that in a large class of models the correlation functions factorize at late times $\langle A(t)B \rangle_\beta \rightarrow \langle A \rangle_\beta \langle B \rangle_\beta$, thus proving that dissipation emerges out of the unitary dynamics of the system. We also show that the fluctuations around this late-time value are bounded by the purity of the thermal ensemble, which generally decays exponentially with system size. For auto-correlation functions we provide an upper bound on the timescale at which they reach the factorized late time value. Remarkably, this bound is only a function of local expectation values, and does not increase with system size. We give numerical examples that show that this bound is a good estimate in non-integrable models, and argue that the timescale that appears can be understood in terms of an emergent fluctuation-dissipation theorem. Our study extends to further classes of two point functions such as the symmetrized ones and the Kubo function that appears in linear response theory, for which we give analogous results.

Two-point correlation functions –or dynamical response/Green’s functions– are the central object of the theory of linear response [1], and appear in the characterization of a wide range of non-equilibrium and statistical phenomena in the study of quantum many-body systems and condensed matter physics [2]. This includes different types of scattering and spectroscopy experiments [3], quantum transport [4, 5], and fluctuation-dissipation relations [6–8].

Here we study the time evolution of such correlation functions in isolated systems evolving under unitary dynamics. More precisely, we focus on functions of the form

$$C^{AB}(t) \equiv \langle A(t)B \rangle_\beta = \text{Tr}(\rho A(t)B), \quad (1)$$

where the evolution is generated by a time-independent Hamiltonian H , $\rho \equiv e^{-\beta H}/Z_\beta$ is a thermal state at inverse temperature β with partition function Z_β , and $A(t) = e^{iHt} A e^{-iHt}$ is the evolved observable in the Heisenberg picture. Both A and B are usually taken to be either local (such as a single-site spin) or extensive operators (such as a global current or magnetization).

Two-point correlation functions have been widely studied before, mostly through numerical methods such as exact diagonalization [9], QMC [10] and tensor networks [11–17], and analytical results exist for specific models, e.g. [18–23]). Also, a number of experimental schemes to measure it directly have been proposed [24–28], which manage to circumvent the obstacle of having to measure two non-commuting observables on a single system. Here, we aim to give rigorous analytical results on their dynamical behavior with as few assumptions on

the Hamiltonian as possible. Our results should apply in particular to most non-integrable Hamiltonians, in which the degeneracy of the energy spectrum is small.

First, for arbitrary local observables A and B we give a rigorous proof of the statement that, for late times, the following signature of dissipation occurs in a large class of models

$$\langle A(t)B \rangle_\beta \xrightarrow{t \rightarrow \infty} \langle A \rangle_\beta \langle B \rangle_\beta. \quad (2)$$

Moreover, we show that the fluctuations around the late-time value are in fact bounded by the effective dimension of the ensemble $d_{\text{eff}}^{-1} \equiv \text{Tr}(\rho^2)$, which decays quickly with system size.

For the particular case of auto-correlation functions, when $A = B$, we also derive an upper bound on the timescale at which the factorization of Eq. (2) happens, which, remarkably, is independent of the size of the system. We provide numerical evidence showing that the bound is in fact a good estimate even for moderate system sizes, and becomes tighter as the size increases.

Our study can be extended to a large class of 2-point correlation functions. For instance, for the symmetrized correlation function, we find that its evolution is dominated by a timescale which is at most of the order of $t^2 \sim \frac{\langle A^2 \rangle_\beta}{\langle [A, H][H, A] \rangle_\beta}$. We argue that this can be interpreted in terms of a fluctuation-dissipation theorem that arises from the unitary dynamics of the system. Finally, we consider the timescales of evolution of the Kubo correlation function that appears in linear response theory [1, 7], which dictates the response of a system at equilibrium to a perturbation in its Hamiltonian.

Late-time behaviour — We now show the rigorous formulation of the late-time factorization of 2-point functions. First, we need the following definition.

* aalhambra@perimeterinstitute.ca

† riddeljp@mcmaster.ca

‡ Corresponding author; luis.garciapintos@umb.edu

Definition 1 (Clustering of correlations). *A state ρ on a Euclidean lattice \mathbb{Z}^D has finite correlation length $\xi > 0$ if it holds that*

$$\max_{X \in M, Y \in N} \frac{|\text{Tr}(\rho X \otimes Y) - \text{Tr}(\rho X) \text{Tr}(\rho Y)|}{\|X\| \|Y\|} \leq e^{-\frac{\text{dist}(M, N)}{\xi}}, \quad (3)$$

where M, N are regions on the lattice separated by a distance of at least $\text{dist}(M, N)$, defined on an Euclidean lattice.

This condition is generic of thermal states at finite temperature away from a phase transition. It has been rigorously shown for 1D systems [29], fermionic [30] and arbitrary models above a threshold temperature [31]. We focus on states that obey it, and that are associated to systems with k -local Hamiltonians, i.e. which can be written as $H = \sum_j h_j$, where h_j couples at most k closest neighbors in a D -dimensional Euclidean lattice \mathbb{Z}^D .

Given that the evolution is unitary and the system is finite-dimensional, limits such as $\lim_{t \rightarrow \infty} C^{AB}(t)$ are not well-defined. Instead, we consider the relevant definition of late-time behaviour to be given by the *infinite-time average* of the correlation functions $\lim_{T \rightarrow \infty} \int_0^T \frac{dt}{T} C^{AB}(t)$.

With these considerations, our first main result is the following.

Theorem 1. *Let H be a k -local, translation-invariant, non-degenerate Hamiltonian on a D -dimensional Euclidean lattice of N sites, and let $[\rho, H] = 0$ be an equilibrium ensemble (such as a thermal state) of finite correlation length $\xi > 0$. Let A, B be local observables with support on at most N^α sites, where α is fixed and such that $0 < \alpha < 1/(D+1)$. Then*

$$\lim_{T \rightarrow \infty} \int_0^T C^{AB}(t) \frac{dt}{T} = \text{Tr}(\rho A) \text{Tr}(\rho B) + \mathcal{O}\left(\xi^{\frac{2D}{D+1}} \log^2(N) N^{-\frac{2}{D+1}}\right) \quad (4)$$

The proof, found in Appendix A1, relies on a weak form of the Eigenstate Thermalization Hypothesis (ETH) shown in [32], which is itself based on previous works on large deviation theory for lattice models [33, 34]. This shows that, in fact, any model obeying the weak ETH and without too many degeneracies will display identical factorization of correlation functions at long times [35] (even if it does not necessarily always thermalize).

Note that we assume that the energy spectrum is non-degenerate, which is accurate for systems without non-trivial symmetries or extensive number of conserved quantities. In particular, non-integrable systems usually display Wigner-Dyson statistics in their fine-grained spectrum, which imply level repulsion [8].

This factorization of the correlation function can be thought of as a signature of the emergence of dissipation due to the unitary dynamics, since the lack of correlations at different times indicates the loss of information about an initial perturbation of B at time $t = 0$, as reflected in the observable A at time t [1].

Fluctuations around late-time value — For most times, the 2-point correlation function is in fact close to its late-time average, with small fluctuations around the equilibrium value. In order to prove this, one needs the extra assumption that the energy gaps are non-degenerate, which again is reasonable in non-integrable systems with connected Hamiltonians [8], where it is generally expected to hold as random perturbations are sufficient to lift degeneracies in energy gaps [36].

Let us define $C_\infty^{AB} = \lim_{T \rightarrow \infty} \int_0^T \frac{dt}{T} C^{AB}(t)$, and the average fluctuations around the late-time value as

$$\sigma_C^2 = \lim_{T \rightarrow \infty} \int_0^T \frac{dt}{T} (C^{AB}(t) - C_\infty^{AB})^2. \quad (5)$$

The following result puts an upper bound on this quantity.

Theorem 2. *Let H be a Hamiltonian with non-degenerate energy gaps, such that*

$$E_j - E_k = E_m - E_l \Leftrightarrow j = m, k = l, \quad (6)$$

and let $[\rho, H] = 0$. It holds that

$$\sigma_C^2 \leq \|A\| \|B\| \max_{j \neq k} \{|A_{kj} B_{jk}|\} \text{Tr}(\rho^2). \quad (7)$$

The proof can be found in Appendix A2. It follows the same steps as the main result in [37]. Here, we also find that the purity $\text{Tr}(\rho^2)$, or *effective dimension*, of the equilibrium ensemble plays a key role. For a microcanonical ensemble $\text{Tr}((1/d)^2) = 1/d$, so the RHS of Eq. (7) is expected to decay exponentially with system size in most situations of interest. Also, notice that for a thermal state $\text{Tr}(\rho_\beta^2) \leq 1/Z_\beta$. Moreover, the ETH predicts that $|A_{kj} B_{jk}| \sim 1/d$ [38].

Timescales of equilibration — Theorems 1 and 2 combined imply that correlation functions of the form $\langle A(t)B \rangle_\beta$ are, for most times $t \in [0, \infty]$, close to the uncorrelated average $\langle A \rangle_\beta \langle B \rangle_\beta$, for a wide class of systems. It is expected that the timescale at which this happens may depend on a number of factors, such as the distance between A and B . If the operators are far apart on the lattice the correlations are limited by the Lieb-Robinson bound [39, 40], and timescales associated with ballistic ($\propto N^{1/D}$) or diffusive ($\propto N^{2/D}$) processes may play a role. However, for the autocorrelation function $C^A(t) \equiv \langle A(t)A \rangle_\beta$, we can show that equilibration to the late-time value occurs in a short timescale, independent of system size. There may also be further effects at larger timescales, such as the Thouless time [41, 42], and for those effects our result limits their relative size.

Let us write the state and observable as

$$\rho = \sum_j \rho_{jj} |j\rangle \langle j|, \quad A = \sum_{jk} A_{jk} |j\rangle \langle k|, \quad (8)$$

where ρ_{jj} and A_{jk} are the respective matrix elements in the energy basis. We can then write

$$\frac{C^A(t)}{C^A(0)} = \sum_{jk} \frac{\rho_{jj}|A_{jk}|^2}{C^A(0)} e^{-i(E_j - E_k)t} \equiv \sum_{\alpha} v_{\alpha} e^{-iG_{\alpha}t}, \quad (9)$$

where we denote pairs of levels $\{i, j\}$ by Greek indexes, and the corresponding energy gaps by $G_{\alpha} \equiv E_j - E_k$. The normalized distribution $v_{\alpha} \equiv \frac{\rho_{jj}|A_{jk}|^2}{C^A(0)}$ incorporates information from state and observable, reflecting the energy gaps that are more relevant to the dynamics of the autocorrelation function, and is central to our proofs. Based on it, we define the following functions.

Definition 2. *Given a normalized distribution p_{α} over G_{α} , we define $\xi_p(x)$ as the maximum weight that fits an interval of energy gaps with width x :*

$$\xi_p(x) \equiv \max_{\lambda} \sum_{\alpha: G_{\alpha} \in [G_{\lambda}, G_{\lambda} + x]} p_{\alpha}. \quad (10)$$

We also define

$$a(\epsilon) \equiv \frac{\xi_p(\epsilon)}{\epsilon} \sigma_G, \quad \delta(\epsilon) \equiv \xi_p(\epsilon), \quad (11)$$

where $\sigma_G = \sqrt{\sum_{\alpha} p_{\alpha} G_{\alpha}^2 - (\sum_{\alpha} p_{\alpha} G_{\alpha})^2}$ is the standard deviation of p_{α} .

Our main result regarding the timescales of correlation functions, proven in Appendix [B 1], is:

Theorem 3. *For any Hamiltonian H and state ρ such that $[H, \rho] = 0$, and any observable A , the time correlation function $C^A(t) = \text{Tr}(\rho A(t)A)$ satisfies*

$$\frac{1}{T} \int_0^T \frac{|C^A(t) - C_{\infty}^A|^2}{(C^A(0))^2} dt \leq 4\pi \left(\frac{a(\epsilon)}{\sigma_G} \frac{1}{T} + \delta(\epsilon) \right), \quad (12)$$

where $a(\epsilon)$ and $\delta(\epsilon)$ are as in Definition 2 for the normalized distribution $v_{\alpha} \equiv \frac{\rho_{jj}|A_{jk}|^2}{C^A(0)}$, and σ_G is given by

$$\sigma_G^2 = \frac{1}{C^A(0)} \text{Tr}(\rho[A, H][H, A]) - \frac{\text{Tr}(\rho[H, A]A)^2}{(C^A(0))^2}. \quad (13)$$

Theorem [3] provides an upper bound of $T_{eq} \equiv \frac{4\pi a(\epsilon)}{\sigma_G}$ on the timescales under which autocorrelation functions approach their steady state value. To see this note that, if for a given T the RHS of Eq. (12) is small, $C^A(t)$ must have spent a significant amount of time in $[0, T]$ near the late-time value C_{∞}^A .

For distributions v_{α} that are uniformly spread over many values of the gaps G_{α} , one can always find an ϵ such that $\delta \ll 1$. In that case, the right hand side of Eq. (12) becomes small on timescales $\mathcal{O}(T_{eq})$. As discussed in [43] and Appendix B 4, if one further assumes smooth unimodal distributions, one also finds that $a \sim \mathcal{O}(1)$, so that the timescale is governed by $1/\sigma_G$. Since σ_G is a

combination of expectation values of local observables, it does not change as one increases the size of the system. In fact, a result of [44] shows that a timescale similar to $1/\sigma_G$ is a lower bound to the timescale of equilibration, which strongly suggests that our upper bound is tight when the conditions on a and δ hold.

As a prime example, for local operators in non-integrable lattice models, in which (as per the ETH) $|A_{jk}|$ are uniformly distributed around a peak at zero energy gap [45, 46], one should be able to choose ϵ such that $a \sim \mathcal{O}(1)$ and $\delta \ll 1$. In Fig. 1 we numerically show that this is indeed the case in a non-integrable Ising model.

Theorem 3 does not make assumptions on the specifics of the Hamiltonian, the observable or the state, making it completely general. However, we do not expect the correlation functions to equilibrate well in all cases, as in some scenarios a and δ will be large—for instance, due to degeneracies—in which case the RHS of Eq. (12) may not become small within reasonable timescales. To illustrate this, in Appendix C 1 we compute these parameters in an integrable model, where we see that the gap degeneracies of the model negatively affect the quantities $a(\epsilon)$ and $\delta(\epsilon)$, making the estimated equilibration timescales longer.

Symmetric correlation functions — The previous results can be extended to other correlation functions, such as

$$C_s^A(t) \equiv \frac{1}{2} \text{Tr}(\rho \{A, A(t)\}) = \frac{C^A(t) + C^A(t)^*}{2}. \quad (14)$$

Along the same lines of Theorem [3], in Appendix [B 2] we prove the following.

Theorem 4. *For any Hamiltonian H and state ρ such that $[H, \rho] = 0$, and any observable A , the time correlation function $C_s^A(t) = \text{Tr}(\rho \{A, A(t)\})$ satisfies*

$$\frac{1}{T} \int_0^T \frac{|C_s^A(t) - C_{s,\infty}^A|^2}{(C_s^A(0))^2} dt \leq 4\pi \left(\frac{a(\epsilon)}{\sigma_G} \frac{1}{T} + \delta(\epsilon) \right), \quad (15)$$

where $a(\epsilon)$ and $\delta(\epsilon)$ are as in Definition [2] for the normalized distribution $v_{\alpha}^s \equiv \frac{\rho_{jj} + \rho_{kk}}{2} \frac{|A_{jk}|^2}{C_s^A(0)}$, and

$$\sigma_G^2 = \frac{1}{C_s^A(0)} \text{Tr}(\rho[A_0, H][H, A_0]). \quad (16)$$

Thus an upper bound for the equilibration timescale is

$$T_{eq} = \frac{4\pi a(\epsilon) \sqrt{C_s^A(0)}}{\sqrt{\text{Tr}(\rho[A, H][H, A])}}, \quad (17)$$

where again $a \sim \mathcal{O}(1)$ for approximately unimodal distributions v_{α}^s . The denominator in T_{eq} can be seen as an “acceleration” of the symmetric autocorrelation function. Eq. (17) can in fact be written as

$$T_{eq} = \frac{4\pi a(\epsilon) \sqrt{C_s^A(0)}}{\sqrt{\left| \frac{d^2 C_s^A(t)}{dt^2} \Big|_0}}. \quad (18)$$

Such timescale turns out to be similar to that of a short-time analysis. A Taylor expansion gives

$$C_s^A(t) = C_s^A(0) \left(1 - \frac{1}{2C_s^A(0)} \frac{d^2 C_s^A(t)}{dt^2} \Big|_0 t^2 \right) + \mathcal{O}(t^3). \quad (19)$$

For early times, the above expression decays on a timescale $\tau = \frac{\sqrt{2}}{4\pi a(\epsilon)} T_{eq}$, identical to our upper bound Eq. (18) up to a prefactor.

The timescale of Eq. (17) suggests an interpretation in terms of an emergent fluctuation-dissipation theorem. Consider *i*) T_{eq} to be the timescale of dissipation of unitary dynamics, meaning that $\langle A(t)A \rangle_\beta \rightarrow \langle A \rangle_\beta \langle A \rangle_\beta$ occurs, and *ii*) $C_s^A(0) = \text{Tr}(\rho A^2)$ as a measure of the fluctuations of A . Then, Eq. (17) gives a proportionality relation between the strength of the fluctuations and the timescale of equilibration, in a similar spirit to what was found in [47] using random matrix theory arguments.

Linear response and the Kubo correlation function — As a further application of our methods, we study the evolution of a quantum system under a perturbation of its Hamiltonian. Let the system start in a thermal state, such that $\rho \propto e^{-\beta(H+\lambda A)}$. Subsequently, the Hamiltonian is slightly perturbed by λA , so that the evolved state is $\rho_t = e^{-itH} \rho e^{itH}$.

It was shown by Kubo [1] that, to leading order in λ , the expectation value of A satisfies $\text{Tr}(\rho A(t)) = C_{\text{Kubo}}(t) \text{Tr}(\rho A)$, where for thermal states the Kubo correlation function can be written as

$$C_{\text{Kubo}}(t) \propto \sum_{j \neq k} \frac{e^{-\beta E_k} - e^{-\beta E_j}}{E_j - E_k} |A_{jk}|^2 e^{it(E_j - E_k)}. \quad (20)$$

Equilibration of $\text{Tr}(\rho A(t))$ is then equivalent to equilibration of the function $C_{\text{Kubo}}(t)$, for which we prove in Appendix B3 that the following holds

Theorem 5. *For any Hamiltonian H , thermal state $\rho \propto e^{-\beta(H+\lambda A)}$, and any observable A , the Kubo correlation function C_{Kubo} satisfies*

$$\frac{1}{T} \int_0^T \frac{|C_{\text{Kubo}}(t) - C_{\text{Kubo},\infty}|^2}{C_{\text{Kubo}}(0)^2} dt \leq 4\pi \left(\frac{a(\epsilon)}{\sigma_G} \frac{1}{T} + \delta(\epsilon) \right), \quad (21)$$

where $a(\epsilon)$ and $\delta(\epsilon)$ are as in Definition [2] for the normalized distribution $w_\alpha \equiv \frac{e^{-\beta E_k} - e^{-\beta E_j}}{E_j - E_k} \frac{|A_{jk}|^2}{C_{\text{Kubo}}(0)}$, and

$$\sigma_G^2 = \frac{1}{C_{\text{Kubo}}(0)} \text{Tr}([A, \rho][A, H]). \quad (22)$$

As before, this implies an upper bound $T_{eq} = \frac{4\pi a(\epsilon)}{\sigma_G}$ on the equilibration timescale of C_{Kubo} , and therefore on the time to return to thermal equilibrium after a perturbation of the system Hamiltonian by A . Once more, if the distribution w_α is smoothly distributed and unimodal then $a \sim \mathcal{O}(1)$ and $\delta(\epsilon) \ll 1$ hold (see Appendix B4).

Simulations — We test Theorem [3] in a spin model governed by the Hamiltonian

$$H = \sum_{j=1}^L (\gamma \sigma_j^X + \lambda \sigma_j^Z) + J \sum_{j=1}^{L-1} \sigma_j^Z \sigma_{j+1}^Z + \alpha \sum_{j=1}^{L-2} \sigma_j^Z \sigma_{j+2}^Z, \quad (23)$$

where σ_j^Z and σ_j^X are the Pauli spin operators along Z and X directions for spin j , and we take open boundary conditions. The field and interaction coefficients $(\gamma, \lambda, J, \alpha)$ characterize the model. We focus on a case corresponding to a system satisfying ETH by choosing $(\gamma, \lambda, J, \alpha) = (0.8, 0.5, 1, 1)$ [48], and study the autocorrelation functions of the observable $A = \sigma_{\frac{L}{2}}^x$. For simplicity we set $\beta = 1$ in our numerics, though no significant changes were observed for $\beta \in [0.1, 5]$. Figure 1 depicts the functions $a(\epsilon)$ and $\delta(\epsilon)$ that appear in Theorem 3, showing that there exist regions of ϵ such that $\delta \ll 1$, ensuring equilibration occurs, and $a \sim 0.4$. Importantly, this is increasingly the case as the size of the system grows.

In Fig. 2 we compare the two sides of bound (12), where it can be seen that the upper bound is off by roughly an order of magnitude, showing the accuracy of estimating T_{eq} as the timescale. Note how the estimate is increasingly better with system size. Details of how the functions required to plot Figs. 1 and 2 are computed can be found in Appendix C.

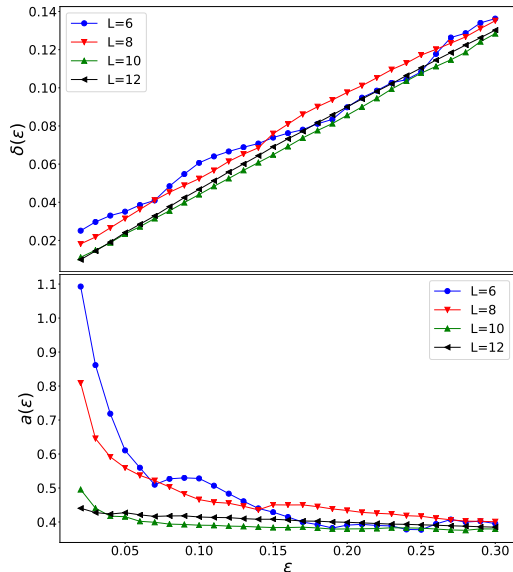


FIG. 1. Plots of $\delta(\epsilon)$ (top) and $a(\epsilon)$ (bottom) for distribution v_α in Theorem 3, obtained by exact diagonalization and a Monte Carlo approximation of the function ξ_v from Def. 2. The plots were generated with 10,000 sampled frequency intervals. Small values of δ imply equilibration occurs for long enough times, while the value of a controls the prefactor in the equilibration timescale Eq. (12). For small ϵ one can satisfy both $\delta \ll 1$ and $a \sim \mathcal{O}(1)$, and this becomes increasingly so for larger system sizes.

Discussion — We derived analytic results on the dynamical behavior of 2-point correlation functions in quantum systems. These include conditions that imply that time-correlation functions factorize for long times, as well as easy-to-estimate upper bounds on the timescales under which such process occurs. Our numerical findings suggest that the upper bounds on timescales we propose are increasingly better estimates as the size of the system grows, and are accurate to within an order of magnitude. This discrepancy could, however, be a finite-size effect, which is also suggested by the bound in the other direction of [44]. A further open problem is the characterization of timescales for correlation functions $C^{AB}(t)$ between arbitrary observables.

We used techniques previously applied in the context of equilibration of quenched quantum systems [43, 49, 50], for which finding rigorous estimates on the timescales is a largely open problem [51–54]. This connection is not surprising, specially considering that previous works [6, 55, 56] have argued that in some situations (that is, for certain initial states, and assuming the ETH holds) one can approximate the out of equilibrium dynamics with the autocorrelation functions covered here.

Given the importance of time-correlation functions in the analysis of a wide range of problems in many-body physics –for instance, in transport phenomena– we anticipate that our results will be useful in the description

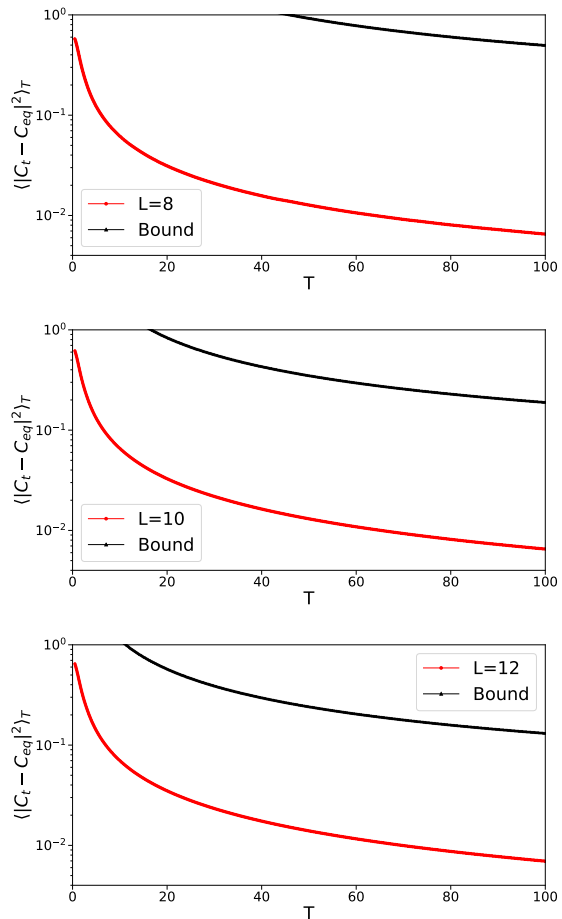


FIG. 2. Comparison of the upper bound in Eq. 12 (RHS) with the simulated evolution of the time-averaged correlation function (LHS) as a function of time, for increasing number of spins L . The evolution obtained from the upper bound approaches the exact dynamics of the system for larger system size.

of closed system dynamics, whose study has surged in recent times due to enormous experimental advances in settings such as cold atoms or ion traps [57, 58].

Acknowledgements — The authors acknowledge useful discussions with Anurag Anshu, Beni Yoshida and Charlie Nation. We are also thankful to Yichen Huang for pointing out an improvement to the error term in Theorem 1 from a previous version. This research was supported in part by the John Templeton Foundation, DOE grant DE-SC0019515, and the Perimeter Institute for Theoretical Physics. Research at Perimeter Institute is supported by the Government of Canada through the Department of Innovation, Science and Economic Development and by the Province of Ontario through the Ministry of Research, Innovation and Science. This research was also supported by NSERC and enabled in part by support provided by (SHARCNET) (www.sharcnet.ca) and Compute/Calcul Canada (www.computeCanada.ca).

-
- [1] R. Kubo, *Journal of the Physical Society of Japan* **12**, 570 (1957).
- [2] G. Rickayzen, *Green's functions and condensed matter*, Techniques of physics (Academic Press, 1980).
- [3] Y. Zhu, *Modern techniques for characterizing magnetic materials* (Springer Science & Business Media, 2005).
- [4] R. Zwanzig, *Annual Review of Physical Chemistry* **16**, 67 (1965).
- [5] X. Zotos, F. Naef, and P. Prelovsek, *Physical Review B* **55**, 11029 (1997).
- [6] M. Srednicki, *Journal of Physics A: Mathematical and General* **32**, 1163 (1999).
- [7] E. Khatami, G. Pupillo, M. Srednicki, and M. Rigol, *Physical review letters* **111**, 050403 (2013).
- [8] L. D'Alessio, Y. Kafri, A. Polkovnikov, and M. Rigol, *Advances in Physics* **65**, 239 (2016).
- [9] R. Steinigeweg and J. Gemmer, *Physical Review B* **80**, 184402 (2009).
- [10] O. Starykh, A. Sandvik, and R. Singh, *Physical Review B* **55**, 14953 (1997).
- [11] J. Sirker and A. Klümper, *Physical Review B* **71**, 241101 (2005).
- [12] T. Barthel, U. Schollwöck, and S. R. White, *Physical Review B* **79**, 245101 (2009).
- [13] A. E. Feiguin and G. A. Fiete, *Physical Review B* **81**, 075108 (2010).
- [14] C. Karrasch, J. Bardarson, and J. Moore, *Physical review letters* **108**, 227206 (2012).
- [15] P. Dargel, A. Wöllert, A. Honecker, I. McCulloch, U. Schollwöck, and T. Pruschke, *Physical Review B* **85**, 205119 (2012).
- [16] T. Barthel, *New Journal of Physics* **15**, 073010 (2013).
- [17] A. Bohrdt, C. B. Mendl, M. Endres, and M. Knap, *New Journal of Physics* **19**, 063001 (2017).
- [18] V. E. Korepin, N. M. Bogoliubov, and A. G. Izergin, *Quantum inverse scattering method and correlation functions*, Vol. 3 (Cambridge university press, 1997).
- [19] A. Its, A. Izergin, V. Korepin, and N. Slavnov, *Physical review letters* **70**, 1704 (1993).
- [20] J. Stolze, A. Nöppert, and G. Müller, *Physical Review B* **52**, 4319 (1995).
- [21] S. Reyes and A. Tsvelik, *Physical Review B* **73**, 220405 (2006).
- [22] J. H. Perk and H. Au-Yang, *Journal of Statistical Physics* **135**, 599 (2009).
- [23] B. Bertini, P. Kos, and T. Prosen, arXiv preprint arXiv:1904.02140 (2019).
- [24] O. Romero-Isart, M. Rizzi, C. Muschik, E. Polzik, M. Lewenstein, and A. Sanpera, *Physical review letters* **108**, 065302 (2012).
- [25] M. Knap, A. Kantian, T. Giamarchi, I. Bloch, M. D. Lukin, and E. Demler, *Physical review letters* **111**, 147205 (2013).
- [26] F. Buscemi, M. Dall'Arno, M. Ozawa, and V. Vedral, arXiv e-prints, arXiv:1312.4240 (2013), arXiv:1312.4240 [quant-ph].
- [27] M. Gessner, F. Schlawin, H. Häfner, S. Mukamel, and A. Buchleitner, *New Journal of Physics* **16**, 092001 (2014).
- [28] P. Uhrich, S. Castrignano, H. Uys, and M. Kastner, *Physical Review A* **96**, 022127 (2017).
- [29] H. Araki, *Communications in Mathematical Physics* **14**, 120 (1969).
- [30] M. Hastings, *Physical review letters* **93**, 126402 (2004).
- [31] M. Kliesch, C. Gogolin, M. Kastoryano, A. Riera, and J. Eisert, *Physical review x* **4**, 031019 (2014).
- [32] F. G. S. L. Brandao, E. Crosson, M. Burak Şahinoğlu, and J. Bowen, arXiv e-prints, arXiv:1710.04631 (2017), arXiv:1710.04631 [quant-ph].
- [33] A. Anshu, *New Journal of Physics* **18**, 083011 (2016).
- [34] T. Mori, arXiv e-prints, arXiv:1609.09776 (2016), arXiv:1609.09776 [cond-mat.stat-mech].
- [35] G. Biroli, C. Kollath, and A. M. Läuchli, *Physical review letters* **105**, 250401 (2010).
- [36] C. Cohen-Tannoudji, B. Diu, F. Laloe, and B. Dui, *Quantum Mechanics (2 vol. set)* (Wiley-Interscience, 2006).
- [37] A. J. Short, *New Journal of Physics* **13**, 053009 (2011).
- [38] J. M. Deutsch, *Reports on Progress in Physics* **81**, 082001 (2018).
- [39] E. H. Lieb and D. W. Robinson (1972) pp. 251–257.
- [40] Z. Huang, X.-K. Guo, et al., *Physical Review E* **97**, 062131 (2018).
- [41] A. Dymarsky, arXiv e-prints, arXiv:1804.08626 (2018), arXiv:1804.08626 [cond-mat.stat-mech].
- [42] M. Schiulaz, E. J. Torres-Herrera, and L. F. Santos, arXiv e-prints, arXiv:1807.07577 (2018), arXiv:1807.07577 [cond-mat.stat-mech].
- [43] L. P. García-Pintos, N. Linden, A. S. L. Malabarba, A. J. Short, and A. Winter, *Phys. Rev. X* **7**, 031027 (2017).
- [44] H. Kim, M. C. Bañuls, J. I. Cirac, M. B. Hastings, and D. A. Huse, *Physical Review E* **92**, 012128 (2015).
- [45] W. Beugeling, R. Moessner, and M. Haque, *Physical Review E* **91**, 012144 (2015).
- [46] R. Mondaini and M. Rigol, *Physical Review E* **96**, 012157 (2017).
- [47] C. Nation and D. Porras, arXiv e-prints, arXiv:1811.03028 (2018), arXiv:1811.03028 [quant-ph].
- [48] K. Kaneko, E. Iyoda, and T. Sagawa, arXiv preprint arXiv:1809.01946 (2018), 10.1103/PhysRevE.99.032128.
- [49] A. J. Short and T. C. Farrelly, *New Journal of Physics* **14**, 013063 (2012).
- [50] A. S. L. Malabarba, L. P. García-Pintos, N. Linden, T. C. Farrelly, and A. J. Short, *Phys. Rev. E* **90**, 012121 (2014).
- [51] H. Wilming, M. Goihl, C. Krumnow, and J. Eisert, arXiv e-prints, arXiv:1704.06291 (2017), arXiv:1704.06291 [quant-ph].
- [52] T. R. de Oliveira, C. Charalambous, D. Jonathan, M. Lewenstein, and A. Riera, *New Journal of Physics* **20**, 033032 (2018).
- [53] A. Dymarsky, arXiv e-prints, arXiv:1806.04187 (2018), arXiv:1806.04187 [cond-mat.stat-mech].
- [54] P. Reimann, *New Journal of Physics* **21**, 053014 (2019).
- [55] J. Richter, J. Gemmer, and R. Steinigeweg, arXiv e-prints, arXiv:1805.11625 (2018), arXiv:1805.11625 [cond-mat.stat-mech].
- [56] J. Richter and R. Steinigeweg, *Physical Review E* **99**, 012114 (2019).
- [57] I. Bloch, J. Dalibard, and W. Zwerger, *Reviews of modern physics* **80**, 885 (2008).

Appendix A: Late time behaviour of two-point functions

1. Proof of late-time equilibration

First, we state the key result from [32] that we use. It says that expectation values for single eigenstates, of the form $\langle E_k | A | E_k \rangle$, are close to the ensemble average $\langle A \rangle_\rho$ with *very high probability*. In contrast, the strong form of the ETH states that the above happens for *all* eigenstates within an energy window. We reproduce the proof of [32] (which itself builds on [34]), with the difference that our version holds for lattices of dimension larger than 1.

Lemma 1 (Proposition 7 [32]). *There exists a constant $0 < \alpha < 1/(D+1)$ such that the following holds. Let H be a translation-invariant, non-degenerate Hamiltonian with N sites on a D -dimensional lattice, ρ an equilibrium ensemble $[\rho, H] = 0$ with finite correlation length ξ , and A some observable with support on a connected region of at most N^α sites. Then, for any $\delta > 0$,*

$$\Pr_{|E_k\rangle \in \rho}(|\langle E_k | A | E_k \rangle - \text{Tr}(\rho A)| \geq \delta) \leq \exp(-c\delta N^{\frac{1}{D+1}} \xi^{-\frac{D}{D+1}}), \quad (\text{A1})$$

where $c > 0$ is a constant, and $|E_k\rangle \in \rho$ indicates that the eigenstates are sampled from the equilibrium distribution ρ .

Proof. We show a bound $\Pr_{|E_k\rangle \in \rho}(\langle E_k | A | E_k \rangle - \text{Tr}(\rho A) \geq \delta)$, and $\Pr_{|E_k\rangle \in \rho}(\text{Tr}(\rho A) - \langle E_k | A | E_k \rangle \geq \delta)$ will follow analogous steps. Notice that since the Hamiltonian is translation-invariant and non-degenerate we can write $\langle E_k | A | E_k \rangle = \langle E_k | \bar{A}/N | E_k \rangle$, where $\bar{A} = \sum_i A_i$ is the extensive observable built out of translations of A . Define $\bar{A}' = \bar{A} - \langle \bar{A} \rangle_\rho$. Then, using Markov's inequality and $e^{\langle \psi | A | \psi \rangle} \leq \langle \psi | e^A | \psi \rangle$ we can write

$$\Pr_{|E_k\rangle \in \rho}(\langle E_k | A | E_k \rangle - \text{Tr}(\rho A) \geq \delta) = \Pr_{|E_k\rangle \in \rho}(e^{\lambda \langle E_k | \bar{A}' | E_k \rangle} \leq e^{\lambda \delta N}) \quad (\text{A2})$$

$$\leq e^{-\lambda \delta N} \sum_k \rho_{kk} e^{\lambda \langle E_k | \bar{A}' | E_k \rangle} \quad (\text{A3})$$

$$\leq e^{-\lambda \delta N} \text{Tr}(\rho e^{\lambda \bar{A}'}). \quad (\text{A4})$$

Now let us decompose $\bar{A}' = \sum_l e^{\lambda a_l} \Pi_l$, and write the average as

$$\text{Tr}(\rho e^{\lambda \bar{A}'}) = \sum_{a_l \leq \delta N/2} e^{\lambda a_l} \text{Tr}(\rho \Pi_l) + \sum_{a_l > \delta N/2} e^{\lambda a_l} \text{Tr}(\rho \Pi_l). \quad (\text{A5})$$

The first term is upper bounded by $e^{\lambda \delta N/2}$. For the second, we write

$$\sum_{a_l > \delta N/2} e^{\lambda a_l} \text{Tr}(\rho \Pi_l) = \sum_j \sum_{\delta N/2 + (j+1) \geq a_l \geq \delta N/2 + j} e^{\lambda a_l} \text{Tr}(\rho \Pi_l) \leq \sum_j e^{\lambda(\delta N/2 + j+1)} \text{Tr}(\rho \Pi_{\geq \delta N/2 + j}), \quad (\text{A6})$$

where $\Pi_{\geq x}$ denotes the projector on the subspace with $a_l \geq x$. The main result of [33] states that

$$\text{Tr}(\rho \Pi_{\geq \delta N/2 + j}) \leq e^{DN^\alpha/\xi} \exp\left(-\frac{c'}{D\xi} (N(\delta/2 + j/N)^2 \xi)^{1/D+1}\right). \quad (\text{A7})$$

Since j is at most $\mathcal{O}(N)$, we can choose some $\lambda = \mathcal{O}\left((N\xi)^{-\frac{D}{D+1}}\right)$ such that, for some constants $c_1, c_2 > 0$,

$$\sum_{a_l > \delta N/2} e^{\lambda a_l} \text{Tr}(\rho \Pi_l) \leq \text{poly}(N) e^{DN^\alpha/\xi} \exp\left(-c_1 N^{\frac{1}{D+1}} \xi^{-\frac{D}{D+1}}\right). \quad (\text{A8})$$

This way, the dominant contribution of Eq. (A5) is the first term. Plugging the bounds back in Eq. (A4) results in the following, for some constant $c > 0$ and large enough N ,

$$\Pr_{|E_k\rangle \in \rho}(\langle E_k | A | E_k \rangle - \text{Tr}(\rho A) \geq \delta) \leq e^{-\lambda \delta N/2} \left(1 + e^{-\lambda \delta N/2} \text{poly}(N) e^{DN^\alpha/\xi} \exp\left(-c_1 N^{\frac{1}{D+1}} \xi^{-\frac{D}{D+1}}\right)\right) \quad (\text{A9})$$

$$\leq \exp\left(-c\delta N^{\frac{1}{D+1}} \xi^{-\frac{D}{D+1}}\right). \quad (\text{A10})$$

□

With it, we are now ready to prove the result on late-time factorization of correlation functions.

Theorem 1. *Let H be a k -local, translation-invariant and non-degenerate Hamiltonian on a D -dimensional Euclidean lattice of N sites, and let $[\rho, H] = 0$ be an equilibrium ensemble (such as a thermal state) of finite correlation length $\xi > 0$. Let A, B be local observables with support on at most N^α sites. Then*

$$\lim_{T \rightarrow \infty} \int_0^T \text{Tr}(\rho A(t) B) \frac{dt}{T} = \text{Tr}(\rho A) \text{Tr}(\rho B) + \mathcal{O}(\xi^{\frac{2D}{D+1}} \log^2(N) N^{-\frac{2}{D+1}}) \quad (\text{A11})$$

Proof. First let us write

$$\rho = \sum_k \rho_{kk} |E_k\rangle \langle E_k|, \quad A = \sum_{kj} A_{kj} |E_k\rangle \langle E_j|, \quad B = \sum_{kj} B_{kj} |E_k\rangle \langle E_j|, \quad (\text{A12})$$

from which we have

$$\text{Tr}(\rho A(t) B) = \sum_{kj} A_{kj} B_{jk} \rho_{kk} e^{it(E_j - E_k)}. \quad (\text{A13})$$

Since the Hamiltonian is non-degenerate by assumption, it holds that

$$\lim_{T \rightarrow \infty} \int_0^T e^{it(E_j - E_k)} \frac{dt}{T} = \delta_{k,j}, \quad (\text{A14})$$

so that the limit becomes

$$\lim_{T \rightarrow \infty} \int_0^T \text{Tr}(\rho A(t) B) \frac{dt}{T} = \sum_k A_{kk} B_{kk} \rho_{kk}. \quad (\text{A15})$$

Now let us define $A_{kk} - \text{Tr}(\rho A) = \Delta_{k,A}$ and $B_{kk} - \text{Tr}(\rho B) = \Delta_{k,B}$, so that [59]

$$\sum_k A_{kk} B_{kk} \rho_{kk} = \text{Tr}(\rho A) \text{Tr}(\rho B) + \sum_k \rho_{kk} (\text{Tr}(\rho A) \Delta_{k,B} + \text{Tr}(\rho B) \Delta_{k,A} + \Delta_{k,A} \Delta_{k,B}) \quad (\text{A16})$$

$$= \text{Tr}(\rho A) \text{Tr}(\rho B) + \sum_k \rho_{kk} \Delta_{k,A} \Delta_{k,B} \quad (\text{A17})$$

Let us define $\Delta \equiv K \log N / N^{\frac{1}{D+1}}$, and split the sum over energies of the error term as

$$\sum_k \rho_{kk} \Delta_{k,A} \Delta_{k,B} = \sum_{k \in \mathcal{S}} \rho_{kk} \Delta_{k,A} \Delta_{k,B} + \sum_{k \notin \mathcal{S}} \rho_{kk} \Delta_{k,A} \Delta_{k,B}. \quad (\text{A18})$$

where $\mathcal{S} \equiv \{k : |\Delta_{k,A}|, |\Delta_{k,B}| \leq \Delta\}$ (that is, the set of k for which both errors are small). Notice that the first term is smaller than Δ^2 by definition. On the other hand, the second term can be bounded as

$$\begin{aligned} \sum_{k \notin \mathcal{S}} \rho_{kk} \Delta_{k,A} \Delta_{k,B} &\leq \max_{k'} \Delta_{k',A} \Delta_{k',B} \sum_{k \notin \mathcal{S}} \rho_{kk} \\ &\leq \max_{k'} \Delta_{k',A} \Delta_{k',B} \left(\sum_{|\Delta_{k,A}| \geq \Delta} \rho_{kk} + \sum_{|\Delta_{k,B}| \geq \Delta} \rho_{kk} \right) \\ &\leq 2 \max_{k'} \Delta_{k',A} \Delta_{k',B} \exp(-c \Delta N^{\frac{1}{D+1}} \xi^{-\frac{D}{D+1}}) \\ &\leq 2 \|A\| \|B\| \left(\frac{1}{N} \right)^{cK \xi^{-\frac{D}{D+1}}}. \end{aligned} \quad (\text{A19})$$

The third line follows from Lemma 1, and the fourth from $|\Delta_{k,A}| \leq \|A\|, |\Delta_{k,B}| \leq \|B\|$. The constant K is arbitrary, so we can choose it such that $cK \xi^{-\frac{D}{D+1}} = \frac{2}{D+1}$. In that case the dominant contribution to Eq. (A18) is that of the first term, and hence $\sum_k \rho_{kk} \Delta_{k,A} \Delta_{k,B} = \mathcal{O}(\Delta^2)$, so that

$$\sum_k A_{kk} B_{kk} \rho_{kk} = \text{Tr}(\rho A) \text{Tr}(\rho B) + \mathcal{O}(\Delta^*), \quad (\text{A20})$$

completing the proof. \square

2. Proof of fluctuations around late-time value

Theorem 2. Let H be a Hamiltonian with non-degenerate energy gaps, such that

$$E_j - E_k = E_m - E_l \Leftrightarrow j = m, k = l. \quad (\text{A21})$$

Then, it holds that

$$\sigma_C^2 \leq \|A\| \|B\| \max_{j \neq k} \{|A_{kj} B_{jk}|\} \text{Tr}(\rho^2). \quad (\text{A22})$$

Proof. Let us expand in the energy eigenbasis.

$$\sigma_C^2 = \lim_{T \rightarrow \infty} \int_0^T \frac{dt}{T} (C(t)^{AB} - C_\infty^{AB})^2 \quad (\text{A23})$$

$$= \sum_{j \neq k} \sum_{l \neq m} \rho_{jj} \rho_{ll} A_{jk} B_{kj} A_{lm} B_{ml} \int_0^T \frac{dt}{T} e^{-it(E_j - E_k + E_l - E_m)} \quad (\text{A24})$$

$$= \sum_{j \neq k} \rho_{jj} \rho_{kk} A_{jk} A_{kj} B_{jk} B_{kj} \quad (\text{A25})$$

$$\leq \sum_{j \neq k} \rho_{jj} \rho_{kk} |A_{jk} A_{kj} B_{jk} B_{kj}| \quad (\text{A26})$$

$$\leq \max_{j \neq k} \{|A_{kj} B_{jk}|\} \sum_{j \neq k} \rho_{jj} \rho_{kk} |A_{jk} B_{kj}| \quad (\text{A27})$$

$$\leq \max_{j \neq k} \{|A_{kj} B_{jk}|\} \sqrt{\sum_{j \neq k} \rho_{jj} \rho_{kk} |A_{jk}|^2} \sqrt{\sum_{j \neq k} \rho_{jj} \rho_{kk} |B_{kj}|^2} \quad (\text{A28})$$

$$\leq \max_{j \neq k} \{|A_{kj} B_{jk}|\} \sqrt{\sum_{j,k} \rho_{jj} \rho_{kk} |A_{jk}|^2} \sqrt{\sum_{j,k} \rho_{jj} \rho_{kk} |B_{kj}|^2} \quad (\text{A29})$$

$$= \max_{j \neq k} \{|A_{kj} B_{jk}|\} \sqrt{\text{Tr}(\rho A \rho A)} \sqrt{\text{Tr}(\rho B \rho B)} \quad (\text{A30})$$

$$\leq \max_{j \neq k} \{|A_{kj} B_{jk}|\} \sqrt{\text{Tr}(A^2 \rho^2)} \sqrt{\text{Tr}(B^2 \rho^2)} \quad (\text{A31})$$

$$\leq \|A\| \|B\| \max_{j \neq k} \{|A_{kj} B_{jk}|\} \text{Tr}(\rho^2). \quad (\text{A32})$$

In the second to the third line we use the assumption of non-degenerate energy gaps. We use the Cauchy-Schwarz inequality in the fifth to sixth line, and once again in going to the eighth line. The last one follows from the fact that for positive operators $\text{Tr}(PQ) \leq \|P\| \text{Tr}(Q)$. □

Appendix B: Dynamics of two-time correlation functions

1. Proof of equilibration timescales of correlation functions

Theorem 3. For any Hamiltonian H and state ρ such that $[H, \rho] = 0$, and any observable A , the time correlation function $C^A(t) = \text{Tr}(\rho A(t)A)$ satisfies

$$\frac{1}{T} \int_0^T \frac{|C^A(t) - C_\infty^A|^2}{(C^A(0))^2} dt \leq 4\pi \left(\frac{a(\epsilon)}{\sigma_G} \frac{1}{T} + \delta(\epsilon) \right), \quad (\text{B1})$$

where $a(\epsilon)$ and $\delta(\epsilon)$ are as in [2] for the normalized distribution $v_\alpha \equiv \frac{\rho_{jj} |A_{jk}|^2}{C^A(0)}$, and σ_G can be readily calculated from knowledge of the state, observable, and Hamiltonian:

$$\sigma_G^2 = \frac{1}{C^A(0)} \text{Tr}(\rho[A, H][H, A]) - \frac{\text{Tr}(\rho[H, A]A)^2}{(C^A(0))^2}. \quad (\text{B2})$$

Proof. Following [43, 50], we get

$$\frac{1}{T} \int_0^T \frac{|C^A(t) - C_\infty^A|^2}{(C^A(0))^2} dt \leq \frac{5\pi}{4} \sum_{G_\alpha \neq G_\beta} v_\alpha v_\beta e^{-|G_\alpha - G_\beta|T}. \quad (\text{B3})$$

Note that the distribution v_α is normalized:

$$\sum v_\alpha = \sum_{jk} \frac{\rho_{jj} |A_{jk}|^2}{C^A(0)} = \frac{\text{Tr}(\rho A^2)}{C^A(0)} = 1. \quad (\text{B4})$$

Proposition 5 in [43] thus implies that

$$\frac{1}{T} \int_0^T \frac{|C_t - C_\infty|^2}{(C^A(0))^2} dt \leq 4\pi \xi_v \left(\frac{1}{T}\right), \quad (\text{B5})$$

with ξ_v as defined in [2]. It was shown in [43] (Proposition 5) that the function $\xi_p(x)$ satisfies

$$\xi_p(x) \leq \frac{a(\epsilon)}{\sigma_G} x + \delta(\epsilon), \quad (\text{B6})$$

with $a(\epsilon) = \frac{\xi_p(\epsilon)}{\epsilon} \sigma_G$ and $\delta(\epsilon) = \xi_p(\epsilon)$. Finally, the standard deviation of the distribution p_v is

$$\begin{aligned} \sigma_G^2 &= \sum_\alpha p_\alpha G_\alpha^2 - \left(\sum_\alpha p_\alpha G_\alpha \right)^2 \\ &= \sum_{jk} \frac{\rho_{jj} |A_{jk}|^2}{C^A(0)} (E_j - E_k)^2 - \left(\sum_{jk} \frac{\rho_{jj} |A_{jk}|^2}{C^A(0)} (E_j - E_k) \right)^2 \\ &= \frac{1}{C^A(0)} \text{Tr}(\rho[A, H][H, A]) - \frac{\text{Tr}(\rho[H, A]A)^2}{(C^A(0))^2}, \end{aligned} \quad (\text{B7})$$

which completes the proof. \square

2. Proof of equilibration timescales of symmetric correlation functions

Theorem 4. For any Hamiltonian H and state ρ such that $[H, \rho] = 0$, and any observable A , the time correlation function $C_s^A(t) = \text{Tr}(\rho\{A, A(t)\})$ satisfies

$$\frac{1}{T} \int_0^T \frac{|C_s^A(t) - C_{s,\infty}^A|^2}{(C_s^A(0))^2} dt \leq 4\pi \left(\frac{a(\epsilon)}{\sigma_G} \frac{1}{T} + \delta(\epsilon) \right), \quad (\text{B8})$$

where $a(\epsilon)$ and $\delta(\epsilon)$ are as in Definition [2] for the normalized distribution $v_\alpha^s \equiv \frac{\rho_{jj} + \rho_{kk}}{2} \frac{|A_{jk}|^2}{C_s^A(0)}$, and

$$\sigma_G^2 = \frac{1}{C_s^A(0)} \text{Tr}(\rho[A_0, H][H, A_0]). \quad (\text{B9})$$

Proof. The symmetric correlation function is defined as

$$C_s^A(t) \equiv \frac{1}{2} \text{Tr}(\rho\{A, A(t)\}) = \frac{C^A(t) + C^A(t)^*}{2}. \quad (\text{B10})$$

The equivalent of Eq. (9) becomes

$$\frac{C_s^A(t)}{C_s^A(0)} = \sum_{jk} \frac{\rho_{jj} + \rho_{kk}}{2} \frac{|A_{jk}|^2}{C_s^A(0)} e^{-i(E_j - E_k)t}, \quad (\text{B11})$$

The proof of Theorem [4] is identical as the previous proof, with the symmetrized distribution $v_\alpha^S \equiv \frac{\rho_{jj} + \rho_{kk}}{2} |A_{jk}|^2$. In this case the variance of the normalized distribution v_α^S becomes

$$\begin{aligned} \sigma_G^2 &= \sum_\alpha p_\alpha^S G_\alpha^2 - \left(\sum_\alpha p_\alpha^S G_\alpha \right)^2 \\ &= \sum_{jk} \frac{\frac{\rho_{jj} + \rho_{kk}}{2} |A_{jk}|^2}{C_s^A(0)} (E_j - E_k)^2 - \left(\sum_{jk} \frac{\frac{\rho_{jj} + \rho_{kk}}{2} |A_{jk}|^2}{C_s^A(0)} (E_j - E_k) \right)^2 \\ &= \frac{1}{C_s^A(0)} \text{Tr}(\rho[A, H][H, A]). \end{aligned} \quad (\text{B12})$$

□

Equilibration then occurs within a timescale

$$T_{eq} = \frac{4\pi a(\epsilon) \sqrt{C_s^A(0)}}{\sqrt{\text{Tr}(\rho[A, H][H, A])}}, \quad (\text{B13})$$

The denominator in T_{eq} can be identified as an ‘‘acceleration’’ of the symmetric autocorrelation function. Indeed,

$$\frac{d^2 C_s^A(t)}{dt^2} = - \sum_{jk} (E_j - E_k)^2 \frac{\rho_{jj} + \rho_{kk}}{2} |A_{jk}|^2 e^{-i(E_j - E_k)t}. \quad (\text{B14})$$

Then, the equilibration timescale is

$$T_{eq} = \frac{4\pi a(\epsilon) \sqrt{C_s^A(0)}}{\sqrt{\left| \frac{d^2 C_s^A(t)}{dt^2} \Big|_0}}. \quad (\text{B15})$$

a. Short-time evolution of symmetric correlation functions

The symmetric autocorrelation functions is given by

$$C_s^A(t) = \sum_{jk} \frac{\rho_{jj} + \rho_{kk}}{2} |A_{jk}|^2 e^{-i(E_j - E_k)t}. \quad (\text{B16})$$

Taking the Taylor expansion of $C_s^A(t)$,

$$\begin{aligned} C_s^A(t) &= C_s^A(0) - \left(i \sum_{jk} (E_j - E_k) \frac{\rho_{jj} + \rho_{kk}}{2} |A_{jk}|^2 \right) t \\ &\quad - \left(\sum_{jk} (E_j - E_k)^2 \frac{\rho_{jj} + \rho_{kk}}{2} |A_{jk}|^2 \right) \frac{t^2}{2} + \mathcal{O}(t^3) \\ &= C_s^A(0) - \frac{d^2 C_s^A}{dt^2} \Big|_0 \frac{t^2}{2} + \mathcal{O}(t^3) \\ &= C_s^A(0) \left(1 - \frac{1}{2C_0} \frac{d^2 C_s^A}{dt^2} \Big|_0 t^2 \right) + \mathcal{O}(t^3). \end{aligned} \quad (\text{B17})$$

For early times, the above expression decays on a timescale

$$\tau \equiv \frac{\sqrt{2} \sqrt{C_s^A(0)}}{\sqrt{\left| \frac{d^2 C_s^A(t)}{dt^2} \Big|_0}}. \quad (\text{B18})$$

3. Proof of equilibration timescales of Kubo correlation functions

Theorem 5. For any Hamiltonian H , thermal state ρ , and any observable A , the Kubo correlation function C_{Kubo} satisfies

$$\frac{1}{T} \int_0^T \frac{|C_{\text{Kubo}}(t) - C_{\text{Kubo},\infty}|^2}{C_{\text{Kubo}}(0)^2} dt \leq 4\pi \left(\frac{a(\epsilon)}{\sigma_G} \frac{1}{T} + \delta(\epsilon) \right), \quad (\text{B19})$$

where $a(\epsilon)$ and $\delta(\epsilon)$ are as in Definition [2] for the normalized distribution $w_\alpha \equiv \frac{e^{-\beta E_k} - e^{-\beta E_j}}{E_j - E_k} \frac{|A_{jk}|^2}{C_{\text{Kubo}}(0)}$, and

$$\sigma_G^2 = \frac{1}{C_{\text{Kubo}}(0)} \text{Tr}([A, \rho][A, H]). \quad (\text{B20})$$

Proof. The Kubo correlation function can be written as

$$C_{\text{Kubo}}(t) \propto \sum_{j \neq k} \frac{e^{-\beta E_k} - e^{-\beta E_j}}{E_j - E_k} |A_{jk}|^2 e^{it(E_j - E_k)}, \quad (\text{B21})$$

with the proportionality constant defined by $C_{\text{Kubo}}(0) = 1$. We can then write

$$\begin{aligned} \frac{C_{\text{Kubo}}(t) - C_{\text{Kubo}}(\infty)}{C_{\text{Kubo}}(0)} &= \frac{\sum_{j \neq k} \frac{e^{-\beta E_k} - e^{-\beta E_j}}{E_j - E_k} |A_{jk}|^2 e^{it(E_j - E_k)}}{\sum_{j,k} \frac{e^{-\beta E_k} - e^{-\beta E_j}}{E_j - E_k} |A_{jk}|^2} \\ &\equiv \frac{\sum_{\alpha \neq 0} w_\alpha e^{-itG_\alpha}}{\sum_\alpha w_\alpha}, \end{aligned} \quad (\text{B22})$$

where we define $w_\alpha \equiv \frac{e^{-\beta E_k} - e^{-\beta E_j}}{E_j - E_k} |A_{jk}|^2 \geq 0$. Given that $w_\alpha \geq 0$, we can perform similar calculations as for Theorem [3], albeit with a different probability distribution. Thus, we also have

$$\left\langle \left(\frac{C_{\text{Kubo}}(t) - C_{\text{Kubo}}(\infty)}{C_{\text{Kubo}}(0)} \right)^2 \right\rangle_T \leq \frac{5\pi}{4} \xi_w(1/T). \quad (\text{B23})$$

Defining the normalized distribution $q_\alpha \equiv w_\alpha / C_{\text{Kubo}}(0)$. The variance is

$$\begin{aligned} \sigma_G^2 &= \sum_\alpha q_\alpha G_\alpha^2 - \left(\sum_\alpha q_\alpha G_\alpha \right)^2 \\ &= \sum_{jk} \frac{1}{C_{\text{Kubo}}(0)} \frac{e^{-\beta E_k} - e^{-\beta E_j}}{E_j - E_k} |A_{jk}|^2 (E_j - E_k)^2 - \left(\sum_{jk} \frac{1}{C_{\text{Kubo}}(0)} \frac{e^{-\beta E_k} - e^{-\beta E_j}}{E_j - E_k} |A_{jk}|^2 (E_j - E_k) \right)^2 \\ &= \frac{1}{C_{\text{Kubo}}(0)} \sum_{jk} (e^{-\beta E_k} - e^{-\beta E_j}) |A_{jk}|^2 (E_j - E_k) \\ &= \frac{1}{C_{\text{Kubo}}(0)} \text{Tr}([A, \rho][A, H]), \end{aligned} \quad (\text{B24})$$

completing the proof of Theorem [5]. □

4. Scaling of a and δ

The proofs of Theorems 3-5 rely on the fact that the function $\xi_p(x)$, defined for any normalized distribution p_α as the maximum distribution that fits an interval x

$$\xi_p(x) \equiv \max_\beta \sum_{\alpha: G_\beta \in [G_\beta, G_\beta + x]} p_\alpha, \quad (\text{B25})$$

satisfies

$$\xi_p(x) \leq \frac{a(\epsilon)}{\sigma_G} x + \delta(\epsilon), \quad (\text{B26})$$

which was shown in [43] (Proposition 5). Here $a(\epsilon) \equiv \frac{\xi_p(\epsilon)}{\epsilon} \sigma_G$ and $\delta(\epsilon) \equiv \xi_p(\epsilon)$, where σ_G is the standard deviation of the distribution p_α . The function $a(\epsilon)$ ends up in the bound of the equilibration timescales, as $T_{eq} = \frac{4\pi a(\epsilon)}{\sigma_G}$, while $\delta(\epsilon)$ governs the long time behavior in the bounds.

Given that $\xi_p(x)$ characterizes how much of the distribution p_α fits an interval x , the value of a in Eq. (B26) depends on how well $1/\sigma_G$ serves to characterize the region where the distribution p_α is supported. Roughly speaking, whenever $1/\sigma_G$ is a good estimate of the width of such small region, then one expects $a \sim \mathcal{O}(1)$. This is well illustrated when considering a unimodal distribution (e.g. a Gaussian). In such case, the fraction of the distribution that fits an interval x is roughly x times the width $1/\sigma_G$ of the window where the distribution is supported, and $\xi_p(x) \sim x/\sigma_G$, so that $a \sim \mathcal{O}(1)$. Multimodal distributions violate such condition, as for them the standard deviation does not characterize the regions in which the distribution has considerable support. At the same time, δ in Eq. (B26) carries information of the fine structure of p_α , indicating the scale at which the distribution can no longer be coarse-grained to a continuous distribution. The only way that $\delta \ll 1$ fails is for distributions that are not smooth, in which a small region of width ϵ is significantly populated. Thus, for distributions that are smooth in a coarse-grained sense, and approximately unimodal, one expects to be able to find a small enough ϵ such that $\delta(\epsilon) \ll 1$ and $a(\epsilon) \sim \mathcal{O}(1)$.

In summary, the problem of proving fast equilibration timescales in our approach can thus be linked to knowing whether the relevant distribution p_α is ‘approximately unimodal’. We argue that for an strongly interacting many-body system this will typically be the case. Consider for instance the case of Theorem 3, where the relevant distribution is given by $v_\alpha \equiv \frac{\rho_{jj} |A_{jk}|^2}{C^A(0)}$.

The large number of energy gaps present in a many-body system implies a dominance of small gaps over larger ones, which favors that, on a coarse-grained sense, the distribution over gaps shows a decay as the size $|G_\alpha|$ of the gap increases. This is reinforced by the tendency of off-diagonal matrix elements $|A_{jk}|$ of local observables to decay as the levels considered are further apart. Existing numerical results on off-diagonal matrix elements of local observables in non-integrable models are consistent with all the requirements listed here [45, 46]. The present arguments suggest distributions v_α that decay for larger values of $|G_\alpha|$, and are therefore unimodal, and also smoothly distributed. This is confirmed in the simulations in Appendix C in a non-integrable model on Fig. 5 (left), and to a somewhat lesser extent in an integrable model too on Fig. 5 (right).

Appendix C: Simulations

To calculate the function given in definition 2 exactly one needs to find the maximum sum of p_α such that $\alpha : G_\alpha \in [G_\lambda, G_\lambda + x]$. This calculation scales quite unfavourably with system size. If we have N energies, the number of intervals one must probe is quadratic in N . For each $x \sim \mathcal{O}(10^{-1})$ the intervals near the center are quite dense, making the entire algorithm for one choice of x approximately scale like $\mathcal{O}(N^3)$. For this reason, we exactly diagonalize the Hamiltonian given in equation 23, and numerically approximate $\xi(x)$. This is done by means of a Monte Carlo scheme where we randomly select intervals defined by G_λ using a normal distribution defined by $\mu_G = \sum_\alpha p_\alpha G_\alpha$ and σ_G given in definition 2.

Figure 3 (left) depicts the accuracy of this scheme. Unsurprisingly $L = 6$ is exactly calculated and is not visible on the except at one location. The other cases show the approximation scheme performs better at larger system sizes. Despite this improvement, the accuracy of the scheme roughly puts us accurate to the fourth digit in all cases, making this scheme more than accurate enough. Quantities such as μ_G and σ_G can be calculated exactly given the exact diagonalization. However the left hand side of Eq. 12 has a time order complexity of $\mathcal{O}(N^4)$, making it again extremely difficult to calculate exactly. To get around this, we simply define a grid $t_k = \Delta k$ where $k = 0, 1, 2 \dots$ and average over the values calculated of $|C^A(t_k) - C_\infty^A|^2$ as,

$$\overline{c(k)}_T = \frac{1}{k+1} \sum_{i=0}^k |C^A(t_i) - C_\infty^A|^2. \quad (\text{C1})$$

Figure 3 (right) shows the forward error of this scheme, showing an expected first order accuracy in time. Since we have an accuracy which is satisfactory for the scales we are comparing with the bound which tends have a roughly 10^{-1} disagreement between the two sides of the bound. Finally to the optimal choice of $a(\epsilon)$ and $\delta(\epsilon)$. For the plots present in figure 2 we simply took the smallest $\delta(\epsilon)$ available to minimize the resolution of our bound and picked the

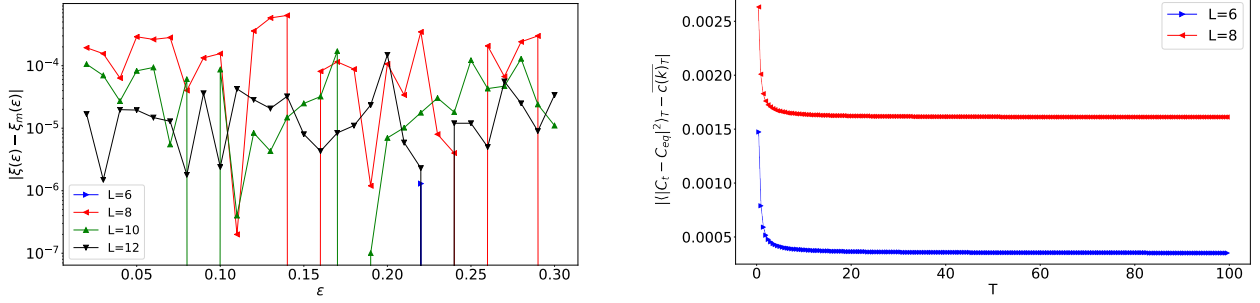


FIG. 3. (left) Forward error plot depicting the accuracy of the Monte Carlo scheme at different values of system size. $\xi(\epsilon)$ is exactly calculated and $\xi_m(\epsilon)$ is calculated using the Monte Carlo scheme with 10,000 samples per value of ϵ . (right) Forward error plot depicting the accuracy of the integral approximation in calculating the left hand side of equation B1 at various values of time and system size. A step size in time of $\Delta t = 0.001$ was used.

corresponding $a(\epsilon)$. This choice has an obvious issue in the $L = 8$ case but begins to be more favourable in the larger system sizes. Looking at figure 1 we see the value $a(\epsilon)$ can grow quite quickly due to finite size effects, making the prefactor outside the $1/T$ term quite large.

1. Integrable models

Next, this section provide an example of showing how our bounds on timescales are affected in integrable models, highlighting the negative effect of degeneracies. Suppose we choose to define our Hamiltonian of Eq. (23) in the main text with parameters $H = (-0.5, 0, -0.5, 0)$. This corresponds to an Ising model with a transverse field. The issue in general with this model comes from investigating the behaviour of the corresponding $\delta(\epsilon)$ and the fact that the frequencies G_α are very degenerate, meaning this function will not necessarily decay to zero as we take $\epsilon \rightarrow 0$.

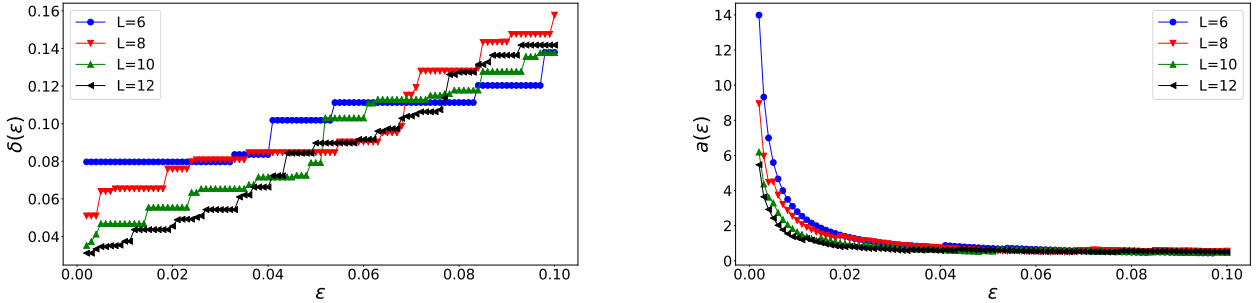


FIG. 4. Plots of $\delta(\epsilon)$ (top) and $a(\epsilon)$ (bottom) for distribution v_α in Theorem 3, obtained by exact diagonalization, and a Monte Carlo approximation of the function from Definition 2. The plots share the same x-axis and were generated with 10,000 sampled frequency intervals. Small values of δ imply equilibration occurs for long enough times, while the value of a controls the prefactor in the equilibration timescale Eq. (B1).

In Figure 4 we see the issue emerging with the bound found in Theorem 3. The degeneracy of the G_α terms cause the decrease in $\delta(\epsilon)$ to happen in discrete steps triggered by calculating $\delta(\epsilon)$ in a small enough region to differentiate two degenerate values of G_α which are close. Thus at small ϵ we still expect our resolution of equilibrium to be quite large. This slow decay of $\delta(\epsilon)$ also causes $a(\epsilon)$ to become quite large very quickly, as one needs $\delta(\epsilon)$ to be roughly linear for $a(\epsilon)$ to be reasonably small. This suggests that perhaps alternative approaches are required to bound the equilibration of two point time correlation functions in integrable models.

2. Distribution of $v_\alpha \equiv \frac{\rho_{jj}|A_{jk}|^2}{C_0}$

Finally, we show the distributions of $v_\alpha \equiv \frac{\rho_{jj}|A_{jk}|^2}{C_0}$ and comment on the differences between the integrable case and the case that obeys the ETH. To proceed we define a coarse grained version \bar{p}_α of $v_\alpha \equiv \frac{\rho_{jj}|A_{jk}|^2}{C_0}$, where we define n bins and bins, $b_1 = [G_{min}, G_{min} + \Delta G]$, $b_2 = [G_{min} + \Delta G, G_{min} + 2\Delta G], \dots$, where $\Delta G = \frac{G_{max} - G_{min}}{n}$. The coarse grained probability is then obtained by summing the associated probabilities, $\bar{p}_\alpha = \sum_{G_\beta \in b_\beta} v_\beta$.

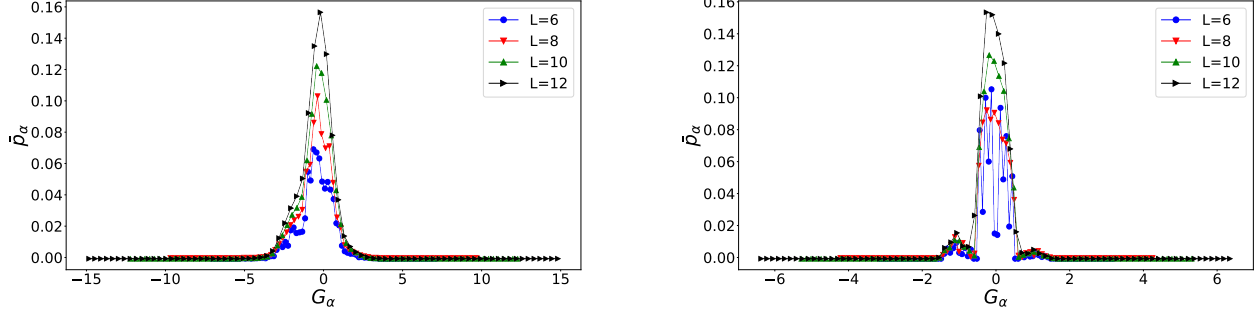


FIG. 5. Plot of \bar{p}_α obtained from coarse-graining $v_\alpha \equiv \frac{\rho_{jj}|A_{jk}|^2}{C_0}$ against frequency, with $n = 80$ bins at various system sizes. The case for which ETH is satisfied is featured on the left, while the integrable case is on the right. For the latter the distribution is less uni-modal, which leads to larger values of $a(\epsilon)$, as depicted on Fig. 4 (right).

The result is given in Figure 5. The ETH case approaches a unimodal distribution quicker than the integrable case, however both distributions appear favorable in the coarse grained probabilities. Note, increasing the number of bins significantly did not significantly affect the shape of the curve.

Chapter 5

Conclusions

In this thesis we introduced the topics of equilibration, thermalization and scrambling. These topics were discussed at length in the introduction and were addressed in three manuscripts in chapters 2, 3 and 4. In chapter 2 we addressed the OTOC in the standard AL model of free fermions and found that the OTOC formed a neck-tie light-cone. The universal power law of equation 1.34 was observed to hold regardless of disorder. Similarly, the wave-front was discussed and it appeared that the universal waveform of equation 1.35 seemed to fail for both the non-disordered and disordered case. Instead we found that regardless of disorder, the form in equation 2.5 was more appropriate. This called into question the proposal of the universal wave-form which had an analytical prediction for equation 1.35 for non-disordered free fermions. We also concluded that a form of weak scrambling existed for the localized phase in late time, with the OTOC settling at a non-zero value in late time. The non-disordered case appeared to relax to zero indicating lack of scrambling. In chapter 3 we continued the discussion from 2 with a quasi-disordered model. The one dimensional AA model was studied, which features a localization transition at a non-zero disorder. The early time growth found in chapter 2 was again observed to be independent of disorder. We added to the discussion posed by 2 by confirming the universal wave form in both the non-disordered case and a small disorder away from the localization transition in the time regime $t \ll \frac{x}{v_B}$. The Gaussian waveform was found again for this model, and had some overlap with the universal form, but is valid surrounding the time $t = \frac{x}{v_B}$. We speculate that this might indicate a fifth time regime of interest for the OTOC directly at the classical wave-front. We then rigorously proved the OTOC equilibrates in finite time to zero for all disorder strengths in the extended region of the model. This constitutes the first rigorous proof of OTOC equilibration that we are aware of. It also implies a lack of scrambling in these models for local operators. In chapter 4 we investigated dynamical correlation functions and their universal properties under reasonable

assumptions. We rigorously proved the equilibration of these functions in the infinite time average limit and in finite time. We similarly proved a late time factorization form given in equation 1.39. The bounds of equilibration were numerically calculated for a model known to obey the strong ETH, and were shown to be reasonably tight. These results are expected to be true for all Hamiltonians with non-degenerate energy values and which at least obey the weak ETH.

Bibliography

- [1] Immanuel Bloch, Jean Dalibard, and Wilhelm Zwerger. Many-body physics with ultracold gases. *Rev. Mod. Phys.*, 80:885–964, Jul 2008.
- [2] Christian Gogolin and Jens Eisert. Equilibration, thermalisation, and the emergence of statistical mechanics in closed quantum systems. *Reports on Progress in Physics*, 79(5):056001, apr 2016.
- [3] Sandu Popescu, Anthony J. Short, and Andreas Winter. Entanglement and the foundations of statistical mechanics. *Nature Physics*, 2(11):754–758, 2006.
- [4] Sheldon Goldstein, Joel L. Lebowitz, Roderich Tumulka, and Nino Zanghì. Canonical typicality. *Phys. Rev. Lett.*, 96:050403, Feb 2006.
- [5] Peter Reimann. Foundation of statistical mechanics under experimentally realistic conditions. *Phys. Rev. Lett.*, 101:190403, Nov 2008.
- [6] Noah Linden, Sandu Popescu, Anthony J. Short, and Andreas Winter. Quantum mechanical evolution towards thermal equilibrium. *Phys. Rev. E*, 79:061103, Jun 2009.
- [7] Luca D’Alessio, Yariv Kafri, Anatoli Polkovnikov, and Marcos Rigol. From quantum chaos and eigenstate thermalization to statistical mechanics and thermodynamics. *Advances in Physics*, 65(3):239–362, 2016.
- [8] J. Eisert, M. Friesdorf, and C. Gogolin. Quantum many-body systems out of equilibrium. *Nature Physics*, 11:124 EP –, Feb 2015. Review Article.
- [9] Giacomo De Palma, Alessio Serafini, Vittorio Giovannetti, and Marcus Cramer. Necessity of eigenstate thermalization. *Phys. Rev. Lett.*, 115:220401, Nov 2015.
- [10] Yuto Ashida, Keiji Saito, and Masahito Ueda. Thermalization and heating dynamics in open generic many-body systems. *Phys. Rev. Lett.*, 121:170402, Oct 2018.

- [11] Angel Rivas and Susana F. Huelga. Open quantum systems. an introduction. *arXiv:1104.5242*, 2011.
- [12] Ulrich Weiss. *Quantum Dissipative Systems*. WORLD SCIENTIFIC, 4th edition, 2012.
- [13] E. B. Davies. Markovian master equations. *Comm. Math. Phys.*, 39(2):91–110, 1974.
- [14] R Alicki. The quantum open system as a model of the heat engine. *Journal of Physics A: Mathematical and General*, 12(5):L103–L107, may 1979.
- [15] Herbert Spohn and Joel L. Lebowitz. Irreversible thermodynamics for quantum systems weakly coupled to thermal reservoirs. *Advances in Chemical Physics*, pages 109–142, 2007.
- [16] M. A. Cazalilla, R. Citro, T. Giamarchi, E. Orignac, and M. Rigol. One dimensional bosons: From condensed matter systems to ultracold gases. *Rev. Mod. Phys.*, 83:1405–1466, Dec 2011.
- [17] Markus Greiner, Olaf Mandel, Theodor W. Hänsch, and Immanuel Bloch. Collapse and revival of the matter wave field of a bose-einstein condensate. *Nature*, 419(6902):51–54, 2002.
- [18] Sebastian Will, Thorsten Best, Ulrich Schneider, Lucia Hackermüller, Dirk-Sören Lühmann, and Immanuel Bloch. Time-resolved observation of coherent multi-body interactions in quantum phase revivals. *Nature*, 465:197 EP –, May 2010.
- [19] Sebastian Will, Deepak Iyer, and Marcos Rigol. Observation of coherent quench dynamics in a metallic many-body state of fermionic atoms. *Nature Communications*, 6:6009 EP –, Jan 2015. Article.
- [20] Toshiya Kinoshita, Trevor Wenger, and David S. Weiss. A quantum newton’s cradle. *Nature*, 440(7086):900–903, 2006.
- [21] M. Gring, M. Kuhnert, T. Langen, T. Kitagawa, B. Rauer, M. Schreitl, I. Mazets, D. Adu Smith, E. Demler, and J. Schmiedmayer. Relaxation and prethermalization in an isolated quantum system. *Science*, 337(6100):1318–1322, 2012.
- [22] Tim Langen, Sebastian Erne, Remi Geiger, Bernhard Rauer, Thomas Schweigler, Maximilian Kuhnert, Wolfgang Rohringer, Igor E. Mazets, Thomas Gasenzer, and

- Jörg Schmiedmayer. Experimental observation of a generalized gibbs ensemble. *Science*, 348(6231):207–211, 2015.
- [23] S. Trotzky, Y.-A. Chen, A. Flesch, I. P. McCulloch, U. Schollwöck, J. Eisert, and I. Bloch. Probing the relaxation towards equilibrium in an isolated strongly correlated one-dimensional bose gas. *Nature Physics*, 8:325 EP –, Feb 2012. Article.
- [24] B. P. Lanyon, C. Hempel, D. Nigg, M. Müller, R. Gerritsma, F. Zähringer, P. Schindler, J. T. Barreiro, M. Rambach, G. Kirchmair, M. Hennrich, P. Zoller, R. Blatt, and C. F. Roos. Universal digital quantum simulation with trapped ions. *Science*, 334(6052):57–61, 2011.
- [25] P. Schindler, M. Müller, D. Nigg, J. T. Barreiro, E. A. Martinez, M. Hennrich, T. Monz, S. Diehl, P. Zoller, and R. Blatt. Quantum simulation of dynamical maps with trapped ions. *Nature Physics*, 9:361 EP –, May 2013. Article.
- [26] R. Blatt and C. F. Roos. Quantum simulations with trapped ions. *Nature Physics*, 8:277 EP –, Apr 2012. Review Article.
- [27] A. K. Tuchman, C. Orzel, A. Polkovnikov, and M. A. Kasevich. Nonequilibrium coherence dynamics of a soft boson lattice. *Phys. Rev. A*, 74:051601, Nov 2006.
- [28] M. Aidelsburger, M. Atala, S. Nascimbène, S. Trotzky, Y.-A. Chen, and I. Bloch. Experimental realization of strong effective magnetic fields in an optical lattice. *Phys. Rev. Lett.*, 107:255301, Dec 2011.
- [29] S. Hofferberth, I. Lesanovsky, B. Fischer, T. Schumm, and J. Schmiedmayer. Non-equilibrium coherence dynamics in one-dimensional bose gases. *Nature*, 449:324 EP –, Sep 2007.
- [30] D. Porras and J. I. Cirac. Effective quantum spin systems with trapped ions. *Phys. Rev. Lett.*, 92:207901, May 2004.
- [31] Marc Cheneau, Peter Barmettler, Dario Poletti, Manuel Endres, Peter Schauß, Takeshi Fukuhara, Christian Gross, Immanuel Bloch, Corinna Kollath, and Stefan Kuhr. Light-cone-like spreading of correlations in a quantum many-body system. *Nature*, 481:484 EP –, Jan 2012.
- [32] T. Langen, R. Geiger, M. Kuhnert, B. Rauer, and J. Schmiedmayer. Local emergence of thermal correlations in an isolated quantum many-body system. *Nature Physics*, 9:640 EP –, Sep 2013.

- [33] J. P. Ronzheimer, M. Schreiber, S. Braun, S. S. Hodgman, S. Langer, I. P. McCulloch, F. Heidrich-Meisner, I. Bloch, and U. Schneider. Expansion dynamics of interacting bosons in homogeneous lattices in one and two dimensions. *Phys. Rev. Lett.*, 110:205301, May 2013.
- [34] S. Popescu, A. J. Short, and A. Winter. The foundations of statistical mechanics from entanglement: Individual states vs. averages. *eprint arXiv:quant-ph/0511225*, November 2005.
- [35] N. Linden, S. Popescu, A. J. Short, and A. Winter. Quantum mechanical evolution towards thermal equilibrium. *Phys. Rev. E*, 79:061103, Jun 2009.
- [36] P. Reimann. Canonical thermalization. *New Journal of Physics*, 12(5):055027, May 2010.
- [37] A. J. Short. Equilibration of quantum systems and subsystems. *New Journal of Physics*, 13(5):053009, 2011.
- [38] N. Linden, S. Popescu, A. J. Short, and A. Winter. On the speed of fluctuations around thermodynamic equilibrium. *New Journal of Physics*, 12(5):055021, 2010.
- [39] S. Goldstein, J. L. Lebowitz, C. Mastrodonato, R. Tumulka, and N. Zanghi. Approach to thermal equilibrium of macroscopic quantum systems. *Phys. Rev. E*, 81:011109, Jan 2010.
- [40] P. Reimann. Foundation of statistical mechanics under experimentally realistic conditions. *Physical Review Letters*, 101(19), Nov 2008.
- [41] Markus P. Müller, Emily Adlam, Lluís Masanes, and Nathan Wiebe. Thermalization and canonical typicality in translation-invariant quantum lattice systems. *Communications in Mathematical Physics*, 340(2):499–561, Dec 2015.
- [42] Luis Pedro García-Pintos, Noah Linden, Artur S. L. Malabarba, Anthony J. Short, and Andreas Winter. Equilibration time scales of physically relevant observables. *Phys. Rev. X*, 7:031027, Aug 2017.
- [43] A. S. L. Malabarba, L. P. García-Pintos, N. Linden, T. C. Farrelly, and A. J. Short. Quantum systems equilibrate rapidly for most observables. *Phys. Rev. E*, 90:012121, Jul 2014.

- [44] A. J. Short and T. C. Farrelly. Quantum equilibration in finite time. *New Journal of Physics*, 14(1):013063, 2012.
- [45] S. Goldstein, T. Hara, and H. Tasaki. Time scales in the approach to equilibrium of macroscopic quantum systems. *Phys. Rev. Lett.*, 111:140401, Oct 2013.
- [46] S. Goldstein, T. Hara, and H. Tasaki. Extremely quick thermalization in a macroscopic quantum system for a typical nonequilibrium subspace. *ArXiv:1402.0324*, 2014.
- [47] Ll. Masanes, A. J. Roncaglia, and A. Acín. Complexity of energy eigenstates as a mechanism for equilibration. *Phys. Rev. E*, 87:032137, Mar 2013.
- [48] F. G. S. L. Brandão, P. Ćwikliński, M. Horodecki, P. Horodecki, J. K. Korbicz, and M. Mozrzykas. Convergence to equilibrium under a random hamiltonian. *Phys. Rev. E*, 86:031101, Sep 2012.
- [49] Vinayak and M. Žnidarič. Subsystem dynamics under random hamiltonian evolution. *Journal of Physics A: Mathematical and Theoretical*, 45(12):125204, 2012.
- [50] A. Hutter and S. Wehner. Dependence of a quantum-mechanical system on its own initial state and the initial state of the environment it interacts with. *Physical Review A*, 87(1), Jan 2013.
- [51] M. Cramer, C. M. Dawson, J. Eisert, and T. J. Osborne. Exact Relaxation in a Class of Nonequilibrium Quantum Lattice Systems. *Physical Review Letters*, 100(3):030602, January 2008.
- [52] M. Kastner. Diverging equilibration times in long-range quantum spin models. *Phys. Rev. Lett.*, 106:130601, Mar 2011.
- [53] P. R. Zangara, A. D. Dente, E. J. Torres-Herrera, H. M. Pastawski, A. Iucci, and L. F. Santos. Time fluctuations in isolated quantum systems of interacting particles. *Phys. Rev. E*, 88:032913, Sep 2013.
- [54] M. van den Worm, B. C. Sawyer, J. J. Bollinger, and M. Kastner. Relaxation timescales and decay of correlations in a long-range interacting quantum simulator. *New Journal of Physics*, 15(8):083007, 2013.
- [55] M. Fuchs, J. Schliemann, and B. Trauzettel. Ultralong spin decoherence times in graphene quantum dots with a small number of nuclear spins. *Phys. Rev. B*, 88(24):245441, December 2013.

- [56] Marek Gluza, Jens Eisert, and Terry Farrelly. Equilibration towards generalized gibbs ensembles in non-interacting theories. *arXiv:1809.08268*, 2018.
- [57] M. Gluza, C. Krumnow, M. Friesdorf, C. Gogolin, and J. Eisert. Equilibration via gaussification in fermionic lattice systems. *Phys. Rev. Lett.*, 117:190602, Nov 2016.
- [58] Jonas Richter, Jochen Gemmer, and Robin Steinigeweg. Impact of eigenstate thermalization on the route to equilibrium. *Phys. Rev. E*, 99:050104, May 2019.
- [59] Jonas Richter and Robin Steinigeweg. Relation between far-from-equilibrium dynamics and equilibrium correlation functions for binary operators. *Phys. Rev. E*, 99:012114, Jan 2019.
- [60] Álvaro M. Alhambra, Jonathon Riddell, and Luis Pedro Garca-Pintos. Time evolution of correlation functions in quantum many-body systems. *arXiv:1906.11280*, 2019.
- [61] Fernando G. S. L. Brandao and Marcus Cramer. Equivalence of statistical mechanical ensembles for non-critical quantum systems. *arXiv:1502.03263*, 2015.
- [62] J. M. Deutsch. Quantum statistical mechanics in a closed system. *Phys. Rev. A*, 43:2046–2049, Feb 1991.
- [63] M. Srednicki. The approach to thermal equilibrium in quantized chaotic systems. *Journal of Physics A: Mathematical and General*, 32(7):1163, 1999.
- [64] M. Rigol, V. Dunjko, and M. Olshanii. Thermalization and its mechanism for generic isolated quantum systems. *Nature*, 452(7189):854–858, 2008.
- [65] M. Rigol and M. Srednicki. Alternatives to eigenstate thermalization. *Phys. Rev. Lett.*, 108:110601, Mar 2012.
- [66] A. Khodja, R. Steinigeweg, and J. Gemmer. Relevance of the eigenstate thermalization hypothesis for thermal relaxation. *Phys. Rev. E*, 91:012120, Jan 2015.
- [67] Rahul Nandkishore and David A. Huse. Many-body localization and thermalization in quantum statistical mechanics. *Annual Review of Condensed Matter Physics*, 6(1):15–38, 2015.
- [68] Kazuya Kaneko, Eiki Iyoda, and Takahiro Sagawa. Work extraction from a single energy eigenstate. *Phys. Rev. E*, 99:032128, Mar 2019.

- [69] Guillaume Roux. Finite-size effects in global quantum quenches: Examples from free bosons in an harmonic trap and the one-dimensional bose-hubbard model. *Phys. Rev. A*, 81:053604, May 2010.
- [70] Giulio Biroli, Corinna Kollath, and Andreas M. Läuchli. Effect of rare fluctuations on the thermalization of isolated quantum systems. *Phys. Rev. Lett.*, 105:250401, Dec 2010.
- [71] S. Genway, A. F. Ho, and D. K. K. Lee. Thermalization of local observables in small hubbard lattices. *Phys. Rev. A*, 86:023609, Aug 2012.
- [72] Clemens Neuenhahn and Florian Marquardt. Thermalization of interacting fermions and delocalization in fock space. *Phys. Rev. E*, 85:060101, Jun 2012.
- [73] R. Steinigeweg, A. Khodja, H. Niemeyer, C. Gogolin, and J. Gemmer. Pushing the limits of the eigenstate thermalization hypothesis towards mesoscopic quantum systems. *Phys. Rev. Lett.*, 112:130403, Apr 2014.
- [74] Hyungwon Kim, Tatsuhiko N. Ikeda, and David A. Huse. Testing whether all eigenstates obey the eigenstate thermalization hypothesis. *Phys. Rev. E*, 90:052105, Nov 2014.
- [75] R. Steinigeweg, J. Herbrych, and P. Prelovšek. Eigenstate thermalization within isolated spin-chain systems. *Phys. Rev. E*, 87(1):012118, January 2013.
- [76] Marcos Rigol. Quantum quenches and thermalization in one-dimensional fermionic systems. *Phys. Rev. A*, 80:053607, Nov 2009.
- [77] Marcos Rigol. Breakdown of thermalization in finite one-dimensional systems. *Phys. Rev. Lett.*, 103:100403, Sep 2009.
- [78] Ehsan Khatami, Guido Pupillo, Mark Srednicki, and Marcos Rigol. Fluctuation-dissipation theorem in an isolated system of quantum dipolar bosons after a quench. *Phys. Rev. Lett.*, 111:050403, Jul 2013.
- [79] Marcos Rigol and Lea F. Santos. Quantum chaos and thermalization in gapped systems. *Phys. Rev. A*, 82:011604, Jul 2010.
- [80] Lea F. Santos and Marcos Rigol. Onset of quantum chaos in one-dimensional bosonic and fermionic systems and its relation to thermalization. *Phys. Rev. E*, 81:036206, Mar 2010.

- [81] Adam Nahum, Jonathan Ruhman, and David A. Huse. Dynamics of entanglement and transport in one-dimensional systems with quenched randomness. *Phys. Rev. B*, 98:035118, Jul 2018.
- [82] James R. Garrison and Tarun Grover. Does a single eigenstate encode the full hamiltonian? *Phys. Rev. X*, 8:021026, Apr 2018.
- [83] Ruihua Fan, Pengfei Zhang, Huitao Shen, and Hui Zhai. Out-of-time-order correlation for many-body localization. *Science Bulletin*, 62(10):707 – 711, 2017.
- [84] Lev Vidmar and Marcos Rigol. Entanglement entropy of eigenstates of quantum chaotic hamiltonians. *Phys. Rev. Lett.*, 119:220603, Nov 2017.
- [85] Fernando G. S. L. Brandao, Elizabeth Crosson, M. Burak Şahinoğlu, and John Bowen. Quantum Error Correcting Codes in Eigenstates of Translation-Invariant Spin Chains. *arXiv e-prints*, page arXiv:1710.04631, Oct 2017.
- [86] Takashi Mori. Weak eigenstate thermalization with large deviation bound. *arXiv e-prints*, page arXiv:1609.09776, Sep 2016.
- [87] Wen Wei Ho, Soonwon Choi, Hannes Pichler, and Mikhail D. Lukin. Periodic orbits, entanglement, and quantum many-body scars in constrained models: Matrix product state approach. *Phys. Rev. Lett.*, 122:040603, Jan 2019.
- [88] C. J. Turner, A. A. Michailidis, D. A. Abanin, M. Serbyn, and Z. Papić. Quantum scarred eigenstates in a rydberg atom chain: Entanglement, breakdown of thermalization, and stability to perturbations. *Phys. Rev. B*, 98:155134, Oct 2018.
- [89] Andrew J. A. James, Robert M. Konik, and Neil J. Robinson. Nonthermal states arising from confinement in one and two dimensions. *Phys. Rev. Lett.*, 122:130603, Apr 2019.
- [90] Itai Arad, Tomotaka Kuwahara, and Zeph Landau. Connecting global and local energy distributions in quantum spin models on a lattice. *Journal of Statistical Mechanics: Theory and Experiment*, 2016(3):033301, 2016.
- [91] Thiago R de Oliveira, Christos Charalambous, Daniel Jonathan, Maciej Lewenstein, and Arnau Riera. Equilibration time scales in closed many-body quantum systems. *New Journal of Physics*, 2018.
- [92] Fabien Alet and Nicolas Laflorencie. Many-body localization: An introduction and selected topics. *Comptes Rendus Physique*, 2018.

- [93] David J. Luitz, Nicolas Laflorencie, and Fabien Alet. Many-body localization edge in the random-field heisenberg chain. *Phys. Rev. B*, 91:081103, Feb 2015.
- [94] Jens H. Bardarson, Frank Pollmann, and Joel E. Moore. Unbounded growth of entanglement in models of many-body localization. *Phys. Rev. Lett.*, 109:017202, Jul 2012.
- [95] Maksym Serbyn, Z. Papić, and Dmitry A. Abanin. Universal slow growth of entanglement in interacting strongly disordered systems. *Phys. Rev. Lett.*, 110:260601, Jun 2013.
- [96] Dong-Ling Deng, Xiaopeng Li, J. H. Pixley, Yang-Le Wu, and S. Das Sarma. Logarithmic entanglement lightcone in many-body localized systems. *Phys. Rev. B*, 95:024202, Jan 2017.
- [97] Marko Žnidarič, Tomaž Prosen, and Peter Prelovšek. Many-body localization in the heisenberg xxz magnet in a random field. *Phys. Rev. B*, 77:064426, Feb 2008.
- [98] Gabriele De Chiara, Simone Montangero, Pasquale Calabrese, and Rosario Fazio. Entanglement entropy dynamics of heisenberg chains. *Journal of Statistical Mechanics: Theory and Experiment*, 2006(03):P03001, 2006.
- [99] Hsin-Hua Lai and Kun Yang. Entanglement entropy scaling laws and eigenstate typicality in free fermion systems. *Phys. Rev. B*, 91:081110, Feb 2015.
- [100] Jonathon Riddell and Markus P. Müller. Generalized eigenstate typicality in translation-invariant quasifree fermionic models. *Phys. Rev. B*, 97:035129, Jan 2018.
- [101] Lev Vidmar, Lucas Hackl, Eugenio Bianchi, and Marcos Rigol. Entanglement entropy of eigenstates of quadratic fermionic hamiltonians. *Phys. Rev. Lett.*, 119:020601, Jul 2017.
- [102] Lev Vidmar, Lucas Hackl, Eugenio Bianchi, and Marcos Rigol. Volume law and quantum criticality in the entanglement entropy of excited eigenstates of the quantum ising model. *Phys. Rev. Lett.*, 121:220602, Nov 2018.
- [103] Lucas Hackl, Lev Vidmar, Marcos Rigol, and Eugenio Bianchi. Average eigenstate entanglement entropy of the xy chain in a transverse field and its universality for translationally invariant quadratic fermionic models. *Phys. Rev. B*, 99:075123, Feb 2019.

- [104] Houssam Abdul-Rahman, Bruno Nachtergaele, Robert Sims, and Gnter Stolz. Localization properties of the disordered xy spin chain. *Annalen der Physik*, 529(7):1600280, 2017.
- [105] Ferenc Iglói, Zsolt Szatmári, and Yu-Cheng Lin. Entanglement entropy dynamics of disordered quantum spin chains. *Phys. Rev. B*, 85:094417, Mar 2012.
- [106] Max McGinley, Andreas Nunnenkamp, and Johannes Knolle. Slow growth of entanglement and out-of-time-order correlators in integrable disordered systems. *arXiv:1807.06039*, 2018.
- [107] Houssam Abdul-Rahman, Bruno Nachtergaele, Robert Sims, and Günter Stolz. Entanglement dynamics of disordered quantum xy chains. *Letters in Mathematical Physics*, 106(5):649–674, May 2016.
- [108] G. Stolz. An introduction to the mathematics of anderson localization. *arXiv preprint arXiv:1104.2317*, 2011.
- [109] Jonathon Riddell and Erik S. Sørensen. Out-of-time ordered correlators and entanglement growth in the random-field xx spin chain. *Phys. Rev. B*, 99:054205, Feb 2019.
- [110] Elliott Lieb, Theodore Schultz, and Daniel Mattis. Two soluble models of an antiferromagnetic chain. *Annals of Physics*, 16(3):407 – 466, 1961.
- [111] A. I. Larkin and Y. N. Ovchinnikov. Quasiclassical method in the theory of superconductivity. *Zh. Eksp. Teor. Fiz.*, 55:2262, 1969. [JETP 28, 1200 (1969)].
- [112] Juan Maldacena, Stephen H. Shenker, and Douglas Stanford. A bound on chaos. *Journal of High Energy Physics*, 2016(8):106, Aug 2016.
- [113] Yasuhiro Sekino and L. Susskind. Fast scramblers. *Journal of High Energy Physics*, 2008(10):065, 2008.
- [114] Subir Sachdev and Jinwu Ye. Gapless spin-fluid ground state in a random quantum heisenberg magnet. *Phys. Rev. Lett.*, 70:3339–3342, May 1993.
- [115] Subir Sachdev. Bekenstein-hawking entropy and strange metals. *Phys. Rev. X*, 5:041025, Nov 2015.
- [116] Daniel A. Roberts, Douglas Stanford, and Leonard Susskind. Localized shocks. *Journal of High Energy Physics*, 2015(3):51, Mar 2015.

- [117] Wenbo Fu and Subir Sachdev. Numerical study of fermion and boson models with infinite-range random interactions. *Phys. Rev. B*, 94:035135, Jul 2016.
- [118] Juan Maldacena and Douglas Stanford. Remarks on the sachdev-ye-kitaev model. *Phys. Rev. D*, 94:106002, Nov 2016.
- [119] Balázs Dóra and Roderich Moessner. Out-of-time-ordered density correlators in luttinger liquids. *Phys. Rev. Lett.*, 119:026802, Jul 2017.
- [120] Yichen Huang, Yong-Liang Zhang, and Xie Chen. Out-of-time-ordered correlators in many-body localized systems. *Annalen der Physik*, 529(7):1600318, 2017.
- [121] Brian Swingle and Debanjan Chowdhury. Slow scrambling in disordered quantum systems. *Phys. Rev. B*, 95:060201, Feb 2017.
- [122] Xiao Chen, Tianci Zhou, David A. Huse, and Eduardo Fradkin. Out-of-time-order correlations in many-body localized and thermal phases. *Annalen der Physik*, 529(7):1600332, 2017.
- [123] Kevin Slagle, Zhen Bi, Yi-Zhuang You, and Cenke Xu. Out-of-time-order correlation in marginal many-body localized systems. *Phys. Rev. B*, 95:165136, Apr 2017.
- [124] W. Miller. *Symmetry Groups and Their Applications*. Computer Science and Applied Mathematics. Academic Press, 1972.
- [125] Daniel A. Roberts and Brian Swingle. Lieb-robinson bound and the butterfly effect in quantum field theories. *Phys. Rev. Lett.*, 117:091602, Aug 2016.
- [126] Xiao Chen, Tianci Zhou, and Cenke Xu. Measuring the distance between quantum many-body wave functions. *Journal of Statistical Mechanics: Theory and Experiment*, 2018(7):073101, jul 2018.
- [127] Cheng-Ju Lin and Olexei I. Motrunich. Out-of-time-ordered correlators in a quantum ising chain. *Phys. Rev. B*, 97:144304, Apr 2018.
- [128] J. Lee, D. Kim, and D. H. Kim. Typical growth behavior of the out-of-time-ordered commutator in many-body localized systems. *arXiv:1812.00357*, 2018.
- [129] J. Bao and C. Zhang. Out-of-time-order correlators in one-dimensional xy model. *arXiv:1901.09327*, 2019.

- [130] Shenglong Xu and Brian Swingle. Accessing scrambling using matrix product operators. *arXiv:1802.00801*, February 2018.
- [131] Vedika Khemani, David A. Huse, and Adam Nahum. Velocity-dependent lyapunov exponents in many-body quantum, semiclassical, and classical chaos. *Phys. Rev. B*, 98:144304, Oct 2018.
- [132] Adam Nahum, Sagar Vijay, and Jeongwan Haah. Operator spreading in random unitary circuits. *Phys. Rev. X*, 8:021014, Apr 2018.
- [133] C. W. von Keyserlingk, Tibor Rakovszky, Frank Pollmann, and S. L. Sondhi. Operator hydrodynamics, otocs, and entanglement growth in systems without conservation laws. *Phys. Rev. X*, 8:021013, Apr 2018.
- [134] Yingfei Gu, Xiao-Liang Qi, and Douglas Stanford. Local criticality, diffusion and chaos in generalized sachdev-ye-kitaev models. *Journal of High Energy Physics*, 2017(5):125, May 2017.
- [135] Shenglong Xu and Brian Swingle. Locality, Quantum Fluctuations, and Scrambling. *arXiv:1805.05376v1*, May 2018.
- [136] Subhayan Sahu, Shenglong Xu, and Brian Swingle. Scrambling dynamics across a thermalization-localization quantum phase transition. *arXiv:1807.06086v1*, cond-mat.str-el, 2018.
- [137] Tibor Rakovszky, Frank Pollmann, and C. W. von Keyserlingk. Diffusive hydrodynamics of out-of-time-ordered correlators with charge conservation. *Phys. Rev. X*, 8:031058, Sep 2018.
- [138] Stephen H. Shenker and Douglas Stanford. Black holes and the butterfly effect. *Journal of High Energy Physics*, 2014(3):67, Mar 2014.
- [139] Aavishkar A. Patel, Debanjan Chowdhury, Subir Sachdev, and Brian Swingle. Quantum butterfly effect in weakly interacting diffusive metals. *Phys. Rev. X*, 7:031047, Sep 2017.
- [140] Debanjan Chowdhury and Brian Swingle. Onset of many-body chaos in the $o(n)$ model. *Phys. Rev. D*, 96:065005, Sep 2017.
- [141] Shao-Kai Jian and Hong Yao. Universal properties of many-body quantum chaos at gross-neveu criticality. *arXiv:1805.12299*, 2018.

- [142] Y. Chen. Universal logarithmic scrambling in many body localization. *arXiv:1608.02765*, 2016.
- [143] Rong-Qiang He and Zhong-Yi Lu. Characterizing many-body localization by out-of-time-ordered correlation. *Phys. Rev. B*, 95:054201, Feb 2017.
- [144] Daniel A. Roberts and Beni Yoshida. Chaos and complexity by design. *Journal of High Energy Physics*, 2017(4):121, Apr 2017.
- [145] Yichen Huang, Fernando G. S. L. Brandão, and Yong-Liang Zhang. Finite-size scaling of out-of-time-ordered correlators at late times. *Phys. Rev. Lett.*, 123:010601, Jul 2019.
- [146] Y. Chen. Universal logarithmic scrambling in many body localization. *arXiv.org*, 2016.
- [147] Beni Yoshida and Norman Y. Yao. Disentangling scrambling and decoherence via quantum teleportation. *Phys. Rev. X*, 9:011006, Jan 2019.
- [148] Brian Swingle, Gregory Bentsen, Monika Schleier-Smith, and Patrick Hayden. Measuring the scrambling of quantum information. *Phys. Rev. A*, 94:040302, Oct 2016.
- [149] Guanyu Zhu, Mohammad Hafezi, and Tarun Grover. Measurement of many-body chaos using a quantum clock. *Phys. Rev. A*, 94:062329, Dec 2016.
- [150] Norman Y. Yao, Fabian Grusdt, Brian Swingle, Mikhail D. Lukin, Dan M. Stamper-Kurn, Joel E. Moore, and Eugene A. Demler. Interferometric approach to probing fast scrambling. *arXiv:1607.01801*, 2016.
- [151] Ipei Danshita, Masanori Hanada, and Masaki Tezuka. Creating and probing the SachdevYeKitaev model with ultracold gases: Towards experimental studies of quantum gravity. *Progress of Theoretical and Experimental Physics*, 2017(8), 08 2017.
- [152] Jun Li, Ruihua Fan, Hengyan Wang, Bingtian Ye, Bei Zeng, Hui Zhai, Xinhua Peng, and Jiangfeng Du. Measuring out-of-time-order correlators on a nuclear magnetic resonance quantum simulator. *Phys. Rev. X*, 7:031011, Jul 2017.
- [153] K. A. Landsman, C. Figgatt, T. Schuster, N. M. Linke, B. Yoshida, N. Y. Yao, and C. Monroe. Verified quantum information scrambling. *Nature*, 567(7746):61–65, 2019.
- [154] Eman Hamza, Robert Sims, and Günter Stolz. Dynamical localization in disordered quantum spin systems. *Communications in Mathematical Physics*, 315(1):215–239, Oct 2012.

- [155] Piers Coleman. *Introduction to Many-Body Physics*. Cambridge University Press, 2015.
- [156] Jonathon Riddell and Erik S. Sørensen. Out of time order correlations in the quasi-periodic aubry-andré model. *arXiv:1908.03292*.
- [157] Serge Aubry and Gilles Andr. Analyticity breaking and anderson localization in incommensurate lattices. *Proceedings, VIII International Colloquium on Group-Theoretical Methods in Physics*, 3, 01 1980.
- [158] Hisashi Hiramoto and Mahito Kohmoto. Scaling analysis of quasiperiodic systems: Generalized Harper model. *Physical Review B*, 40(12):8225–8234, October 1989.
- [159] Giacomo Roati, Chiara D’Errico, Leonardo Fallani, Marco Fattori, Chiara Fort, Matteo Zaccanti, Giovanni Modugno, Michele Modugno, and Massimo Inguscio. Anderson localization of a non-interacting Bose–Einstein condensate. *Nature*, 453(7197):895–898, June 2008.
- [160] B Deissler, M Zaccanti, G Roati, C D’Errico, M Fattori, M. Modugno, G Modugno, and M. Inguscio. Delocalization of a disordered bosonic system by repulsive interactions. *Nature Physics*, 6(5):354–358, April 2010.
- [161] E Lucioni, B Deissler, L Tanzi, G Roati, M Zaccanti, M. Modugno, M. Larcher, F Dalfovo, M. Inguscio, and G Modugno. Observation of Subdiffusion in a Disordered Interacting System. *Physical Review Letters*, 106(23):133–4, June 2011.
- [162] Michael Schreiber, Sean S Hodgman, Pranjal Bordia, Henrik P Lüschen, Mark H Fischer, Ronen Vosk, Ehud Altman, Ulrich Schneider, and Immanuel Bloch. Observation of many-body localization of interacting fermions in a quasirandom optical lattice. *Science*, 349(6250):842–845, August 2015.
- [163] Henrik P Lüschen, Pranjal Bordia, Sean S Hodgman, Michael Schreiber, Saubhik Sarkar, Andrew J Daley, Mark H Fischer, Ehud Altman, Immanuel Bloch, and Ulrich Schneider. Signatures of Many-Body Localization in a Controlled Open Quantum System. *Physical Review X*, 7(1):37–13, March 2017.
- [164] Henrik P Lüschen, Pranjal Bordia, Sebastian Scherg, Fabien Alet, Ehud Altman, Ulrich Schneider, and Immanuel Bloch. Observation of Slow Dynamics near the Many-Body Localization Transition in One-Dimensional Quasiperiodic Systems. *Physical Review Letters*, 119(26):18–6, December 2017.